EARTHQUAKE SPECTRA

Earthquake Spectra
2024, Vol. 40(1) 5–88

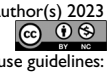

DOI: 10.1177/87552930231215428
journals.sagepub.com/home/eqs
Sage

# The 2023 US 50-State National Seismic Hazard Model: Overview and implications

**Mark D Petersen, M.EERI[1,2], Allison M Shumway[1], Peter M Powers, M.EERI[1], Edward H Field, M.EERI[1], Morgan P Moschetti, M.EERI[1], Kishor S Jaiswal, M.EERI[1], Kevin R Milner, M.EERI[3], Sanaz Rezaeian[1], Arthur D Frankel, M.EERI[4], Andrea L Llenos[1], Andrew J Michael, M.EERI[5], Jason M Altekruse[1], Sean K Ahdi, M.EERI[1,6], Kyle B Withers[1], Charles S Mueller[1], Yuehua Zeng[1], Robert E Chase, M.EERI[1,7], Leah M Salditch[1,8], Nicolas Luco, M.EERI[1], Kenneth S Rukstales[1], Julie A Herrick[1], Demi L Girot[1], Brad T Aagaard[1], Adrian M Bender[9], Michael L Blanpied[10], Richard W Briggs[1], Oliver S Boyd, M.EERI[1], Brandon S Clayton[1], Christopher B DuRoss[1], Eileen L Evans[11], Peter J Haeussler[9], Alexandra E Hatem[1], Kirstie L Haynie[1], Elizabeth H Hearn[12], Kaj M Johnson[13], Zachary A Kortum[1], N Simon Kwong, M.EERI[1], Andrew J Makdisi, M.EERI[1], H Benjamin Mason[1,14], Daniel E McNamara[15], Devin F McPhillips[16], Paul G Okubo[17], Morgan T Page[16], Fred F Pollitz[5], Justin L Rubinstein[5], Bruce E Shaw[18], Zheng-Kang Shen[19], Brian R Shiro[1], James A Smith[1], William J Stephenson[1], Eric M Thompson[1], Jessica A Thompson Jobe[1], Erin A Wirth[4], and Robert C Witter[9]**

**Abstract**

The US National Seismic Hazard Model (NSHM) was updated in 2023 for all 50 states using new science on seismicity, fault ruptures, ground motions, and probabilistic techniques to produce a standard of practice for public policy and other engineering applications (defined for return periods greater than ~475 or less than ~10,000 years). Changes in 2023 time-independent seismic hazard (both increases and decreases compared to previous NSHMs) are substantial because the new model considers more data and updated earthquake rupture forecasts and ground-motion components. In developing the 2023 model, we tried to apply best available or applicable science based on advice of co-authors, more than 50 reviewers, and hundreds of hazard scientists and end-users, who attended public workshops and provided technical inputs. The hazard assessment incorporates new catalogs, declustering algorithms, gridded seismicity models, magnitude-scaling equations, fault-based structural and deformation models, multi-fault earthquake rupture forecast models, semi-empirical and simulation-based ground-motion models, and site amplification models conditioned on shear-wave velocities of the upper 30 m of soil and deeper sedimentary basin structures. Seismic hazard calculations yield hazard curves at hundreds of thousands of sites, ground-motion maps, uniform-hazard response spectra, and disaggregations developed for pseudo-spectral accelerations at 21 oscillator periods and two peak parameters, Modified Mercalli Intensity, and 8 site classes required by building codes and other public policy applications. Tests show the new model is consistent with past ShakeMap intensity observations. Sensitivity and uncertainty assessments ensure resulting ground motions are compatible with known hazard information and highlight the range and causes of variability in ground motions. We produce several impact products including building seismic design criteria, intensity maps, planning scenarios, and engineering risk

[1]Geologic Hazards Science Center, US Geological Survey, Golden, CO, USA
[2]Denver Federal Center, Denver, CO, USA
[3]University of Southern California, Los Angeles, CA, USA
[4]Earthquake Science Center, US Geological Survey, Seattle, WA, USA
[5]Earthquake Science Center, US Geological Survey, Moffett Field, CA, USA
[6]AECOM, Los Angeles, CA, USA
[7]Lettis Consultants International, Boulder, CO, USA
[8]Guy Carpenter, Chicago, IL, USA
[9]US Geological Survey, Anchorage, AK, USA
[10]US Geological Survey, Reston, VA, USA
[11]California State University, Northridge, Northridge, CA, USA
[12]Capstone Geophysics, Portola Valley, CA, USA
[13]Indiana University, Bloomington, IN, USA
[14]College of Engineering, Oregon State University, Corvallis, OR, USA
[15]EarthScope Consortium, Washington, DC, USA
[16]Earthquake Science Center, US Geological Survey, Pasadena, CA, USA
[17]Hawaiian Volcano Observatory, US Geological Survey, Hilo, HI, USA
[18]Lamont-Doherty Earth Observatory, Palisades, NY, USA
[19]University of California, Los Angeles, Los Angeles, CA, USA

**Corresponding author:**
Mark D Petersen, Denver Federal Center, P.O. Box 25046, MS 966, Denver, CO 80225, USA.
Email: mpetersen@usgs.gov

assessments showing the potential physical and social impacts. These applications provide a basis for assessing, planning, and mitigating the effects of future earthquakes.

**Keywords**
National Seismic Hazard Model, earthquake rupture forecast, ground-motion model, probabilistic seismic hazard maps, earthquake engineering and risk

Date received: 31 May 2023; accepted: 8 October 2023

## Introduction

A recent joint study led by the US Geological Survey (USGS) and Federal Emergency Management Agency (FEMA) forecasted direct average economic losses of $14.7 billion per year from ground-shaking–related damage to buildings across the United States (Jaiswal et al., 2023). The USGS National Seismic Hazard Model (NSHM, Petersen et al., 2020) forms the underlying ground-shaking hazard layer applied in this risk assessment and is made by developing the nation's fault and fold deformation databases, interpreting crustal and volcanic seismicity, and evaluating the probabilistic ground-shaking levels for various earthquake sizes, distances, tectonic regimes, and site conditions. The projected rates of earthquakes and economic risk in some urban areas pose a threat to citizens and infrastructure. The USGS has continued to develop the NSHM over the past five decades and revises these models regularly to reflect newly published earthquake science on earthquake hazards (e.g. Algermissen and Perkins, 1976; Frankel et al., 1996, 2002; Petersen et al., 1996, 2008, 2014, 2015a, 2020, 2021 for the conterminous United States (CONUS); Wesson et al., 2007 and Appendix D of Electronic_Supplement_1.pdf for Alaska; and Klein et al., 2001 and Petersen et al., 2022 for Hawaii). In addition, the NSHMs are calculated for US territories (Puerto Rico: Mueller et al., 2010; Guam and Mariana Islands: Mueller et al., 2012; American Samoa: Petersen et al., 2012) that also face significant risk from earthquakes; the NSHMs for these territories are planned to be revised following this 50-state update. In this article, we describe the basis of the 2023 NSHM that is available publicly on the GitLab website (source models (HI: Powers and Altekruse, 2022b; CONUS: Powers and Altekruse, 2022a; AK: Powers and Altekruse, 2023) and *nshmp-haz* computer code (Powers et al., 2022)), OpenSHA website (Field et al., 2003), USGS ScienceBase Catalog (HI: Rukstales et al., 2021; CONUS and AK: Petersen et al., 2023), and through supporting information (e.g. logic trees) from papers listed in the references and Electronic_Supplement_1.pdf. The 2023 NSHM represents a living model which for this version applies the best available science as of the end of calendar year 2023. Any minor adjustments needed for policy applications (e.g., applications of $V_{S30}$ dependent tapered adjustments to central and eastern U.S. ground motion models and Alaska recurrences that are more compatible with geologic observations) will be updated and tracked via the USGS ScienceBase data releases and *nshmp-haz* computer code version numbers.

The NSHM seismic hazard products provide information needed to save lives and property through application in life-safety–based building design codes; by assisting the public and industry in identifying, preparing for, and mitigating against economic and infrastructure losses; and by supporting functional recovery and resilient community development through effective disaster management and seismic safety planning. Earthquake resistant building provisions rely on the NSHMs to guide construction of new and existing buildings, highways, bridges, railroads, dams, pipelines, energy systems, and hazardous waste disposal. Besides application in building codes, these models have also influenced policy

and industry safety and continuity plans including FEMA risk assessments and mitigation grants, governmental and military disaster management strategies, state-wide and local government seismic safety plans and legislation, critical infrastructure assessments, business and industry planning tools, and insurance risk applications. Given the importance of these applications, we routinely engage and foster evaluation and feedback from the end-users of the NSHMs. For example, as part of this update, we hosted a user-needs workshop and several other user-specific meetings with participation from leaders from industry, academia, government, and insurance to enfranchise a larger user base.

Earthquakes are quite common across the United States with most activity focused within the western United States (WUS), Alaska, and Hawaii but with occasional earthquakes scattered across the central and eastern United States (CEUS). The seismic activity rates and ground-motion levels are thought to differ between the CEUS and WUS because of varying tectonic processes and distance to the plate margin, earthquake source and attenuation characteristics, and underlying geologic conditions. For example, CEUS earthquakes typically have larger stress drops and can be felt at larger distances than comparable sized WUS earthquakes due to differences in crustal properties (USGS, 2018). Disparities in earthquake faulting mechanisms (strike-slip, normal, or reverse motions) can also result in regional variability in ground-shaking levels. More than half of the United States (27 states) have experienced potentially damaging earthquakes of moment magnitude (M)5+ since 1900 according to the USGS Advanced National Seismic System Comprehensive Earthquake Catalog (USGS, Earthquake Hazards Program (ComCat), 2022; depicted as shaded regions in Figure 1). An additional 10 CEUS states have historical records of pre-1900 activity of M5+ earthquakes (e.g. depicted with hatched lines in Figure 1). Only 13 states have not experienced earthquakes above M5 in ComCat (depicted with lighter shading). Therefore, 37 of the 50 states (74%) have some past record of significant earthquake activity and face the potential of future damaging shaking. Understanding the historical and prehistoric earthquakes is important because these data are used to forecast locations, rates, and ground shaking of future earthquakes.

Figure 1 highlights several large or significant earthquakes that have occurred over the past few hundred years across the United States (described below). The largest US earthquakes are produced from plate convergence in subduction processes along the Pacific Northwest Cascadia subduction zone (M~9 1700 (offshore Washington, Oregon, California)) and Alaska-Aleutian Arc (M9.2 1964; M8.7 1965; M8.6 1946 and 1957; M8.3 1906; M8.2 1938 and 2021; and M8.0 1949, 1985, 1986, and 1995). Large damaging earthquakes are also produced along major plate boundary transform (strike-slip) faults spread mostly across California (M7.9 1857 (Fort Tejon); M6.8 1868 (Hayward); M7.4 1872 (Owen's Valley); M7.9 1906 (San Francisco); M6.9 1989 (Loma Prieta); M7.3 1992 (Landers); M7.1 1999 (Hector Mine); M7.2 2010 (El Mayor Cucapah, northern Baja, Mexico); M7.1 2019 (Ridgecrest)); and Alaska (M7.9 2002 (Denali)); reverse and strike-slip faults in California (M7.5 1952 (Kern County); M6.7 1994 (Northridge)); normal and strike-slip Basin and Range earthquakes (M6.9 1915 (Pleasant Valley, Nevada); M7.3 1932 (Cedar Mountain, Nevada); M7.3 1954 (Fairview Peak, Nevada); M6.9 1954 (Dixie Valley, Nevada); M7.2 1959 (Hebgen Lake, Montana); M6.9 1983 (Borah Peak, Idaho)); and along ancient re-activated tectonic margins in the CEUS, including three events near New Madrid, Missouri (M~7.3–8.0 1811–1812) and an earthquake near Charleston, South Carolina (M~7 1886). Geologic evidence of large prehistoric earthquakes has also been identified at sites across the United States, including large fault offsets and prehistoric evidence of damaging earthquakes along the San Andreas Fault, Cascadia subduction

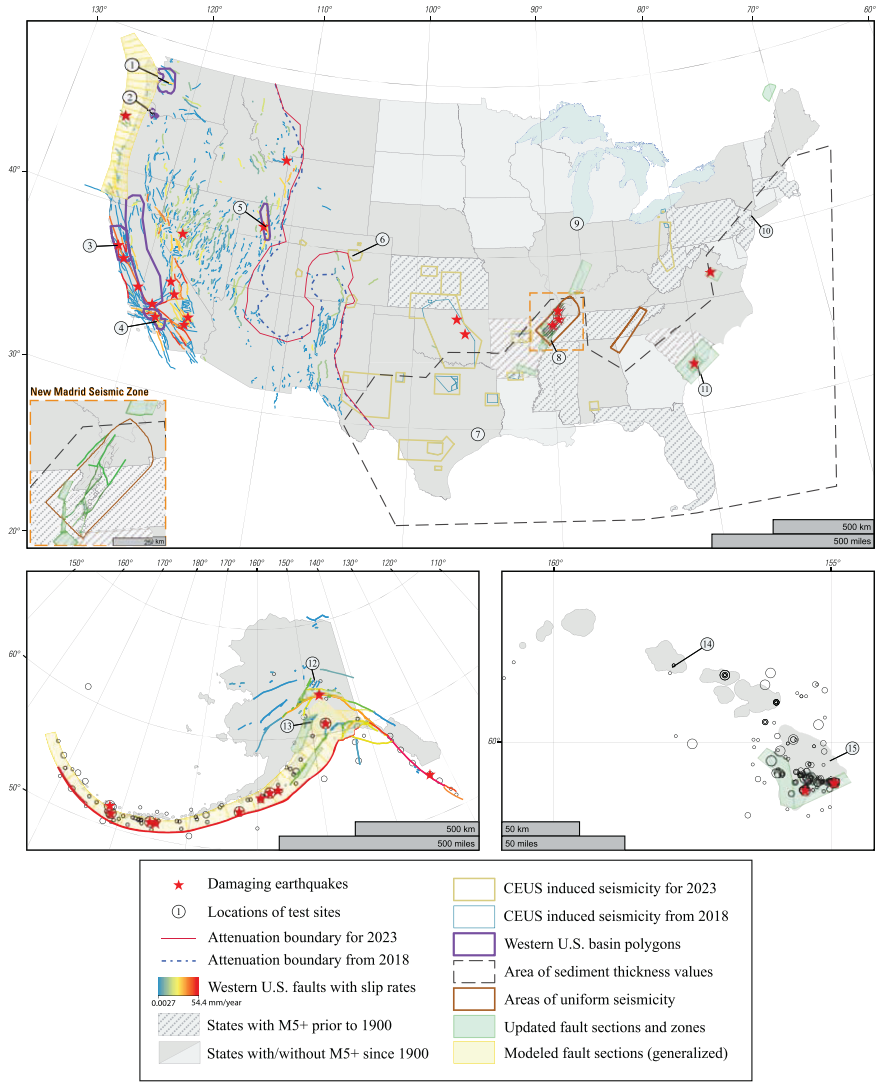


**Figure 1.** Maps show faults, zones applied in the CEUS, and zones of ground-motion model (GMM) amplification for the 2023 50-State National Seismic Hazard Model. The inset map is a close-up view of the New Madrid seismic zone area (orange dashed boundary). Spatial boundaries include potentially induced earthquakes for the update and the previous 2018 zones, 2023 central and eastern United States (CEUS)–western United States (WUS) attenuation boundary update and 2018 boundary, WUS basins, and two areas of uniform seismicity. Fault sections for the WUS (Hatem et al., 2022a, 2022b) and for Alaska from Bender et al. (2021) are shown colored according to slip rates. Fault sections in the CEUS are not shown according to slip rates but all slip rates are less than 0.2 mm/year. The Alaska megathrust is represented by 14 segmented zones. Damaging earthquake locations are shown in all three maps. In addition, we show seismicity for Alaska (M7+) and Hawaii (M5+) (Petersen et al., 2021; Rukstales et al., 2021). Fifteen sites chosen for sensitivity and scenario testing (including disaggregation and uncertainty for a subset of the test sites) are called out sequentially: (1) Seattle, Washington; (2) Portland, Oregon; (3) San Francisco and (4) Los Angeles, California; (5) Salt Lake City, Utah; (6) Denver, Colorado; (7) Houston, Texas; (8) Memphis, Tennessee; (9) Chicago, Illinois; (10) New York, New York; (11) Charleston, South Carolina; (12) Fairbanks and (13) Anchorage, Alaska; and (14) Honolulu and (15) Hilo, Hawaii (See Electronic_Supplement_2.pdf for a layered, interactive version of this file).

zone, Wasatch fault, Walker Lane, and Central Nevada seismic zone, as well as from liquefaction features dispersed across the central and northeastern parts of the country. The Island of Hawai'I has also experienced large, damaging volcanic and fault-based earthquakes (M7.9 1868; M7.7 1975; M6.9 2018). The US territories have experienced large and damaging earthquakes in Puerto Rico (M7.7 1943; M6.4 2020), near Guam (M7.8 1993), and a tsunamigenic earthquake affecting American Samoa (M8.1 2009).

Along with the large earthquakes on plate boundaries, many smaller- to moderately large-sized earthquakes ($3.0 \leqslant M < 7.0$) have ruptured along known or previously unidentified faults across the United States and can cause damaging levels of ground shaking over more limited areas. The maps and scale bar charts in Figure 2 show the locations and numbers of earthquakes of M3+ through time for four regions (CEUS, WUS, Alaska, Hawaii). Moderately large-sized earthquakes typically occur in regions that historically have been very active (e.g. WUS, Alaska), but they can also occur in places where earthquakes have not been common during the recent past (e.g. CEUS, 2011 M5.8 Mineral, Virginia; 1755 M~5.9 offshore of Cape Ann, Massachusetts; and WUS 2022 M5.7 Magna, Utah). Although CEUS moderate-size earthquake rates are typically lower than other places, this is not always the case and rates substantially increased over the past decade due to thousands of induced earthquakes triggered by industrial fluid injection of wastewater with a peak about 2015 (Figure 2). Such induced earthquakes can cause damaging ground motions (e.g. 2011 M5.3 Trinidad, Colorado; 2011 M5.7 Prague, Oklahoma; 2016 M5.8 Pawnee, Oklahoma earthquakes). The induced earthquakes are not included in these policy-based models because they are generally transient features of the seismicity, and mitigation actions can translate into rapid changes in earthquake rates. Instead, we supplement these NSHMs with short-term earthquake shaking forecasts that account for industrial injection and hydrofracturing based earthquakes (Petersen et al., 2015b, 2016a, 2016b, 2017, 2018). Short-term (1 year) model forecasts have not been made since 2018 but may be reconsidered if seismicity rates ramp up substantially again. Even though induced seismic activity has subsided in many areas over the past few years due to management efforts, seismicity remains higher than normal in Oklahoma, Kansas, and the Permian Basin of Texas (refer to Appendix B of Electronic_Supplement_1.pdf). WUS earthquakes continue with persistently high numbers that fluctuate in time due to aftershocks following large earthquakes. The Alaska seismicity reflects earthquakes on a major subduction interface along the Aleutian arc, deeper intraslab events in the subduction zone, shallow crustal fault events, and volcanic activity. Earthquakes in Alaska appear to increase with time (Figure 2), but this observation likely is an artifact caused by the increased number of deployed seismographs rather than being associated with any underlying physical changes. The numbers of earthquakes across Alaska are quite high compared to other regions. The Island of Hawai'i has recently had high earthquake counts, mostly due to recent volcanic eruptions of Kilauea and Mauna Loa. Figure 2 also shows the 2023 NSHM averaged gridded smoothed seismicity models for each of the 50 states along with M4+ earthquakes in the WUS, Alaska, and Hawaii and M2.7+ in the CEUS that are used to produce the seismicity models.

The USGS NSHM Project applies the new science on the potential locations, sizes, and rates of future earthquakes as well as the probable strength of ground motions and integrates this information into seismic hazard curves, ground-motion maps, and other supporting information. These hazard assessments are constructed using well-accepted time-independent probabilistic seismic hazard analysis (PSHA, Baker et al., 2021; Cornell, 1968) that allow for consideration of a broad range of alternative earthquake models

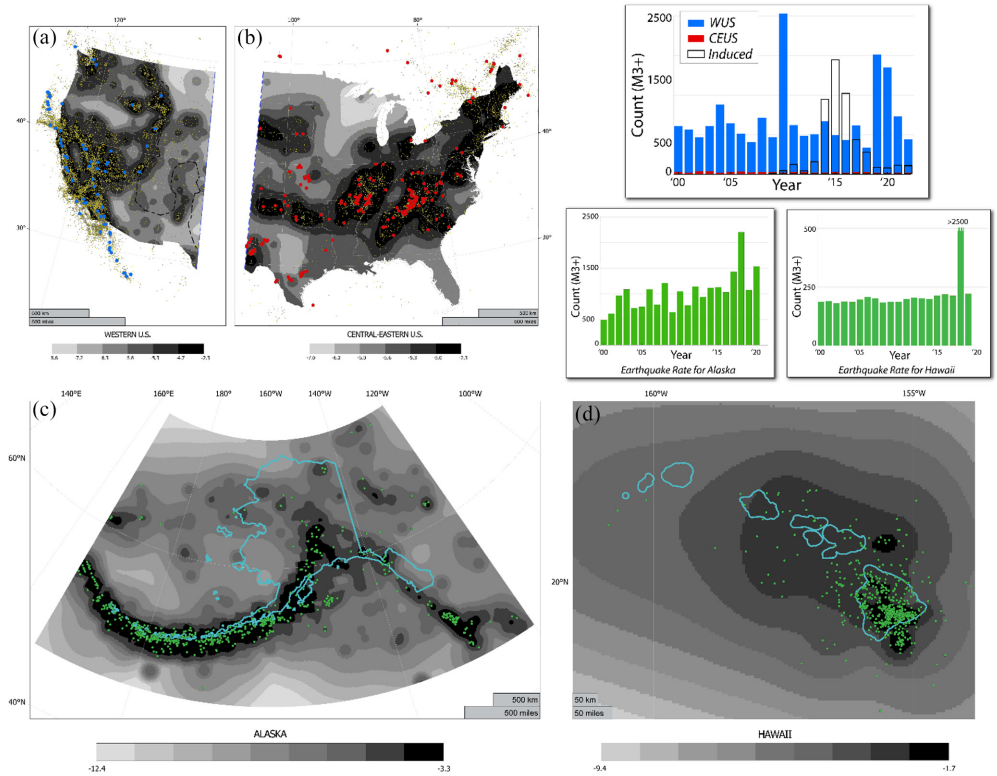


**Figure 2.** Normalized probability density function grids of seismicity-based earthquake rates (no fault models) are displayed for (a) the western United States (WUS), (b) the central and eastern United States (CEUS), (c) Alaska, and (d) Hawaii. For (a) and (b), values were weighted 0.4/0.4/0.2 across the three declustering methods (NN/GK/R85) and 0.4/0.6 for fixed/adaptive smoothing for conterminous United States and Alaska and 1.0 for adaptive smoothing Hawaii. Seismicity since May 2019 is shown for magnitude 4 and greater in the WUS (blue circles); magnitude 2.7 and greater in the CEUS (red circles); and the full catalog with yellow circles. The boundary between the eastern and western earthquake catalogs is shown as (a) and (b), respectively. The updated CEUS/WUS attenuation boundary is shown with a black dashed line. Averaged and normalized grids for Alaska (c) show the three layers (crustal, interface, and slab) based on equal weights across the three declustering methods with 100% adaptive smoothing. Seismicity since May 2019 with magnitude 4 and greater is shown as green circles. (d) Normalized and averaged grids of shallow seismicity for Hawaii show the nearest neighbor declustering with 100% adaptive smoothing for the three grid regions (northern, southern, and summit); magnitude 4 and greater events are shown as green circles. Inset plots of time-history represent counts of magnitude 3 and greater earthquakes in the WUS, CEUS, induced events, Alaska, and Hawaii seismicity. The CEUS/WUS/induced-seismicity time histories are superimposed with the same zero line and not stacked plots.

available in the science and engineering communities. Because aftershocks are not an independent Poisson process as assumed in the standard PSHA methodology (Cornell, 1968), the NSHM hazard values may not be appropriate for return periods much less than about 475 years in some applications (Field et al., 2023). This could be corrected with additional research on time-dependent spatially and temporally dependent earthquake cluster models (Field et al., 2021). Difficulties in understanding prehistoric earthquake data also make it challenging to forecast seismicity beyond about 10,000 years without extensive fault specific studies as implemented in siting of nuclear facilities or important dams. Therefore,

our PSHA estimates are best defined for return periods between about 475 and 10,000 years. Earth processes are naturally complex, and earthquakes are very difficult to forecast over short times, so our analyses here focus on long-term forecasts—50 years with probabilities of exceedance ranging from 2% to 10%.

The 2023 NSHM is based on a new earthquake rupture forecast (ERF) that describes the probabilistic locations, sizes, and rates of potential earthquakes and a ground-motion model (GMM), which defines probabilistic levels of ground shaking conditioned on an earthquake rupture and site characteristics. The ERF are described in detail by Field et al. (2023) for CONUS, this paper for Alaska, and Petersen et al. (2022) for Hawaii. The GMMs are described by Moschetti et al. (2023a) for an overview of CONUS, Rezaeian et al. (2023) for Cascadia subduction, this paper for Alaska, and Petersen et al. (2022) for Hawaii. This seismic hazard assessment considers several new ERFs and GMMs that have been developed since the previous NSHM update:

1. Seismicity-based earthquake grids are founded on new earthquake catalogs compiled with alternative new declustering algorithms, induced-seismicity identifications for CEUS, and gridded (smoothed) seismicity assessments (Field et al., 2023; Petersen et al., 2022; this paper for Alaska). The 2023 model considers full-catalog rates (as recommended by the ERF panel) with spatially smoothed seismicity kernels from declustered catalogs, rather than only using the declustered catalogs as in previous NSHMs.
2. Fault-based deformation models include new geologic (Hatem et al., 2022a, 2022b) and joint geologic and geodetic inversions (Pollitz et al., 2022; this paper for Alaska).
3. New magnitude-scaling equations provide estimates of sizes of earthquakes for shallow crustal, deep crustal, subduction, and stable continental environments (Shaw, 2023).
4. A new inversion-based methodology for inclusion of multi-fault ruptures, including a wider range of epistemic uncertainties, was applied across the WUS region (Milner and Field, 2023). New traditional (classic) rate models were developed for the CEUS (Shumway et al., 2023), Alaska (this paper), and Hawaii (Petersen et al., 2022).
5. New semi-empirical Next Generation Attenuation (NGA)-Subduction GMMs are implemented for pseudo-spectral accelerations (SAs) and peak parameters (Bozorgnia et al., 2022; Rezaeian et al., 2023). New region adjusted coefficients were implemented for Alaska.
6. New CEUS adjusted revisions to the stable continental GMMs (Moschetti et al., 2023a) are also implemented.
7. New three-dimensional (3D) ground-motion simulations for the Seattle and Los Angeles regions are considered in assessing ground motions from earthquake ruptures that have not been instrumentally recorded (Frankel et al., 2018; Moschetti et al., 2023a; Wirth et al., 2018a).
8. Basin-depth amplification models based on NGA-West2 are constructed and applied for the San Francisco Bay Area, Los Angeles, Great Valley of California, and Portland/Tualatin regions (Ahdi et al., 2023; Moschetti et al., 2023a).
9. New amplification models are constructed and implemented for the Atlantic and Gulf Coastal Plains that account for sediment thickness (Boyd et al., 2023).
10. New CEUS-WUS boundaries are developed and applied for earthquake catalogs, fault models, and GMMs.

The component models and overall hazard model updates were reviewed by several expert panels, together consisting of more than 50 scientists and engineers.[1] These expert panels deemed the new components to be reasonable for inclusion in the 2023 NSHM, and furthermore that they account for a more complete range of uncertainty than previous seismic hazard models (ERF review—Jordan et al., 2023, GMM review—Electronic Supplement of Moschetti et al., 2023a, NSHM Steering Committee review—Electronic_Supplement_1.pdf, Appendix H). The NSHM Steering Committee (NSHM-SC), which oversaw the review process, was requested to provide feedback on (1) whether the model was adequately reviewed, (2) whether the USGS response appropriately addressed the review comments and recommendations, and (3) whether the model is suitable for release and to serve as the basis for hazard mitigation. It was the consensus of the NSHM-SC that the level of technical review for the conterminous US, Alaska, and State of Hawaii were adequate, that the USGS responded acceptably to most panel comments and recommendations, and that the models are suitable for use in building code and similar applications at return periods of 475 years and longer. The NSHM-SC and the Alaska Review Panel reviewed the ERF and GMMs for Alaska and found them to be suitable for use in policy applications, subject to additional documentation and verification (Electronic_Supplement_1.pdf, Appendix H).

An example 2023 seismic hazard map developed as part of this study is shown in Figure 3 that is based on Modified Mercalli Intensity (MMI, a macroseismic measure of earthquake effects and damage that describes the strength of earthquake shaking inferred from intensity observations). The probabilistic seismic hazard and risk is quite variable across the United States. Earthquake hazard is high along West Coast population centers due to potential of earthquakes associated with the Cascadia subduction zone and San Andreas Fault System, across the densely populated Wasatch Front and up through the Teton Range/Yellowstone region, within the Walker Lane and central Nevada seismic belt, near the New Madrid seismic zone (NMSZ) and Charleston seismic zone, Aleutian Island chain of southern Alaska, and across the southern Island of Hawai'i. Moderately high hazard and risk is found across many of the WUS states, and areas of pre-existing faulting across the CEUS, central Alaska, and central islands of the Hawaiian chain. Lower hazard and numbers of earthquakes are observed across northern and central portions of the Midwest and southern regions of the country as well as in the northern portion of Alaska and farthest northwest islands of Hawaii. Nevertheless 26 states have moderate to higher probabilities of shaking - 25 percent or reater chance of experiencing damaging shaking (MMI VI+) in 100 years (Figure 3).

One of the greatest challenges in constructing this 2023 NSHM has been to evaluate and then implement only the best available or applicable science into the policy model. Best available science is defined as including well-vetted and published hazard input component models with adequately documented assumptions, is consistent with open and timely science principles, encompasses a scientifically reasonable range of earthquake ruptures and ground-motion effects that improve the basis of the 2023 NSHM, assesses variability and uncertainties in such information, and ensures that the end-product is reasonable for and consistent with the intended purposes (e.g. Title 40 CFR § 702.33). The ERF review panel suggests the following elements need to be included as part of the best available/applicable science: relevance, inclusiveness, objectivity, transparency and openness, timeliness, and peer review; in their report, objectivity is replaced with verification and validation (Jordan et al., 2023). Best science evaluations require each of these science-based criteria and include well-vetted and published hazard information and models that are accepted through a comprehensive review process and encompass a reasonable

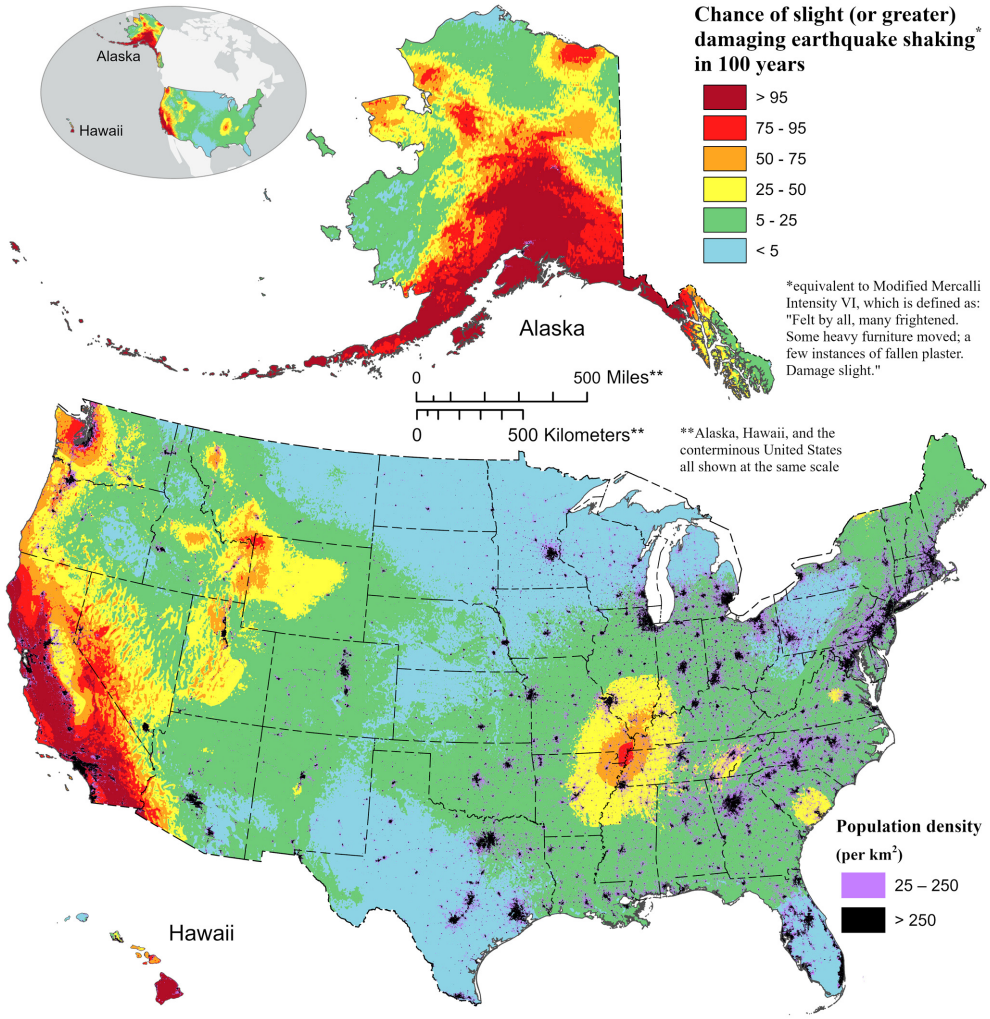


**Figure 3.** Map showing the chance of any level of damaging earthquake shaking in 100 years from the 2023 50-State National Seismic Hazard Model. The shaking is equivalent to Modified Mercalli Intensity VI and higher and is based on the average peak ground acceleration and 1-s horizontal spectral response acceleration (using Worden et al., 2012 model without uncertainty). Ground motions are amplified using hybrid $V_{S30}$ estimates (Heath et al., 2020). Population density (LandScan, Dobson et al. (2000) with 1 km×1 km resolution from Oak Ridge National Laboratory) is superimposed on the map.

scientific range of earthquake characteristics and effects for updating the 2023 NSHM. This version of the NSHM is meant for seismic policy applications, and we attempt to adhere to the definitions given above for best applicable science. In terms of peer review, openness, transparency, inclusiveness, and objectivity, the NSHM input models included in this update are evaluated with a thorough (over 50 reviewers), open (dozens of public workshops and a public comment period), and transparent review process (tools, data, and documentation available on NSHM Project website). In addition, the model incorporates comprehensive and defensible representations of epistemic uncertainty (lack of

knowledge that is reducible through additional studies) and aleatory variability (intrinsic randomness in the earthquake process). Through scientific studies, we can sometimes convert apparent variability into epistemic uncertainty (e.g. consideration of non-ergodic GMMs). We plan to follow this policy-based study with research and development models that explore additional input parameters and models that were not considered in previous NSHMs so that end-users can evaluate impacts and explore implementation issues (refer to section "Discussion").

To confirm the models are based on the current best science, that the results are reasonable, and the products are useful, the resulting NSHM outputs were tested using historical intensity data, evaluated based on published inclusion criteria (Rezaeian et al., 2015), and appraised extensively by the science and engineering communities through more than 25 public workshops and the publication process. The draft model was available in written form and in a public workshop for comment by any interested person during an open-review period in April and May 2023. The model was examined and evaluated by hundreds of earthquake science and hazard experts who participated in regional and topical workshops and members of several review committees (see Note 1) who analyzed details of component models. The NSHM research strategies have benefited extensively from direct involvement of the NSHM-SC, consisting of nine renowned seismic hazard experts—who review inputs and outputs of models, recommend model improvements, promote comprehensive uncertainty assessments and testing of the model, and advocate for improved science directions.[1] Reviews by the ERF review panel (Jordan et al., 2023), GMM review panel (Moschetti et al., 2023a Electronic Supplement), Alaska review panel (Appendix G of Electronic_Supplement_1.pdf), Tiger Team (also known as the GMM advisory panel; Appendix F of Electronic_Supplement_1.pdf), Hawaii review panel (Petersen et al., 2022), and NSHM-SC (Appendix H of Electronic_Supplement_1.pdf) are available for the public's consideration.

In terms of timeliness for consideration of input components for the 2023 NSHM, any ERF and GMM models published before 31 December 2020, deadline were given full consideration for inclusion in the model. Information that became available after this date may or may not have been considered for model development. NSHM Project scientists, in consultation with the NSHM-SC, exercised their discretion and judgment regarding utilization of recent results, and do so when justified in terms of the result's scientific credibility and significance to hazard. Concerns and objections were expressed by some reviewers dealing with the following issues: inclusion of input models that came in late, lack of adequate documentation during the review process, lack of adequate time for review, and desire for more discussion of review comments that were not accepted. These objections and the possibility that the model may be premature in some regions were considered by the review panels and NSHM project members. In those cases, we followed the consensus (but not unanimity) of the review panels and project members in making these decisions of whether to include models or not. USGS personnel had to make difficult decisions about which review comments were feasible for implementation and did not conflict with other guiding principles of the model development (e.g. weighting and epistemic uncertainty considerations).

This overview paper is written for a variety of audiences, and the scope is broader than in many papers. The introduction and overview of methodology sections were written for the informed scientists/engineers who may be interested in why we calculate seismic hazard, where damaging earthquakes occur, the types of data that are used to assess hazard, the intensity measures of hazard, and a description of how we can use these hazard

maps and mitigate the effects of future events. The ERF and GMM sections are technical and written for scientists and engineers who want to understand the breadth of issues with input models—pointing to other companion papers for details, how models are derived and evaluated, and the basis for weighting models. The results section is written for the users of 2023 NSHM with descriptions of where, why, and how much the hazard has changed compared to the previous NSHM versions. The discussion section describes hazard issues that the project members, review committees, and other scientists debated including the evaluation of best available science for each input model type as well as the associated epistemic uncertainty and aleatory variability, descriptions of the input component model sensitivities and uncertainty assessments, and description of policy as well as research and development models that can be considered for various engineering purposes. The references are extensive and may be useful for anyone needing more detailed information than that provided in this overview article.

## Overview of model components and integration into the NSHM

The highest hazard areas in the 2023 NSHM are concentrated in places where large damaging earthquakes have or are thought to have occurred in historic and prehistoric times as discerned through earthquake records, historical intensity recordings, and geologic and geodetic fault studies. Nevertheless, damaging earthquakes can also occur in places where they have not been observed in the recent past. For assessing the probabilistic hazard, we develop an ERF (Field et al., 2023) that specifies the probabilistic locations, sizes, and rates of future earthquakes, and a GMM (Moschetti et al., 2023a; Rezaeian et al., 2023) that specifies the probabilistic ground-motion distributions resulting from earthquakes of various sizes, distances, alternative rupture mechanisms, and site conditions. Both inputs control the shaking levels for pseudo-SAs for multiple oscillator periods, peak acceleration and velocity, and alternative site classes at hundreds of thousands of sites across the 50 states. In developing the forecast, we try to (1) ensure that input data are properly processed and robust for the purpose of policy hazard applications, especially in urban areas; (2) work with internal and external USGS partners to build probabilistic ERF and GMM input component models that consider available data, physics-based constraints, empirical-based regressions, computer simulations, and to ensure that models are consistent with known physics principles in extrapolating models into regions with poor data availability; (3) incorporate new input data, models, and methods through interaction with our NSHM-SC and an extensive review process; (4) ensure that NSHM captures the breadth of epistemic uncertainty and by assigning justifiable weights based on data, model residual analysis, and expert judgment; and (5) develop robust, reasonable, and useful seismic hazard models describing the expected frequency of exceeding a set of ground-motion thresholds.

To understand the spatial and size distributions of past earthquakes, we develop an earthquake catalog that lists 66,272 events M2.7–7.9 from 1568 to 2022 for CONUS, 36,878 events M3.5–9.2 from 1882 to 2020 for Alaska, and 32,782 events M2.5–7.9 from 1790 to 2019 for Hawaii (Figure 2). We remove suspected induced, mining, and other manmade earthquakes from the CEUS catalogs that occur within time periods of known earthquake inducing industrial activity and within spatially defined zones where known injection or other earthquake stimulating activities occurred (Field et al., 2023). The forecasted earthquake rates are assumed to follow a Gutenberg–Richter (GR; Gutenberg and Richter, 1944) exponential magnitude-frequency distribution (MFD) that is observed globally with *b*-values (slope of the MFD) that are considered based on regional earthquake

observations. The distribution is truncated at a maximum magnitude (Mmax) based on sizes of historic earthquakes, physics-based considerations, or global analogs. Typically, this Mmax is set to be close to M8 for background earthquakes, which is higher than in early NSHMs and more consistent with global earthquakes in various tectonic settings. Larger earthquakes can also occur on known faults included in the model. The minimum magnitude where we begin integration of the ground-motion contributions is still set at the standard M5 even though we recognize that M4+ earthquakes can cause damaging shaking at nearby locations (we may consider revisions in the future). The gridded seismicity model accounts for moderate- or large-sized earthquakes along faults and in places where fault sources are unrecognized. We apply several declustering methods, some of which are applied for the first time in the 2023 NSHM. This model assumes that future large earthquakes will occur where past seismicity is concentrated. We develop a grid of earthquake rates over a regular interval of points with 6 km spacing. Smoothing grids are shown in Figure 2 and are based on smoothing the declustered earthquake catalogs and then scaling the seismicity rates at each grid point to be consistent with the full rate of earthquakes $M \geqslant 5.0$ for WUS and $M \geqslant 4.7$ for CEUS. This model is more effective for forecasting future earthquakes in places of high seismic areas where past seismic activity is concentrated but is less effective where seismicity is low. We also apply broad zones to account for a base level of seismicity across a wide area where seismicity is low but cannot be ruled out.

We consider geologic fault studies to assess the fault structure and seismicity rates for faults with geologically recent (late Quaternary or Holocene) activity. The ERF accounts for potential locations, rates, and sizes of future earthquakes on mapped faults (Field et al., 2023). Figure 1 shows locations of faults included in the model (Hatem et al., 2022a, 2022b). The new WUS fault database contains about 1000 fault sections and slip rates based on both geologic and geodetic interpretations, an increase of about 350 faults compared to the previous NSHM for CONUS. This fault assessment was coordinated with state geological surveys that have parallel and intersecting responsibilities for earthquake safety. Deformation models were constructed using geologic and geodetic deformation data and joint geologic and geodetic inversion models (Hatem et al., 2022a, 2022b; Petersen et al., 2013; Pollitz et al., 2022). We assess earthquake sizes by analyzing magnitude-scaling equations that consider a collection of data showing moment magnitudes as a function of empirical rupture areas and physics-based energy constraints (Shaw, 2023). The resulting fault geometry and slip rates, earthquake magnitudes, and several other filters, constraints, and modeling components are used to develop a broad range of earthquake rate models, which include multi-segment or multi-fault ruptures that are similar to complex ruptures observed globally. These models span from the classic model that is similar to prescriptive models that account for historical and prehistoric ruptures and were applied in most previous NSHMs, to the inversion-based fault-system solutions that apply generalized simulated annealing inversions initially developed for California (Field et al., 2009, 2013) and extended to ruptures across the WUS that account for a broad range of multi-fault ruptures (Milner et al., 2022). We account for alternative ERFs to populate logic trees that are applied for capturing and incorporating uncertainty into the probabilistic NSHM ground motions.

Semi-empirical GMMs account for probabilistic distributions of shaking levels using ground-motion recordings from past earthquakes, 3D numerical ground-motion simulations of large earthquakes, and amplification models that are conditioned on the characteristics of the rock/soils beneath the site (e.g. $V_{S30}$ is the time-averaged velocity in the

upper 30 m, $Z_{1.0}$ is the depth to the 1.0 km/s shear-wave velocity, and $Z_{2.5}$ is the depth to the 2.5 km/s shear-wave velocity horizon). The 2023 NSHM uses semi-empirical GMMs including new NGA-Subduction models, 3D simulations for Seattle and Los Angeles, sedimentary thickness-based amplification models for the CEUS (Gulf and Atlantic Coastal Plains) and WUS (Seattle, Portland/Tualatin, San Francisco/California Great Valley, Los Angeles), and a revised CEUS-WUS attenuation boundary. Details of these models, implementations, and sensitivity studies are found in Rezaeian et al. (2023) for subduction zone GMMs, and in Moschetti et al. (2023a) for the remaining GMMs in the WUS and CEUS. We examined the distribution of implemented GMMs to ensure that the models are encompassing a reasonable level of epistemic uncertainty (higher in the CEUS and Hawaii where data are sparser than in the WUS and Alaska) and we also add additional epistemic uncertainty to account for earthquakes that may occur outside of the empirical databases applied in developing the GMMs. Some reviewers felt that the additional epistemic uncertainty and its application in the calculations need further refinement. These requests came late in the process and there are also applications in San Francisco and Los Angeles that show the importance of including these "unknown unknown" contributions (refer to Appendix B of Electronic_Supplement_1.pdf). Moschetti et al. (2023a) provide details on sediment-thickness- and seismic-velocity-based amplification models and 3D numerical simulations of large ruptures. Details of GMMs for Alaska and Hawaii NSHMs are provided in Appendix D of Electronic_Supplement_1.pdf and Petersen et al. (2022), respectively. Selected GMMs for all regions and their assigned weights are summarized in Table SA-4 of Electronic_Supplement_1.pdf and are based on the revised GMM selection criteria published in Rezaeian et al. (2021).

The weight assignments, as in previous cycles of the NSHMs, are based on a consensus building process that involves consideration of expert judgment, published selection criteria (e.g. Petersen et al., 2014; Rezaeian et al., 2015, 2021, 2023), data residual analyses (e.g. McNamara et al., 2020), and a thorough review of between-model dispersion as well as important characteristics and limitations. This process requires extensive analysis for both ERF and GMM components in developing scientific-based weighting schemes. In the past, we have applied a three-point distribution with weights 0.185, 0.63, and 0.185 representing the 95% confidence levels for ERF and GMM models, and sometimes, these were applied as one instead of two standard deviations in previous NSHMs. However, these branches do not represent commonly used percentiles of a normal distribution, and we currently apply these weights to $\mu - 1\sigma$, $\mu$, and $\mu + 1\sigma$ instead (Keefer and Bodily, 1983). We generally assign equal weights to models if we do not identify advantages to a specific model or significantly better fits with data. When input component models have advantages over other considered models, we typically assign ratio weights (e.g. 1/3–2/3, 1/4–3/4) or percentage-based weights (e.g. 20%–80%) reflecting preferences of the project members, NSHM-SC, review panels, and the informed community on the best science. It is important to recognize that outliers can significantly modify the mean of a distribution, especially toward the high end (Field et al., 2023). We try to include the best input component models that are justified by science-based principles; however, we sometimes down-weight newer or less studied models. In addition, we include models that are valuable to illuminate and broaden the range of epistemic uncertainty because the principal objective is to capture the true range of epistemic uncertainty (e.g. deformation models, Coastal Plain amplification models). Additional epistemic uncertainty has been added to the GMMs in the WUS because in some cases the range of uncertainty is artificially low for certain periods and the models are developed together in a consensus fashion using similar data sets and commonly agreed on methods. We sometimes classify alternative models by class or individual modeler and then

assign weights to different suites of models based on expert judgment as in CEUS GMMs. We apply backbone models or more complicated models such as the Sammons mapping applied in NGA-East (Goulet et al., 2021a) for which a mean/median model is applied with a range of epistemic uncertainty models that is deemed reasonable by the science community (e.g. Atkinson et al., 2014). We retire older models as they are updated, proposed for exclusion by modelers, recognized as having deficiencies, or considered to be encompassed in the range of models already considered in the updated model. Occasionally, we phase out older models over multiple update cycles instead of eliminating them in one cycle when they are still viable but utilize less information compared to the newer equations. Below we provide an overview of the science input models described in detail for ERF (Field et al., 2023) and the GMM (Moschetti et al., 2023a; Rezaeian et al., 2023).

It is difficult to separate epistemic uncertainties from aleatory variability (especially for GMMs) but is necessary for development of hazard fractiles (Marzocchi and Jordan, 2018). For this analysis, we assess the center, the body, and the range of ground motions included in the NSHM to define a representative suite of models that capture the epistemic uncertainty. We spent a great deal of effort evaluating residuals from input data and models using various performance metrics to assess the best science data, methods, and weighting for models (e.g. McNamara et al., 2020). Inclusion of many additional proponent models in the hazard assessment does not necessarily capture a reasonable range of epistemic uncertainty, so we have also put an emphasis on assessing the scientifically defensible range of epistemic uncertainty that is consistent with available data, tectonic regime considerations, and other specific conditions (Atkinson et al., 2014). Where needed we have added additional epistemic uncertainty to account for a scientifically reasonable range of uncertainty that is dependent on the amount and distribution of data (empirical and synthetic), span of available models, physical understanding of the earthquake process, and assessment of variability in epistemic uncertainty that considers global analogs. For portfolio applications, one would need to consider the spatial correlations in the epistemic uncertainties (standard deviation) to avoid overestimating the risk.

For this update, we evaluated epistemic uncertainties in the ground-motion hazard for 2% and 10% probabilities of exceedance in a 50-year hazard level using a logic-tree approach, which sweeps through alternative weighted ERF and GMM epistemic inputs (weighted branches) to discern fractiles of potential ground motions at a handful of representative sites (Anchorage, Alaska; Honolulu, Hawaii; Los Angeles, California; New York City, New York; Salt Lake City, Utah; San Francisco, California). The formation of a logic tree ideally spans the mutually exclusive and completely exhaustive set of possibilities or logic-tree branches. However, sometimes this assessment of available models does not satisfy the wide uncertainties allowed by science-based principles and global observations (Atkinson et al., 2014). We evaluated full uncertainties at six sites and partial ERF uncertainties at dozens of sites but would have preferred to make these uncertainty assessments at all grid sites across the country. During our assessment, we realized that more effort is required to separate the aleatory and epistemic components, improve the computing facilities, and understand the correlations as described in the sections on uncertainties and discussion below.

## ERF models and weights

Details of the input models and forecasts for CONUS, Alaska, and Hawaii are described in Field et al. (2023), this paper for Alaska, and Petersen et al. (2022), respectively. In this

section, we discuss model issues, sensitivity, weighting schemes, and hazard results. The input ERF component models include the following: the earthquake catalog, declustering models, spatial smoothing applications, fault and deformation models (geologic and geodetic), magnitude-scaling equations, Mmax assessments, and earthquake rate models for all 50 states.

An ERF, also referred to as a seismic source characterization in some studies, gives a complete list of potentially damaging fault ruptures in a region and over a specified timespan (or suites of synthetic earthquake catalogs, especially for fully time-dependent models). This section summarizes the time-independent ERFs developed for the 2023 NSHM, restricting attention here to changes that are new and innovative and consequential with respect to implied hazard. The ERFs presented here represent updates to those utilized in the 2018 NSHM for CONUS (Petersen et al., 2020), which largely utilized unmodified ERF components from the 2014 NSHM for CONUS (Petersen et al., 2014, 2015a).

Several broader goals with respect to ERF developments are described by Field et al. (2023) including (1) a more comprehensive representation of epistemic uncertainties; (2) increased uniformity in model assumptions and methodologies across regions (involving de-regionalization of model component developments); (3) simplification wherever it can be achieved without degrading model usefulness; (4) more operationalization of model component creation; (5) model extensibility with respect to adding time dependencies (including spatiotemporal clustering, swarms, and induced seismicity); (6) utilizing more physics to make up for sparse data at larger magnitudes; and (7) providing more complete documentation to minimize the need to comb through previous publications when learning about or reproducing models. All these goals are aimed at improving the rate and efficiency with which future model improvements can be rolled out nationwide.

ERF development is a system-level problem that uses constraints from a broad range of disciplines (e.g. earthquake geology, tectonic geodesy, statistical seismology, and earthquake physics). As such, a modular design is critical to managing workflows and to enable different groups of scientists to focus within their respective areas of expertise. Field et al. (2023) summarize the various components presently defined and utilized, including (1) fault models, defining physical attributes of explicitly modeled faults; (2) deformation models, specifying fault slip rates as constrained by geology and assessing the influence of each fault and in some cases "off-fault" deformation rates; (3) earthquake rate models, specifying the long-term rate of each earthquake rupture; and (4) probability models, which specify conditional probabilities based on elastic rebound, spatiotemporal clustering, swarms, and induced events. Given the general time-independent nature of NSHMs, the main topic here is the earthquake rate models, which generally (with exceptions) get applied using Poisson probabilities. This 2023 US NSHM ERF was constructed at the same time as update efforts in New Zealand, and although the two models are quite distinct from one another in methodologies and goals, many of the concepts were discussed together (Gerstenberger et al., 2023).

Each earthquake rate model is composed of two types of earthquake sources, which are generally categorized as fault-based (i.e. explicitly modeled faults) versus "off-fault" or "gridded" seismicity, with measures often being taken to avoid double counting between these two. It is important to clarify that off-fault earthquakes as described above still occur on fault sources, but they are on uncharacterized faults that have not been detected or studied sufficiently for inclusion in this model. It is difficult to define potential ruptures in areas between known faults where future ruptures could occur as fresh ruptures or

subsidiary fault ruptures. Fault-based sources are also distinguished by (1) "Classic" fault models, generally applied to individual faults and with prescribed attributes (e.g. the shape of the MFD); (2) fault-zone sources where a distinct fault surface is not identifiable (also applied with prescribed attributes); and (3) fault-system solutions, which are aimed at acknowledging and including many plausible multi-fault ruptures. The latter are generally inversion based, as described below for WUS, but were also derived from multi-cycle physics-based simulators (Milner et al., 2022). We start with the CONUS region because it embodies all types of components, and then follow with differences and exceptions reflected in the Hawaii and Alaska ERFs. Each section also discusses epistemic uncertainty representation, treatment of aftershocks, and the review process.

## *CONUS ERFs*

The most consequential updates for the CONUS ERF are the addition of faults, new slip-rate constraints, changes in gridded seismicity components, and the inclusion of multi-fault ruptures in the WUS outside California. The innovation in the fault and deformation models is to allow for multi-fault ruptures, which have been observed in several recent large earthquakes in California, Mexico, New Zealand, and Turkey. We also expanded the representation of epistemic uncertainties for most components, and we were able to conduct extensive branch sensitivity studies with respect to WUS hazard. Epistemic uncertainties for the Cascadia subduction zone were based on several workshops prior to the 2014 NSHM update and on an extensive logic tree that included many alternative input component models. Epistemic uncertainties for the CEUS fault sources are based on extensive logic trees developed by the US Nuclear Regulatory Commission (CEUS–SSCn) (2012) project. The model update relied on several component developments, including those represented in the publications listed in Table 1 of Field et al. (2023).

*Fault and deformation models.* Fault model and geologic constraint updates for the WUS were compiled by Hatem et al. (2022a, 2022b), with about 350 new faults being added (mostly outside California), which were previously excluded due to lack of site-specific geologic slip-rate constraints. Hatem et al. (2022a, 2022b) also compiled geologic slip-rate estimates at points where site-specific studies are available, and applied default categorical estimates for the faults that lack such explicit constraints. Some of the fault ruptures had narrow faults when considering fault creep. The ERF review panel discussed this issue but felt that the narrow faults were reasonable for inclusion in the 2023 NSHM.

The five WUS deformation models utilized in the 2023 NSHM are described in a special issue of Seismological Research Letters (e.g. refer to the overview paper by Pollitz et al. (2022)). Again, the main inferences from these models are slip-rate estimates for each fault section in the WUS Fault Model. One model is based almost entirely on geologic constraints (Hatem et al., 2022a), whereas the four others also utilize Global Positioning System (GPS) or geodetic constraints that were updated by Zeng (2022b). Two of these models represent updates to those utilized in the 2018 NSHM (Zeng (2022a) and Shen and Bird (2022)), both of which generally honor the geologic constraints unless GPS data strongly indicate otherwise. The other two models are new: one from Pollitz (2022) and another from Evans (2022) that effectively permit wider excursions from geologic values than the older models by relaxing geologic constraints and allowing for more freedom to follow the geodetic data. Further enhancements include corrections for potential viscoelastic effects (the "ghost transients" described by Hearn (2022)), and much more thorough

inferences and corrections for fault creep processes (Johnson et al., 2022). Because the models have considerable dispersion between one another, it is important to point out that consideration of all these models can lead to substantial effects on the uncertainty assessments and can be important considerations for certain classes of end-users. These inter-model deformation differences are also important in assessing off-fault slip rates and their associated uncertainties.

Given the complexity and importance of these models, a special review team (Deformation Review Panel for CONUS chaired by Kaj Johnson (see Note 1)) was convened to advise on the reliability of each modeling approach (and to suggest logic-tree branch weights). This analysis involved scoring each model based on 15 different metrics. The review panel recommended relatively low branch weights for the two new models, Pollitz (2022) and Evans (2022), due mostly to their having more anomalous slip rates, but also emphasized that these models are nevertheless viable and allow the model to capture a broad range of epistemic uncertainty. However, and as discussed in Field et al. (2023), initial hazard calculations revealed that some slip-rate outliers were having a disproportionate and concerning effect on mean hazard. We use the results of the Deformation Review Panel for CONUS as input into our deliberations on weighting of the deformation models and generally follow these recommendations but modify them based on further considerations by the ERF Review Panel and others: Geologic 26%, Zeng 32%, Shen and Bird 32%, Pollitz 8%, and Evans 2% shown in Table SA-1. As noted below, further deformation-model development is one of our highest priorities with respect to planned future work, especially with respect to better quantification of slip-rate uncertainties and covariance between faults. Another priority research topic is the off-fault deformation estimates provided by some of these models, which were deemed too immature for application (e.g. as a gridded seismicity constraint) at this time.

The fault model and geologic constraints for the CEUS were updated by Thompson Jobe et al. (2022a, 2022b), including the addition of five new faults (Central Virginia, Saline River, Joiner Ridge, Crowley's Ridge (South), and Crowley's Ridge (West)). They also made fault-geometry adjustments to four previously utilized faults (Axial, Bootheel, New Madrid West, and Reelfoot), and added explicit surfaces to five faults previously represented with zones (Commerce, Eastern Margin (North), Eastern Margin (South), Crittenden County, and Meeman-Shelby, the latter of which was previously called River Picks). They also summarize the slip rate or paleo event-rate constraints available for each fault, with the latter typically involving some number of paleoliquefaction events inferred over some period. No WUS-style deformation models were developed for CEUS faults, owing mostly to the lack of deformation rate constraints.

### *Earthquake rate models*

*WUS fault-system solutions.* The biggest innovation with respect to earthquake rate models is the inclusion of multi-fault ruptures throughout the WUS, made possible by a new inversion-based fault-system solution developed by Milner and Field (2023). This builds of the so-called "grand inversion" approach used in the Uniform California Earthquake Rupture Forecast version 3 (UCERF3; Field et al., 2014; Page et al., 2014), but with important improvements with respect to computational efficiency, better control with respect to fitting various data constraints, an expanded set of diagnostics and model-evaluation plots, and better reproducibility (our intent is to enable anyone to conduct such calculations themselves). Perhaps most importantly, we added variable segmentation constraints, enabling us to define a much wider range of models with respect to multi-fault

ruptures. Specifically, we have a "Classic" segmentation branch that is consistent with previous UCERF1 and UCERF2 (Field et al., 2009; Petersen et al., 2007) and other models outside California (where extensive multi-fault ruptures are prohibited), three branches that apply a range of jump-distance–based penalties, and an unsegmented branch that applies no penalty for jumps up to 15 km (UCERF3 had one branch that applied no penalty for jumps up to 5 km, Field et al., 2023). Note that the extreme branches are partially a proxy for the fault model being incorrect with respect to the actual distance between faults (i.e. the classic branch might be most appropriate where jump distances are much larger than implied by the fault model, or the unsegmented branch might be appropriate where an unknown connector fault exists). After considerable deliberations, the classic model and unsegmented branch models were each given lower weight (10%) compared to the other fault segmentation models (low 20%, medium 30%, and high 30%). These weights were based on recommendations from the ERF Review Panel and observations that the classic model has a magnitude–frequency curve bulge and assumes that faults cannot rupture together more than that observed in the geologic data. The classic model does not generally allow ruptures that extend beyond geologic observations and results in shorter ruptures, smaller magnitudes, and shorter recurrence times compared to the longer ruptures, larger magnitudes, and longer recurrence times associated with the three multi-fault rupture models that allow various ranges of rupture jumps. Therefore, the classic model typically has larger ground-motion hazard than the multi-fault rupture models.

Another improvement is the ability to map out a wider range of models via a supra-seismogenic *b*-value constraint (defined further below), which sets the slope of a GR density distribution (not cumulative distribution) at large magnitudes. In UCERF3 (Field et al., 2014), inversion solutions were constrained to stay as close as possible to the previous model (UCERF2, Field et al., 2009), which might have been justifiable from a policy perspective (do not change the model any more than needed to fit the data), but this limited the range of models considered. In other words, a wider range of models may fit the data equally well, which represents epistemic uncertainty that warrants being accounted for. The supra-seismogenic *b*-value constraint is our way of doing this, with five discrete branches between values of 0.0 and 1.0, which is effectively a way of adjusting the total rate of events on each fault section; in fact, we do not constrain the entire implied MFD on each fault section in the inversion, but rather we constrain this implied total rate. We do, however, sum the fault-section MFDs to also provide a total regional MFD constraint in the inversion, which likely is an improvement over how the total fault MFD target was defined in UCERF3 and provides a path to check the model against historical data.

This inversion approach starts with the fault model and applies a new plausibility filter (Milner et al., 2022) to define the ruptures that have a non-zero likelihood of occurrence (to reduce an effective infinite number of ruptures to a manageable and representative set, resulting in 580,000 different WUS ruptures here). Figure 9 of Field et al. (2023) shows the implied inter-connectivity among WUS faults (where multi-fault ruptures can occur in the model). The magnitude and average slip for each of these ruptures are computed from one of six scaling relations, the options of which are based on new recommendations from Shaw (2023). The inversion then solves for the rate of each rupture by satisfying the chosen deformation model slip rates, as well as the paleoseismic recurrence intervals updated by McPhillips (2022) for sites in California and those compiled by Valentini et al. (2020) for the Wasatch fault. Because slip rates may be inconsistent with nearby paleoseismic recurrence intervals, we added three paleoseismic data-fit branches that adjust how well these data are fit (relative to slip rates), providing a wider range of models than utilized in

UCERF3. Fault creep is assumed to reduce rupture area, except for highly creeping faults where it is applied as a slip-rate reduction as well.

In summary, we have five deformation models, six scaling relationships, five target supra-seismogenic *b*-values, five segmentation models, and three paleoseismic data-fit options represented on the logic tree, which amounts to 2250 different inversion-based fault-system solutions for WUS (Figure 4). This new ERF consists of rates of 580,000 alternative but possible fault ruptures across the entire WUS. The ratio plots show each model compared to the average of all models within a similar logic-tree branch. Large differences in earthquake rates are found between the geologic and geodetic deformation models, fault segmentation models, and the declustering and gridded (smoothing) components of the seismicity-based rate models. As such, we think we now have a fully comprehensive representation of the viable range of models, at least with respect to the propensity of multi-fault ruptures (i.e. leaving aside slip-rate uncertainty questions). This new ERF consists of rates of 580,000 alternative but possible fault ruptures across the entire WUS. A much more detailed summary of inversion-based fault-system solutions is available in Field et al. (2023). In addition, we point the users to further information on how branch weights were decided, references to other related studies, full implementation details, quantification of data-fit improvements, and various sensitivity analyses (Field et al., 2023).

*CEUS fault sources.* CEUS fault-based sources, described by Shumway et al. (2023), are based on the updated fault models and geologic constraints discussed above (Thompson Jobe et al., 2022a, 2022b). All are either represented with a fault zone (area source) or with an explicit fault surface. Figure 1 shows faults and zones for CEUS sources. All these models also adopt the Repeating Large-Magnitude Earthquake (RLME) hypothesis introduced by the US Nuclear Regulatory Commission CEUS–SSCn (2012), which assumes that each source produces only a narrow range of magnitudes (or a single-magnitude event in the case of past and present USGS NSHMs). For this 2023 NSHM, we use a flexible definition of RLME because some faults are only characterized by evidence from a single earthquake rupture rather than evidence of repeating ruptures. The magnitude of these characteristic events is inferred from a scaling relationship using either fault-surface area, the maximum length of a fault zone, or the spatial extent of paleoliquefaction deposits. The mean rate of the RLME source is either inferred by moment balancing if a slip-rate estimate is available or from an observation of $N$ events having occurred in some timespan $T$ (e.g. from paleoliquefaction deposits) using calculations of likelihood. Although there is no aleatory variability in source magnitude, considerable epistemic uncertainties are accounted for with respect to what the characteristic magnitude is, the recurrence rate implied by the geologic constraints, and sometimes the area assigned to fault-zone sources.

With respect to fault-zone sources (Figure 1), the following changes have occurred since the 2018 NSHM for CONUS: three have been added in the NMSZ (Joiner Ridge, Crowley's Ridge (south), and Crowley's Ridge (west)); two were added elsewhere in the CEUS (Saline River and Central Virginia); five were converted from zones to explicit fault surfaces (Commerce, Eastern Rift Margin (North), and Eastern Rift Margin (South), which includes three fault segments); and four were unchanged (Wabash Valley, Charleston, Charlevoix, and Marianna). We weighted these five new rupture models with 50% on the new ERF model and 50% on the gridded seismicity characterization based on discussions with the authors on limitations of the paleoliquefaction studies and uncertainty on whether these sources represent unique sources relative to the background gridded seismicity sources in the model (Field et al., 2023; Shumway et al., 2023).

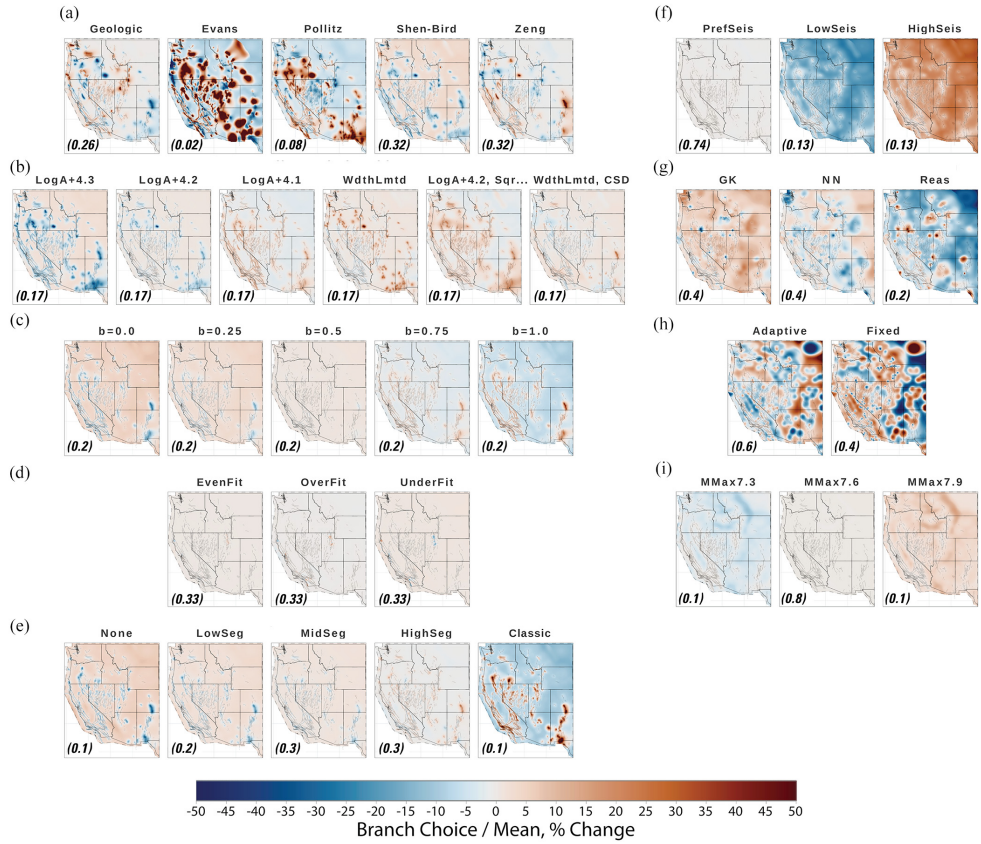


**Figure 4.** Plots showing ratios of the various parameters/models to the average of the group shown on each row or each of the logic-tree branches (weights are shown in the lower left-hand corners): deformation model (a), scaling relationship (b), supra-seismogenic *b*-value (c), paleoseismic data uncertainties (d), segmentation model (e), regional seismicity rate (f), seismicity declustering algorithm (g), seismicity smoothing kernel (h), and off-fault Mmax (i). Colors range from dark brown (very high ratios) to dark blue (very low ratios) after Field et al. (2023). Appendix A (Table SA-1) provides weights for the models.
Source: Modified from Field et al. (2023).

There are 12 CEUS faults modeled with an explicit fault surface, none of which is new, none of which has had any changes in source magnitudes or rates, and only one of which is outside the NMSZ. The latter, the Meers fault in Oklahoma, is now known to extend farther to the west, which increased computed hazard in that area. The only other consequential modification is with respect to the Axial fault, which was extended to the southwest and produced a computed hazard increase in that area too (Field et al., 2023; Shumway et al., 2023). Although the other fault-based sources in the NMSZ did not undergo any other consequential changes since the 2018 NSHM, it is worth noting that they embody additional complexity with respect to some single and multi-fault ruptures (each of which still honors the RLME assumption) and there are branches that assume ruptures always come as doublets or triplets. A more extensive summary of these fault-based sources is given in Field et al. (2023), and full details, including logic-tree descriptions for each, are given by Petersen et al. (2008, 2014) and Shumway et al. (2023).

Field et al. (2023) also describe some improvements that could be made to these models. One is to relax the RLME assumption to acknowledge a wider range of possibilities (i.e. increase aleatory variability in source magnitudes). Another would be to streamline logic trees to reduce the number of logic-tree branches and avoid over-complication of the modeling. Finally, the interconnected fault system in the NMSZ seems like a prime candidate for an inversion-based fault-system solution, although lack of mapped surface faults with accompanying slip rates will lead to a much broader range of fault-based solutions. Furthermore, assumptions on the earthquake clustering and recurrence times between sequences of New Madrid events could be improved with more information on paleoliquefaction timing constraints and additional global analogs.

*Cascadia subduction zone.* The Cascadia subduction zone model is essentially a fault-based source with a more sophisticated 3D representation of the subducting interface that includes three down-dip widths. Updates relative to the 2018 NSHM for CONUS, summarized in Field et al. (2023), are based on new paleoseismic constraints and discussions at a virtual workshop in February 2021. These led to the addition of an alternative segmentation model proposed by Goldfinger et al. (2017), which has ruptures extending farther north, and swapping out a 2000-year M $\geqslant$ 8 recurrence branch with two alternatives (800-year vs 2300-year recurrence) inferred from on-shore data by Nelson et al. (2021). We also added a cluster model for which, 10% of the time, a sequence of smaller ~M8 ruptures sweep down the subduction zone over a short period of time (Electronic_Supplement_1.pdf, Table SA-2 and Figure SB-1). Finally, Goldfinger et al. (2017) and Nelson et al. (2021) include an optional time-dependent probability for full subduction zone ruptures assuming a Brownian Passage Time distribution. This model assumes a recurrence interval of 529 years and a coefficient of variation of 0.5, with the last event having occurred in 1700. The model applies the magnitude-scaling equations from the 2018 model as well as a new equation by Shaw (2023, M = logA + 4). This time-dependent assessment produces a 50-year probability of 12.5%, which is a factor of ~1.4 greater than the time-independent probability of 9% (Petersen et al., 2002). There was a consideration of whether to include time-dependent probabilities for recurrence of the largest Cascadia rupture M9; however, in the end, the review panels felt that these additions should not be included here. Changes are caused by new turbidite results, new magnitude-scaling equations, and new subduction GMMs. The logic tree is displayed in Electronic_Supplement_1.pdf (Figure SB-1). The changes in computed hazard produced by these modifications are generally less than 10%. Hazard sensitivity calculations have also been performed of implied along-strike variation in slip for the three different down-dip width branches of the logic tree, revealing that the choice of the location of the up-dip limit of rupture has a large impact on implied slip rate, and adjusting this rupture bound may be considered in future updates.

Subduction intraslab earthquake sources are modeled as a gridded seismicity source in the Cascadia model. The 2018 NSHM, and prior NSHMs, used three different depth slice horizons to mimic the down going geometry of the subducting slab. In the 2023 NSHM, we have updated this approach using depths from the Slab2 Cascadia model (Hayes et al., 2018). This smoothly varying depth model is an improvement over the prior "stair-step" model and is consistent with the intraslab implementation for the Alaska–Aleutian subduction zone in the 2023 NSHM for Alaska. The intraslab rate model has not been updated for the 2023 NSHM. The Mmax model has also not been updated, and normally caps at M7.2, but some branches have Mmax as high as M8 (GR branch with Mmax = 7.95).

*Gridded seismicity sources.* Gridded seismicity sources are meant to account for the fact that our fault models are incomplete with respect to representing all possible fault-rupture surfaces, especially at smaller magnitudes. These sources are represented in the NSHM using the following: (1) a polygon defining the region and a spatial discretization interval (0.1 degrees here) to define the grid cells; (2) a spatial probability distribution defining the relative rate of earthquake nucleation within each grid cell; (3) a total M $\geqslant$ 5 rate and *b*-value for the region; (4) an assumed maximum magnitude for the region or a set of subregions; (5) a probability distribution of focal mechanisms for each grid cell; and (6) rules for converting a nucleation point into a finite-rupture surface. Steps are also taken to ensure that gridded seismicity sources are not double counted with fault-based sources. Campbell and Gupta (2018) suggest an efficient method of modeling random orientation of virtual faults that avoids biases and could be considered in future NSHMs.

The models utilized here are based on observed seismicity, so the first step was to update the earthquake catalog through 2022 using the methodology of Mueller (2019), taking care to exclude induced-seismicity events. Due to catalog completeness heterogeneities and other differences, the following steps were conducted separately for the WUS, CEUS, and the deep seismicity near the Cascadia subduction zone. The total M $\geqslant$ 5 rate and *b*-value for each region were inferred by Field et al. (2023), including a best estimate and 95% confidence bounds (*a* rate and *b*-value pair for each). The spatial probability distribution of grid-cell rates was calculated by Field et al. (2023), which involved declustering the earthquake catalog to avoid bias from aftershock sequences, spatially smoothing the resultant declustered catalog, and normalizing by the total rate so that grid-cell values sum to 1.0. This process results in a spatial probability density function (PDF) map. Additional epistemic uncertainty was accounted for in the declustering process, because no methodology is universally accepted as the best way to decluster earthquakes from the catalog, with some models removing more large earthquakes and some removing fewer events. The algorithms of Reasenberg (1985) and Zaliapin and Ben-Zion (2020) were added to the traditional approach (Gardner and Knopoff, 1974), resulting in three weighted logic-tree branches. We reduced the weight on the Reasenberg model to half (20%) that of the other two declustering models (40% each) because the ERF review panel felt that the Reasenberg model did not adequately remove aftershocks for some events and it likely spreads seismicity too far in some areas (Field et al., 2023). The full and declustered catalogs, for both the CEUS and WUS, are available at the USGS ScienceBase Catalog (Petersen et al., 2023).

The same two spatial smoothing algorithms applied in the 2018 NSHM for CONUS were again utilized here, both of which implement a two-dimensional Gaussian kernel (Field et al., 2023). The first applies a "fixed" correlation length that, using the convention of Frankel (1995), is $\sqrt{2}$ times the standard deviation of the Gaussian, which was set as 50 km in the WUS and between 50 and 70 km in the CEUS (depending on assumed minimum magnitude of completeness). The second "adaptive" approach sets the smoothing width as the distance to the *N*th nearest event ($N = 3$ in the WUS and $N = 4$ in CEUS), providing greater spatial resolution in higher seismicity areas. These nearest neighbor numbers were reoptimized using likelihood tests for the updated catalogs but are similar to the 2014 NSHM values (Field et al., 2023; Moschetti, 2015; Petersen et al., 2014). The fixed smoothing approach can produce dubiously low seismicity rates in areas that have had few or no observed events, in which case rates are prevented from going below a specified floor rate; this is now only applied in CEUS. The adaptive weighting approach was given more weight (60%) compared to the fixed weighting model, which was given less weight (40%) in the 2023 NSHM compared to that in 2018. This change allows for the use of more

nearest neighbor earthquakes than in 2018 NSHM for CONUS (based on comments from the ERF review panel, Jordan et al., 2023). A new boundary between CEUS and WUS catalogs was suggested at longitude −104°W, which also led to new differences in the catalogs and applicable processing (Field et al., 2023). This boundary was changed so that both faults and gridded seismicity sources modeled using the WUS fault-system solutions would have the same areal extent.

Three branches are utilized for gridded seismicity Mmax, with the options and weights for the WUS being adopted from UCERF3 and those for the CEUS being adopted from the 2018 NSHM for CONUS (Figure 2). Likewise, the spatial distribution of focal-mechanism likelihoods remains unchanged since the 2018 NSHM for CONUS, as is the procedure for assigning finite-rupture surfaces to gridded seismicity events. Finally, adjustments were made to avoid double counting seismicity on faults in the WUS.

*Treatment of aftershocks in hazard calculations.* As noted above, the removal of aftershocks is arguably necessary when inferring the long-term spatial distribution of seismicity rates. The question addressed here is whether aftershocks should be included in time-independent hazard assessments. Previous NSHMs applied declustered models to honor the Poisson hazard assumption, a decision that had only a minor impact on results because the declustering algorithm used at that time, Gardner and Knopoff (1974), does not generally remove events above M6.5. The problem is that more modern, best available declustering algorithms (e.g. based on the ETAS model of Ogata (1988, 1998) or the Zaliapin and Ben-Zion (2020) approach as applied here) tend to remove about half the events at all magnitudes, which would be highly inappropriate for hazard assessments. A significant body of literature asserts that, for 2% or 10% in 50-year hazard, keeping aftershocks and assuming a Poisson process are better than declustering with antiquated or biasing methodologies (Field et al., 2021; Marzocchi and Taroni, 2014; Michael and Llenos, 2022; Wang et al., 2022).

We follow UCERF3 in terms of including the rates of all M5+ events in the time-independent ERFs presented here, a decision our review panel agreed with. UCERF3 included an optional Gardner–Knopoff filter for hazard calculations, which was applied in the 2018 NSHM for CONUS for consistency with other regions, but there is no longer any scientific rational or sensible procedure for perpetuating this practice, especially given the available additional declustering algorithms. The consequence of this modification may be minimal for building code applications that apply 2%, 5%, or 10% probability of exceedances (PEs) in 50 years; however, the impact may be more significant for probabilities of exceedance greater than 10% or for smaller probabilities where gridded seismicity controls the hazard (Field et al., 2023). Therefore, modifications for applications that require these higher exceedance probabilities (e.g. risk community) may be warranted.

## Model evaluations

Model validation is an important exercise for ensuring the model results are robust and acceptable to the wider science community and demonstrating that the model is consistent with all kinds of data. Model evaluations were performed to validate the ERF model against different data sources. Several model-evaluation metrics are described in Field et al. (2023), including model-implied MFDs and their comparison with observations for various regions, inversion misfits with respect to slip-rate and paleo recurrence interval constraints, implied segmentation and rates of multi-fault ruptures, implied hazard curves

and hazard maps, an explanation of changes with respect to the 2018 NSHM for CONUS (summarized below), and sensitivities of the above with respect to the WUS logic-tree branches. Figure 23 of Field et al. (2023) exemplifies the latter with respect to maps of the PGA that has a 2% chance of exceedance in 50 years. However, we cannot create such plots for CEUS fault-based sources due to the logic-tree complexity and heterogeneity described above.

In addition to the Deformation Model Review Team for CONUS discussed above, we also convened a 19-member ERF review panel chaired by Tom Jordan (see Note 1). Their feedback led to model improvements, including assessments of the slip-rate outliers and additional constraints on the rate of very long ruptures ($\geqslant$ 700 km) (Jordan et al., 2023). The WUS fault-system solutions were also carefully scrutinized by an *ad hoc* group of USGS geologists, which also led to a number of model adjustments as well as some future recommendations (Hatem et al., 2022a, 2022b). All these model evaluations allow us to conclude that this new model represents a substantial improvement in assessing epistemic uncertainties (Jordan et al., 2023).

### *Alaska ERF*

The 2023 Alaska NSHM, previously updated in 1999 and 2007 (Wesson et al., 1999, 2007), is documented in this paper and Appendix D of Electronic_Supplement_1.pdf and updates all ERF and GMM components. The Alaska NSHM was subject to review by an independent panel of Alaska hazard experts (i.e., AK Review Panel chaired by Mike West)[1] and a Tiger Team of GMM developers (chaired by Norm Abrahamson) enlisted to evaluate the Alaska subduction GMMs[1]. Reports from the Tiger Team and Alaska Review Panel can be found in Electronic_Supplement_1.pdf, Appendix F and G, respectively. The 2023 Alaska ERF describes earthquake rupture potential in the active-crust, subduction interface, and subduction intraslab tectonic settings. The 2023 crustal fault model includes over 100 faults, and we use estimates of slip rates derived from geodetic data for both crustal fault and subduction interface ERF components. The 2023 Alaska NSHM also includes a new subduction segmentation and recurrence model, new approaches to developing gridded seismicity, and the structure of the Alaska-Aleutian subduction interface is constrained to Slab2 (Hayes et al., 2018).

The crustal fault model (Bender et al., 2021; Haeussler et al., 2023) consists of 105 fault sections, increased from 9 in 2007 and was developed following the same methods applied in the CONUS region (Hatem et al., 2022a,b). Important additions include a connector fault through the Chugach and Wrangell-St. Elias Ranges, which permits slip transfer from the Queen Charlotte—Fairweather system to the Totschunda and Denali faults. The model also adds numerous reverse and strike-slip faults in the complex zone of deformation where localized strike-slip motion on the Queen Charlotte—Fairweather system gives way to compressional deformation at the east end of the Alaska-Aleutian arc. The crustal fault ERF assigns both geologic (Haeussler et al., 2023) and geodetic block model (Elliott and Freymueller, 2020) slip rates to crustal faults. We downweight the geodetic block model (1/3 weight) because it provides lower estimates of slip rate on the Denali and Queen Charlotte faults where the long-term geologic rates are better constrained. Faults that do not coincide with block boundaries are assigned geologic rates with full weight. For the fast-slipping strike-slip faults of the interconnected Denali–Totschunda–Fairweather–Queen-Charlotte system, the ERF accommodates multi-fault ruptures and along-strike variations in slip rate. The crustal ERF also includes several area source zones in regions where numerous active structures are

mapped, but for which slip-rates are poorly constrained. Rupture magnitudes and areas in the crustal fault model are computed using a width-limited magnitude-area scaling relation by Shaw (2023) and we impose a regional Mmax of $7.9 \pm 0.34$.

The Alaska ERF includes gridded (smoothed) seismicity models for all tectonic settings that are based on an earthquake catalog that includes events through 2020. For crustal and intraslab settings, the gridded seismicity model forecasts earthquake rates for M5 up to M7.9 events. For active-crust, the Mmax distribution is M7.5 (0.9 weight) and M7.9 with a tapered MFD (0.1 weight), consistent with the gridded seismicity model for active-crust in the 2018 CONUS NSHM (Petersen et al., 2020). For the subduction interface, the gridded seismicity model accounts for the numerous small M57 earthquakes not covered by the finite fault model used for M7+ earthquakes. Development of the gridded seismicity models included the novel application of a probabilistic earthquake classifier to segregate the catalog into crustal, subduction interface, and subduction intraslab events. Each catalog was then processed using the same three declustering, two smoothing, and rate modeling methods as used in the development of the CONUS ERF update (Field et al., 2023; Table SA-1) and applied with identical weights as the CONUS model. Point earthquake sources for the interface and instraslab grids are modeled at depths derived from Slab2 (Hayes et al., 2018). Their spatial extent is also limited to the extent of the Slab2 contours with the interface grid further limited to depths shallower than 50 km. Similarly, gridded seismicity model rates (a-and b-values in the Gutenberg-Richter MFD) for Alaska are based on the full-catalog rate and not the declustered catalog rate that was used in prior NSHMs.

For the Alaska-Aleutian subduction zone, large magnitude (M8+) megathrust earthquakes occur on updated structural and segmentation models that consider both geologic and geodetic recurrence rates (Briggs et al., 2023). We give the geologic branch 80% weight and the geodetic branch a lower 20% weight because it implies very high rates of M8 earthquakes which are plausible but are only rarely observed in the historic record. Future analysis could focus on the higher M8 rates implied by the geodetic model. We performed sensitivity studies showing the relative contributions of the ERF and GMM models and find that for most sites the GMM modifications are much more substantial in increasing the hazard compared to the ERF modifications (e.g., site in Anchorage shows that overall changes are based on a 2/3 contribution from GMM changes and 1/3 contribution from ERF changes, Appendix D of Electronic_Supplement_1.pdf). The ERF branches without the geodetic models result in higher ground motions than in the 2007 NSHM for Alaska and the geodetic branch increases this further. The geologic branch of the megathrust model considers two down-dip widths (narrow and wide) constrained to depth contours of the Slab2 model (Hayes et al., 2018). Magnitudes are computed using the scaling relations applied for the 2018 Cascadia model supplemented with a new alternative model by Shaw (2023; $\log A + 4$). For the geodetic branch, rupture areas are constrained to the modeled locked portions of each subduction interface section. On the geologic branch, we allow ruptures to consist of either 1, 2, or 3 contiguous rupture sections of the megathrust (with equal weights of 1/3; refer to Table SA-3 in Electronic_Supplement_1.pdf). Four of the multi-section models match the rupture extents of historic interface earthquakes in 1788, 1957, 1965, and 1964, the Great Alaska earthquake. The multi-section rate models are constrained to not exceed the single-section geologic recurrences with any residual rate assigned to single section ruptures.

### Hawaii ERFs

As in other parts of the United States, the Hawaii seismicity source model was developed using gridded seismicity and fault-based deformation models. To update the gridded seismicity model, we applied a new earthquake catalog, declustering methods, spatial smoothing algorithms, and earthquake rate models for moderate to large earthquakes and caldera collapses to update the previous model developed in 2001 (Klein et al., 2001). The Hawaii model prescribes full weight on the classic model that is built from geologic observations and paleoseismic studies of prehistoric ruptures. The new Hawaii earthquake catalog was first separated into two regions (north and south) and five subregions based on alternative earthquake mechanisms and depths (shallow summit, shallow non-summit, deep summit, deep non-summit, and caldera collapse, with shallow and deep defined as less than or greater than 20 km, respectively). Rate models were computed for each subregion independently. The catalog was further subdivided into three different time periods (1840–1899, 1900–1959, 1960–2019) to account for spatial and time-dependent variability in the earthquake rates. We used the same decluster methods now considered in CONUS and Alaska but have excluded Gardner and Knopoff (1974) because it does not fit the clustered earthquake behavior observed across Hawaii. Full and declustered catalogs can be found at the USGS ScienceBase Catalog (Rukstales et al., 2021). Seismicity across the Hawaiian island chain varies spatially from the dense distribution of earthquakes on the Island of Hawai'i to the much sparser distribution of earthquakes found across the islands located to the northwest. In 2001, the spatial distribution of this seismicity was characterized using fixed spatial smoothing combined with a ramp-type smoothing model that allowed for a linear spatial decay of earthquake rates toward the less seismically active northern islands (Klein et al., 2001; Petersen et al., 2022). For the 2021 NSHM, we only applied the adaptive smoothing model because it naturally results in decaying rates from the southern to the northern islands and does not require the complex ramp (fixed smoothing) modeling techniques of Klein et al. (2001). We also apply a caldera collapse shaking model to account for ground motions near the Kilauea caldera that caused damage to nearby structures during the 2018 Kilauea eruption (Michael and Llenos, 2022). We apply maximum magnitudes ranging from M7.5 to M8 that account for seismicity that was observed on the southern and western flanks of the islands as well as a new interpretation of a large earthquake with M 7.5 located near Lanai (Butler, 2020). The earthquake rates are based on a GR distribution of earthquakes with *b*-values derived from each declustered catalog (Petersen et al., 2022). As an alternative, the rates and *b*-values were also calculated using the full catalog combined with declustered catalog spatial distributions (e.g. Field et al., 2021; Marzocchi and Taroni, 2014).

The Hawaii fault-based model was updated with 20 years of additional seismicity data, new fault deformation GPS data, and a geologically recent (Quaternary) fault database (Klein et al., 2001; Petersen et al., 2021). The new fault model considers moderate to large earthquakes on low angle dipping décollement faults recognized or inferred on the southern and western portions of the Island of Hawai'i at depths between 8 and 12 km based on seismic reflection studies and seismicity patterns. The ERF fault model allows for several alternative (epistemic) south and west flank sources derived from seismic moment of large historic earthquakes, slip rates across the southern and western flank regions, and historical inter-event earthquake recurrence information. Forecasted earthquakes on major low-dipping décollement sources are similar to the 1868 Ka'ū (M7.9, M7.0 aftershock) and the 1975 and 2018 Kalapana earthquakes (M7.7, M6.9) on the southern coast and the 1929 $M_s$6.5 near Hualālai and the 1951 M6.9 earthquake near Kona along the western coast of

the Island of Hawai'i. The geologic and geodetic deformation model is based on slip rates inferred across a network of 66 telemetered GPS stations on the Island of Hawai'i and shows significantly higher potential for large earthquakes in the southern flank region compared to the western flank of other areas of the island. Maximum magnitudes were increased to M7.5–8.2 across the southern and western flanks of the Island of Hawai'i to account for potential large earthquakes, similar to those observed historically on the south flank. The décollement zones were weighted with recurrence information described in Petersen et al. (2021). The models were reviewed by the Hawaii Earthquake and Tsunami Advisory Council for use in the 2023 NSHMs (Petersen et al., 2021).

## GMMs

The 2023 NSHM applies new and modified GMMs (NGA-Subduction, CEUS NGA-East), 3D numerical ground-motion simulations (Seattle-M9 and Los Angeles region-CyberShake), sedimentary thickness-based amplification models for the CEUS (Gulf and Atlantic Coastal Plains) and WUS sedimentary basins (Seattle, Portland/Tualatin, San Francisco, California Great Valley, Los Angeles), and a revised CEUS-WUS attenuation boundary. Details of these models, implementations, and sensitivity studies are found in Rezaeian et al. (2023) for subduction zone GMMs and in Moschetti et al. (2023a) for the GMMs in WUS and CEUS. Past NSHMs applied semi-empirical GMMs that were based on abundant moderate-size earthquakes recorded in the WUS and were supplemented with larger and great earthquakes recorded globally to characterize ground shaking. Stochastic- and physics-based simulations and hybrid- and reference-empirical GMMs were applied for earthquakes in the CEUS. The 2023 NSHM includes 3D-simulated ground motions for the first time for earthquakes on the Cascadia subduction zone and for faults across the Los Angeles basin (Moschetti et al., 2023a). Moschetti et al. (2023a) also provide details on sediment-thickness- and seismic-velocity-based amplification models and 3D numerical simulations of large ruptures. Details of GMMs for Alaska and Hawaii NSHMs are provided in this paper and Appendix D of Electronic_Supplement_1.pdf and Petersen et al. (2022), respectively. Selected GMMs for all regions and their assigned weights are summarized in Tables SA-4 to SA-9 of Electronic_Supplement_1.pdf and are based on the revised GMM selection criteria published in Rezaeian et al. (2021). The weight assignments, as in previous cycles of NSHMs, are based on a consensus building process that involves consideration of expert judgments, data residual analyses, and a thorough review of each model's characteristics such as magnitude and distance scaling and limitations such as applicability ranges of the model parameters. Example logic trees for GMMs with weights are shown in Figure 5.

We made several additions and modifications to GMMs applied in the 2023 NSHMs. For subduction zones, we have implemented new semi-empirical NGA-Subduction for Cascadia and Alaska subduction sources (Rezaeian et al., 2023). We supplement these NGA equations with two older GMMs for Cascadia that provide additional epistemic uncertainty at longer periods; these are similar and developed using computer simulated data for longer periods ($T \geqslant 1$ s) but are downweighted because they are older and did not have the benefit of the most recent data. We implement adjustment factors to the CEUS GMMs to reduce bias with regional records; these adjustment factors are incorporated with reduced weight because they are new and less tested. New region-specific GMMs are implemented for Hawaii with one model (Wong et al., 2015) being downweighted because the residuals with data were much larger than for the other GMMs.

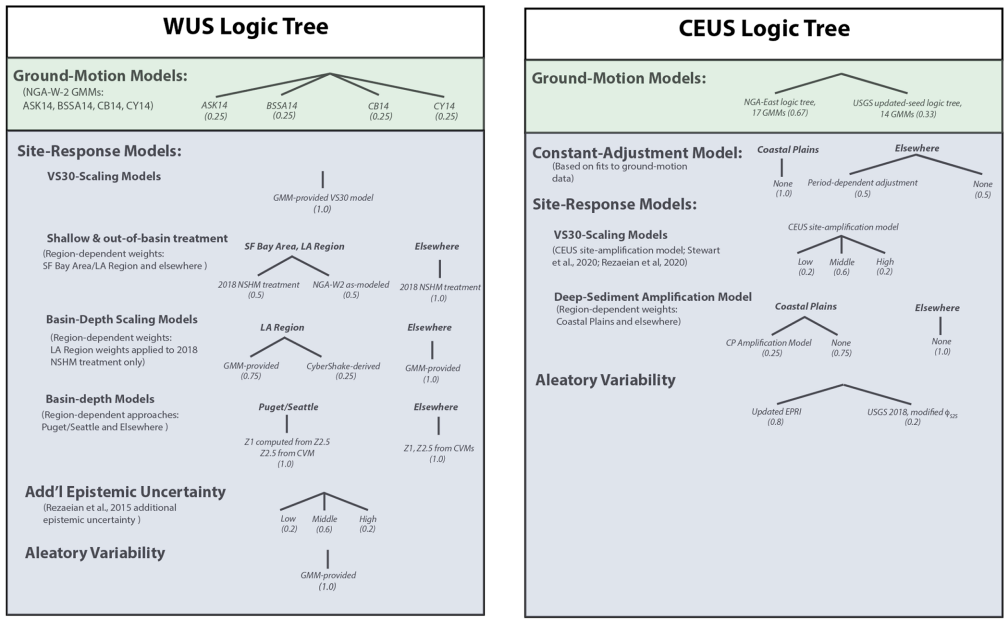


**Figure 5.** Logic trees for western United States (WUS) and central and eastern United States (CEUS) ground-motion models (GMMs). The GMMs include Abrahamson et al. (2014) (ASK14); Boore et al. (2014) (BSSA14); Campbell and Bozorgnia (2014) (CB14); Chiou and Youngs (2014) (CY14). Other abbreviations include the Community Velocity model (CVM), Electric Power Research Institute (EPRI), Site-to-Site variability ($\varphi_{S2S}$). Other details including additional epistemic uncertainty implementation may be found in Rezaeian et al., 2021, 2023.

Weights were presented at regional workshops and the CONUS GMMs were evaluated by the review panels.

Comparisons of the average weighted GMMs with some of the older GMMs are shown in Figure 6 for the median response spectral ground motions and standard deviations. Generally, the median ground motions for shallow crustal, subduction interface, and subduction intraslab earthquakes are similar to one another within about a factor of 2. However, the CEUS model medians and sigmas are considerably higher than for WUS GMMs, especially at short periods. In particular, Alaska interface and intraslab standard deviations are much higher than the earlier versions, which substantially affects hazard calculations.

To evaluate earthquake ground shaking for the hazard model, it is important to understand details of how ground motions are influenced by earthquake magnitude, distance, shallow soils ($V_{S30}$), deep sedimentary basin deposits ($Z_{1.0}$ and $Z_{2.5}$) and other factors. Tens of thousands of strong ground-motion records from earthquakes have been recorded over the past century that provide insights into ground-shaking characteristics. The Pacific Earthquake Engineering Research (PEER) Center has developed ground-motion databases for earthquakes located within different tectonic regimes. For shallow crustal earthquakes, the NGA-West2 project (Bozorgnia et al., 2014) used 21,192 three-component records from 599 shallow crustal events M3–M7.9 (Ancheta et al., 2014). For stable continental earthquakes, the NGA-East project used 27,000 records from 82 earthquakes

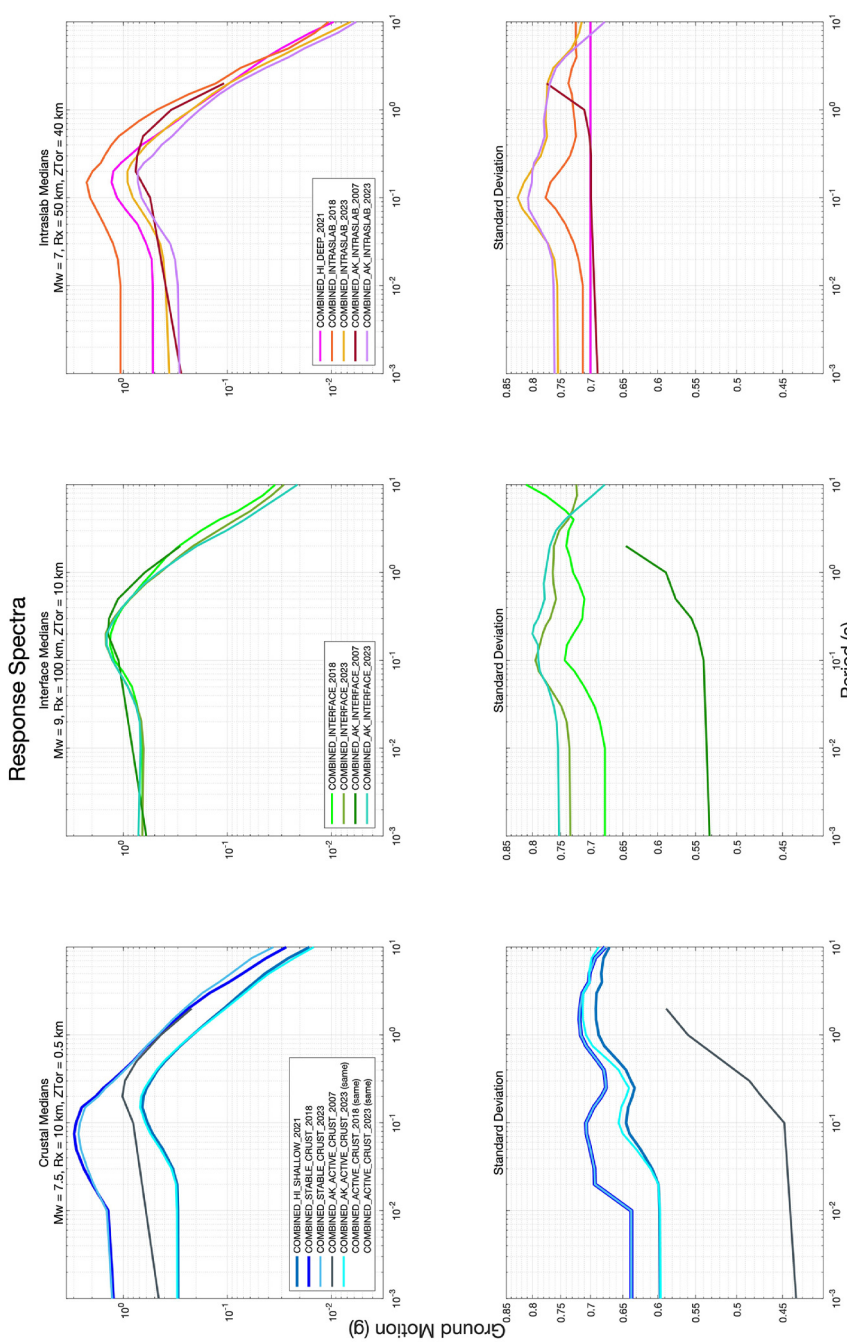


**Figure 6.** Ground-motion model comparisons for the median response spectral ground motions as a function of period (shortest periods similar to PGA) (top) and standard deviations (bottom) for shallow (left), interface (center), and deep (right) earthquakes on a 760 m/s $V_{S30}$ site condition. Shallow plot parameters: M7.5; interface plot parameters: M9, distance = 100 km, depth to top of rupture = 10 km; deep plot parameters: M7, $R_x$ = 50 km, and $Z_{TOR}$ = 40 km. The ground-motion models are combined average models, so the full range of epistemic uncertainty is not shown here (refer to Rezaeian et al., 2023 for more detail on all input GMMs).

M2.5–M6.9 (Goulet et al., 2021a, 2021b) enhanced by simulations for larger magnitude earthquakes. For subduction zone earthquakes, the NGA-Subduction project (Bozorgnia et al., 2022) used 71,340 three-component recordings from 1883 events M4–M9 (Mazzoni et al., 2021). We do not apply all the available GMMs for this 2023 modeling but instead implement models that form a reasonable distribution of alternative input models that are broad enough so that we can capture epistemic uncertainty (i.e. center, body, and range). Figure 5 shows logic trees for WUS and CEUS GMMs that are described in detail in Moschetti et al. (2023a) and described more generally in the sections below.

For this 2023 NSHM, we modify the site response terms of some existing GMMs with data from numerical simulations and from seismic observations (Moschetti et al., 2023a). These GMMs and modifications to those equations apply realistic 3D basin-specific geometries and computer simulations using shear-wave velocity profiles, mostly from community velocity models, to guide GMM development. We consider region-specific measurements and proxy-based maps of time-averaged shear-wave velocities in the upper 30 m of the crust ($V_{S30}$) (e.g. Heath et al., 2020; Wald and Allen, 2007) and community velocity models that define the deeper sedimentary sequences quantified by $Z_{1.0}$ and $Z_{2.5}$—the depths to the 1.0 and 2.5 km/s shear-wave velocity horizons (Aagaard, 2023a, 2023c; Aagaard and Hirakawa, 2021; Ahdi et al., 2023; Lee et al., 2014; Magistrale et al., 2008; Shah and Boyd, 2018; Simpson and Louie, 2020; Stephenson et al., 2017)—to test basin-scaling models developed in the NGA-West2 GMMs to the Great Valley of California, to the Reno, Nevada, and Portland/Tualatin, Oregon basins, and to the Atlantic and Gulf Coastal Plains. In addition to the empirical GMMs, 3D numerical simulations are now used in Seattle (Frankel et al., 2009, 2018; Wirth et al., 2018a) and Los Angeles (CyberShake, Graves et al., 2011) to model basin effects. The effects of these new GMMs and sedimentary basin models are described in the sections below and in Moschetti et al. (2023a).

We commissioned a GMM review panel chaired by Jon Stewart to review the input models for the 2023 NSHMs. This review is presented in Appendix C in Electronic_Supplement_1.pdf of Moschetti et al. (2023a).

### *WUS active crustal GMMS*

We apply the same GMMs in the WUS active crustal regions as considered in the 2018 NSHM using the NGA-West2 (Abrahamson et al., 2014, hereafter ASK14; Boore et al., 2014, hereafter BSSA14; Bozorgnia et al., 2014; Campbell and Bozorgnia, 2014, hereafter CB14; Chiou and Youngs, 2014, hereafter CY14). In addition to what is listed in Table SA-4 of Electronic_Supplement_1.pdf, we considered inclusion of the Graizer (2018) GMM for WUS. This GMM was not incorporated in this update cycle due to obstacles in implementation, but there are no known reasons why this GMM would not be included in future NSHMs—with additional implementation inputs. We retain the model of additional epistemic uncertainty developed for the 2014 NSHM to account for models that could vary from the NGA-West2 versions included in this update (Petersen et al., 2015a, 2015b; Rezaeian et al., 2015). Example logic trees for the WUS are shown in Figure 5.

We considered implementation of directivity models into the 2023 NSHM and active crustal GMMs, but decided to delay their use in NSHM until we have more complete vetting and agreement in the ground-motion modeling community concerning how to represent these earthquake effects. Withers et al. (2023) evaluated the effect of seismic directivity on hazard by implementing a median and aleatory adjustment to ground motion that

accounts for the averaged effect of possible hypocenter locations along a fault plane. They focused on strike-slip faults with near-vertical dips, where directivity model predictions are generally consistent and implemented the directivity adjustments for the UCERF3 rupture forecast. Withers et al. (2023) found that azimuthal amplification can substantially increase hazard at the end of individual fault rupture traces but is substantially reduced when applied probabilistically, where there is interference from multiple, overlapping seismic sources. In order to further investigate directivity effects from complex fault geometries and better understand epistemic uncertainty, we support continued investigations into the directivity models and their effects on seismic hazard.

### *WUS subduction GMMS*

Compared to previous subduction GMMs, the NGA-Subduction project represents a substantial improvement in uniform data processing, multiple modeling platforms for alternative regions across the globe, and extensive review and evaluations. We updated the subduction GMMs using three of the new NGA-Subduction models (Abrahamson and Gülerce, 2022, hereafter AG20; Kuehn et al., 2020, hereafter KBCG20; Parker et al., 2022, hereafter PSBAH20). Various weighting schemes were considered that allow for combining regional (Cascadia and Alaska) and global versions of the new NGA-Subduction models and some of the older 2018 NSHM models. We considered a broad range of potential GMMs because the regional Cascadia models of AG20, KBCG20, and PSBAH20 suffer from very limited Cascadia strong-motion data. The final selected models include the three new NGA-Subduction GMMs while maintaining two of the three older models to better account for epistemic uncertainty at periods greater than 1 s (Atkinson and Macias, 2009, hereafter AM09; and Zhao et al., 2006, hereafter Zhao06). The AG20 GMM was considered as an update to the Abrahamson et al. (2016) which was applied in 2018. The NGA-Subduction models were supplemented with lower weighted older models (AM09 and Zhao06) to allow for additional epistemic uncertainty, especially for long-period ground motions. These older models are more consistent with the AG20 and M9 computer simulations than the new NGA-Subduction models.

A magnitude-scaling break point parameter is new in the NGA-Subduction GMMs (Campbell, 2020). This can result in substantial differences to ground-motion forecasts for large earthquakes where the rate of increase flattens beyond the break point. We did not incorporate variations of this parameter in this cycle, but sensitivity analyses are provided in Rezaeian et al. (2023). We could not adequately implement this improvement in the 2023 NSHM; however, this might be a topic for modifying epistemic uncertainty for large ground motions in future versions of NSHM.

We considered weighting the median GMMs and the lognormally distributed aleatory variabilities separately in logic-tree branches, but this was considered at a late stage in the update process and consensus on how to weight these models was not readily achieved. To represent epistemic uncertainty, we applied combinations of GMMs that were thought to be consistent with Cascadia and Alaska strong-motion data. For Cascadia subduction interface earthquakes, we apply the adjusted version of AG20 with weight 25% and the KBCG20 and PSBAH20 Cascadia versions with equal weight (25% each) along with the AM09 and Zhao06, which together receive 25% weight. For intraslab earthquakes, we apply AG20 Cascadia and Cascadia-adjusted equations, which receive a total weight of 25%—with most weight assigned to the adjusted version. The rest of the weight for intraslab events is given to KBCG20 and PSBAH20 Cascadia along with the older Zhao06

(equally weighted with 25%). An important improvement is the incorporation of epistemic uncertainties on the median ground motion, which were implemented as a three-point representation of a lognormal distribution for all three GMMs. Table SA-4 in Electronic_Supplement_1.pdf lists GMMs and weights.

### CEUS GMMS and adjustment factors

The 2018 NSHM applied 17 final NGA-East models and 14 updated seed models with weights described by Petersen et al. (2020) and Rezaeian et al. (2021). For this 2023 NSHM, the CEUS ground-motion modeling implementations include two changes. One change involves a new correction to the nonlinear portion of the amplification model (Hashash et al., 2020) that is used in applying the NGA-East GMMs ($V_{S30}$ = 3000 m/s) to other $V_{S30}$ site conditions. The linear portion of the site amplification model as described by Stewart et al. (2020) has not changed. The second change involves a period-dependent modification to NGA-East GMMs to improve the fits of the residuals to updated compilations of CEUS strong-motion data (Moschetti et al., 2023a). Data misfits with the GMMs indicate an overprediction of ground motions for oscillator periods less than about 1 s and an underprediction at periods greater than 3 s (Moschetti et al., 2023a). These corrections apply to all $V_{S30}$ soil classifications. It is still unclear whether the GMM adjustment factors for the CEUS should be partitioned between NGA-East and site amplification models or whether the factors should be completely based on the NGA-East models alone. Adjusment factors were applied to reduce the bias of the model compared to regional observations (misfit). We convened a Tiger Team (also known as a GMM advisory team, see Note 1) to evaluate how we implement the NGA-East models. The recommendation of the Tiger Team (see Appendix F in Electronic_Supplement_1.pdf) was to taper the VS30 term between 1000 and 2000 m/s based on the residuals (Ramos-Sepulveda et al., 2023). In the current version of the model, we have not made this modification because the changes are relatively small. However, this could be considered for future updates. Figure 5 shows as example logic tree for CEUS GMMs. Table SA-4 in Electronic_Supplement_1.pdf provides a list of GMMs and weights.

### Alaska and Hawaii GMMS

In the case of Alaska, older GMMs that were used in the 2007 Alaska NSHM do not meet our GMM inclusion criteria and are therefore not considered. For earthquakes in active crustal regions, we apply the four NGA-West2 GMMs and a model of epistemic uncertainty in a logic tree of equally weighted branches consistent with that used for active crustal earthquakes in the CONUS model over the last few update cycles. Average crustal GMM medians in the 2023 Alaska NSHM are lower and aleatory variability (sigma) is higher than in the 2007 model (Figure 6). For Alaska subduction earthquakes, we implemented and evaluated both the global and Alaska regionalized NGA-Subduction interface and intraslab equations (AG20, KBCG20, and PSBAH20) along with the epistemic uncertainty and aleatory variability models specified in each. Our analysis of the NGA-Subduction GMMs for interface raised some questions and we therefore enlisted the help of a Tiger Team consisting of NGA-Subduction and other GMM experts to advise and make recommendations on the application of these new GMMs in the Alaska NSHM. The Tiger Team noted that the Alaska ground motion database is limited to moderate magnitude events at large distances and that there are issues with the Alaska regionalized models. At the recommendation of the Tiger Team, we applied the three global NGA-Subduction

GMMs for interface with 1/6 weight each and bias-corrected versions of each model, also with 1/6 weight each. The bias corrections were developed using records that post-date the NGA-Subduction database and which are located closer to the population centers of south-central Alaska than the events used to develop the GMMs. Median ground motions are generally lower for the NGA-Subduction models, except at shorter distances and periods where they are higher (Appendix D of Electronic_Supplement_1.pdf). Average aleatory variability of the NGA-Subduction GMMs is higher (Figure 6), with individual NGA-Subduction models having sigma as high as 0.9 (e.g., PSBAH20). At the recommendation of the Tiger Team, we modified the KBCG20 aleatory variability model to match the published CB14 model to account for nonlinear site effects. The Tiger Team recommended the use of the Alaska regionalized NGA-Subduction intraslab GMMs as published because they are constrained by more data. For this update, we did not include amplification of long period ground motions over deep sedimentary basins as in the CONUS NSHM. Appendix A of Electronic_Supplement_1.pdf provides full details and weights (Table SA-4) of the GMMs selected for the 2023 AK NSHM.

We also updated the Hawaii shallow and deep GMMs in developing the 2023 NSHM (Petersen et al., 2022). The new 2023 NSHM considers five shallow GMMs (Atkinson, 2010; A10, ASK14, BSSA14, CB14, CY14) and three deep GMMs (A10, Zhao06, Wong et al., 2015; W15) that were compared to the strong ground-motion records on Hawaii to identify the equations that best fit the data. We used a total residual approach that compares the PDF for both mean and standard deviations and a log-likelihood test that considers the best GMMs for use in the model (McNamara et al., 2020). The new equations for Hawaii are shown in Table SA-4 of Electronic_Supplement_1.pdf with weights described in Petersen et al. (2022). We weighted the models based on residual analyses (McNamara et al., 2020; Petersen et al., 2022). In addition, we applied additional epistemic uncertainty similar to the 2018 NSHM and applied the empirical corrections to the A10 model for estimating ground motions from caldera collapses (A10_Caldera, Petersen et al., 2020). Site effects are implemented by evaluating soil profiles for Hawaii and the available strong ground-motion database. Hawaii sedimentary basin models are not available for amplifying long-period ground motions. Moreover, the $V_{S30}$ models do not seem to perform as well in Hawaii as they do in the WUS.

## Sediment depth-based amplification models

The 2023 NSHM provides maps for several values of $V_{S30}$ and sedimentary basin depth. These factors are important for many of the largest western cities. Relevant basin-specific data and models to implement these factors are not universally available, but NSHM applies them where there is confidence that available data are sufficient to result in an improvement in hazard estimates. For the 2018 NSHM, we applied sedimentary depth-based amplification models for WUS basins (Seattle, San Francisco, Los Angeles, and Salt Lake City); well-defined depth-based amplification models were not available for the CEUS or most other regions for this analysis. The semi-empirical models are conditioned on depth to a particular velocity horizon to account for amplification effects related to deeper velocity structure. Basin-depth models modify the active crustal, stable continental, and subduction GMMs for a proxy depth parameter included in the model: depth to the 1.0 km/s ($Z_{1.0}$) or the 2.5 km/s shear-wave horizon ($Z_{2.5}$). For active crustal and subduction GMMs, these are typically defined by each of the modeling teams for their GMM. These basin-amplification factors are correlated with the $V_{S30}$ amplification factors and cannot be used independently. We only applied the long-period basin amplification and

not the deamplifications in several basins (Wasatch near Salt Lake City, Seattle, Portland, Tualatin, Seattle, and the Great Valley of California) where velocity data and available models have not been applied for this purpose, strong-motion recordings are lacking, and amplification models need to be tested further. We allow for deamplification in Los Angeles and San Francisco, as described below using a logic-tree approach. We did not amplify or deamplify ground motions within the Reno basin for similar reasons. For Reno the improvement was not substantial when using these local depth-based models, uncertainty in published velocity models is high, and there is not much additional amplification due to basin-depth scaling compared to that captured by $V_{S30}$ scaling model.

For this 2023 NSHM, we apply basin-depth amplification models for CONUS where local basin-depth models are available, but not for Alaska or Hawaii where there are no accepted community velocity models available. We also use a model that can be applied to the NGA-East GMMs and seed models to account for the deep-sediment effects of the Atlantic and Gulf Coastal Plains. For updating the basin-amplification models in the WUS, we considered updated community seismic velocity models in the San Francisco Bay Area (Ahdi et al., 2023), new basin-depth models for the California Great Valley (Ahdi et al., 2023), Reno (which was not ultimately implemented), and Portland–Tualatin basins (Ahdi et al., 2023), new treatment of basin-amplification models at shallow-basin and out-of-basin sites, as well as the M9 simulations for the Puget Lowlands region (Frankel et al., 2018; Wirth et al., 2018b) and CyberShake simulations for the greater Los Angeles metropolitan region (Graves et al., 2011). The M9 and CyberShake simulations are not directly used to establish ground-motion levels. However, these data are used to modify the GMMs through implementation of amplification factors that are a function of sediment depth. This modification was also suggested by Nweke et al. (2022a) with further discussion presented in Moschetti et al. (2023a).

### *WUS amplification models*

We apply the basin depths from seismic velocity models for Seattle, San Francisco, Great Valley, Los Angeles/Ventura, Portland/Tualatin, and Salt Lake City (Aagaard, 2023a, 2023c; Aagaard and Hirakawa, 2021; Lee et al., 2014; Magistrale et al., 2008; Simpson and Louie, 2020; Stephenson, 2007; Stephenson et al., 2017) to assess $Z_{1.0}$ and $Z_{2.5}$ depth parameters. The basin-amplification models are derived along with the NGA-West2 equations (ASK14; BSSA14; CB14; CY14). We evaluated the basin-depth models in Reno (Aagaard, 2023b; Simpson and Louie, 2020) and found that because the basins were relatively shallow, the equations did not predict substantial amplifications in those regions. Using the local basin-depth models did not provide additional predictive capability (Ahdi et al., 2023)—similar to our 2018 analysis for Salt Lake City (Petersen et al., 2020). Ground-motion amplifications have been observed in each of these regions but scanty strong-motion data from large earthquakes are available to assess basin amplifications. Additional work would be beneficial to evaluate geometric basin influences and amplification characteristics and evaluate differences between these shallow basins and the deeper basins in California where most of the strong-motion data are located that underpin the development of these amplification models. We weight each of the basin-depth models with 100% weight because we are improving the information using $Z_{1.0}$ and $Z_{2.5}$ depth information that is not applied in the pre-2018 NSHMs. We could not add additional epistemic uncertainty to the amplification models (e.g. depth uncertainties of $Z_{1.0}$ and $Z_{2.5}$) because the methodology is currently not available.

We give full weight to the Great Valley $Z_{1.0}$ and $Z_{2.5}$ models because no alternatives are available. We applied the $Z_{1.0}$ and $Z_{2.5}$ in zones shown in Figure 7. Basin-depth models for Reno, the Wasatch Front, and Portland/Tualatin are shallower than the basins in California, resulting in amplification at very few sites, relative to the basin-amplification effects implicit in $V_{S30}$-scaling models built into the NGA-West2 GMMs. The Great Valley of California is much deeper and results in amplifications for long periods, especially in the southwestern portion of the zone.

In preparing the 2018 NSHM, we debated whether to modify ground motions from the NGA-West2 models based on sedimentary thickness inside and outside of basins. This led to many discussions with our NSHM-SC and in open workshops (Petersen et al., 2020). In the end, we decided that we lacked sufficient information to warrant lowering predicted ground motions from GMMs at the basin-edge regions where past earthquakes caused extensive damage and ground-motion variability was large (e.g. Santa Monica, California; West Seattle, Washington). Thus, for the 2018 hazard assessment, we amplified ground motions only in the deepest portions of the sedimentary basins and reverted to average GMMs everywhere else with no basin-amplification terms being applied.

For the 2023 NSHM, we revisit this decision considering new region-specific analyses for the San Francisco Bay Area and the greater Los Angeles region presented in Moschetti et al. (2023a) and in Nweke et al. (2020, 2022b). We tested the new California models for their effectiveness in predicting amplifications throughout these urban regions and found that the NGA-West2 model with basin response terms $Z_{1.0}$ and $Z_{2.5}$ perform well in these two regions (Moschetti et al., 2023a). For this 2023 NSHM, we develop a logic tree that accounts for modified ground motions in areas outside of basins, at basin edges, and inside of basins (Moschetti et al., 2023a). We consider a logic-tree uncertainty with half weight given to the 2018 model that only amplifies ground motions within the deepest portion of the basins, and half weight given to empirical basin-depth amplification models ($Z_{1.0}/Z_{2.5}$) of NGA-West2 that deamplify long-period ground motions for relatively shallow sediments and amplify motions in deeper sediments (refer to Table SA-6 for the San Francisco GMM logic tree and Table SA-7 for the Los Angeles GMM logic tree in Electronic_Supplement_1.pdf). Deamplifications of ground motions have been observed in relatively small or shallow sedimentary structures (e.g. the valley province in Nweke et al. 2022b).

We apply these logic trees because our studies indicate that the NGA-West2 model is appropriate for use with the current database of strong motion in the San Francisco and Los Angeles regions, which lower ground motions by about 30% in both of these urban areas (Moschetti et al., 2023a). However, it is important to recognize that there are large epistemic uncertainties and aleatory variabilities that have not been explored that could influence these results in the future. For example, (1) this is the first time we are using the community velocity models for this purpose of amplifying ground motions in shallow soils and we need to ensure that the models are appropriate for this purpose; (2) we do not have strong-motion recordings from large San Andreas system earthquakes, so these effects have not been recorded or explained; and (3) there exist several unmodeled uncertainties such as at basin-edge sites due to converted waves and in recent work by Withers et al. (2023), which shows about 5% increases in the hazard at the 2% in 50-year level when applying the Watson-Lamprey (2018) directivity equations for the San Francisco Bay Area. For other regions we will need to carry out a similar analysis as we did in the urban areas of California to ensure that these basin models are consistent with the NGA-West2 amplification models. Therefore, for this 2023 update, we applied a logic-tree structures to

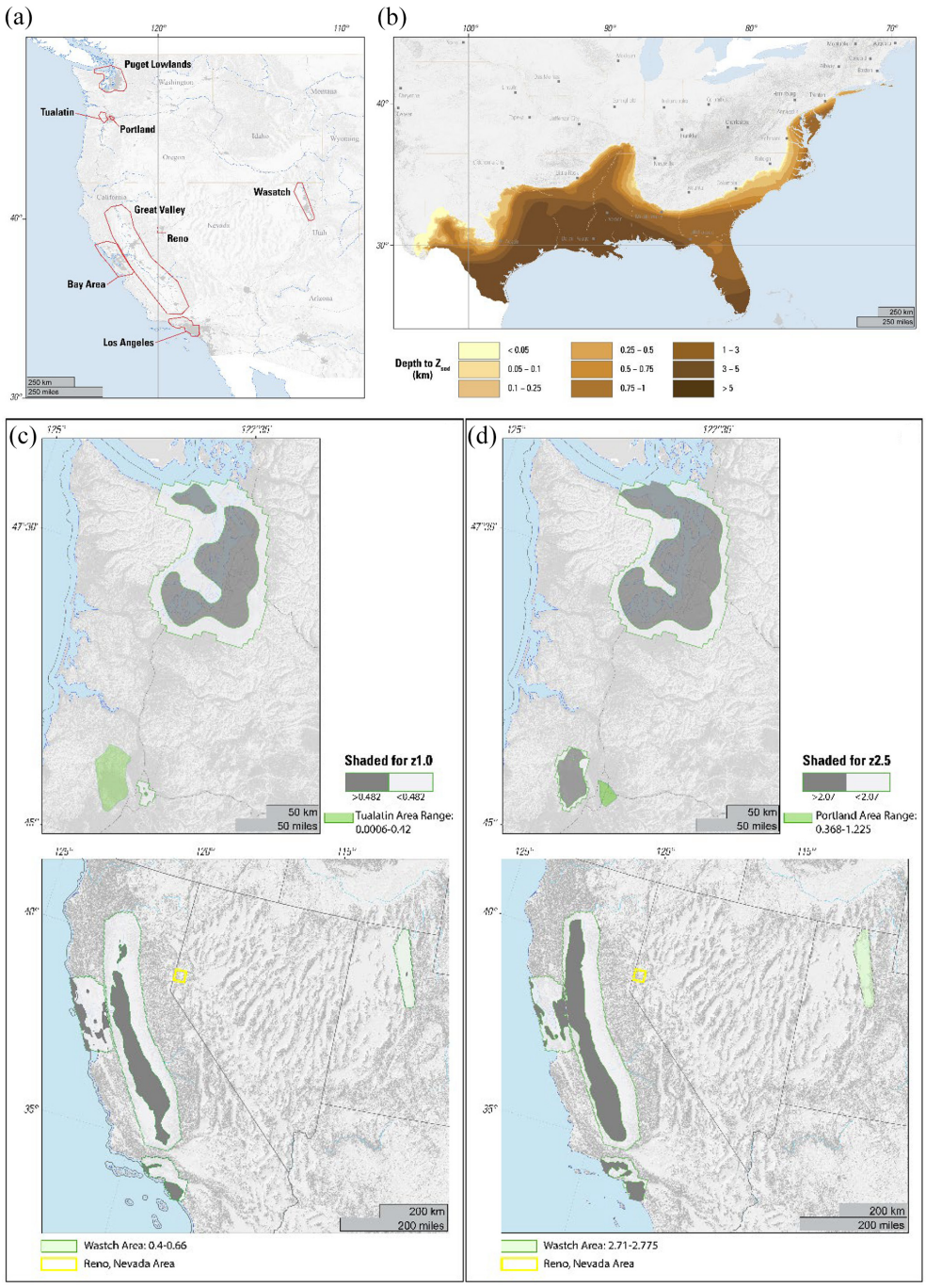


**Figure 7.** (a) The seven western United States (WUS) basin polygons (red solid lines) that were assessed for amplification; dashed lines represent two zones that were tested but not incorporated into the final model. (b) The extent of the coastal plain shaded for the depth to sediment base ($Z_{sed}$; Boyd et al., 2023). (c) Seven WUS basins assessed for amplification for $Z_{1.0}$ at $V_{S30}$ 260 m/s. (d) Seven WUS basins assessed for amplification for $Z_{2.5}$ for $V_{S30}$ 260 m/s; green shading fills areas too shallow for amplification. The basins shown were applied in the 2023 model with the exception of the Reno basin.

account for the NGA-West2 models as well as unknowns associated with the unmodeled uncertainties.

We did not develop basin-amplification models for Alaska or Hawaii. We did not have sufficient data to develop a good $V_{S30}$ or sedimentary basin models that could be used for this purpose. If developed, these models will be an important addition to future hazard models.

### 3D simulation-based models

The 3D simulations are used to modify the NGA-West2 and subduction GMMs to account for basin effects from large-magnitude earthquakes. We consider the CyberShake 3D ground-motion simulations (Graves et al., 2011) that are based on earthquake sources across the Los Angeles region, a kinematic rupture generator, and reasonable structural and velocity representations of the Los Angeles basin. We use the simulated ground motions in the southern California region to develop alternative basin-depth scaling terms for the NGA-West2 GMMs (Moschetti et al., 2023b). The simulation-derived basin-depth scaling models are centered on the GMMs and use the $V_{S30}$-scaling models of each GMM; however, we also allow for non-zero amplifications at zero differential depths, following recent work in southern California. After considerable discussions, correction factors were applied that are described further in Moschetti et al. (2023b) based on Nweke et al. (2022a). Modified basin-amplification factors apply the functional forms of each of the NGA-West2 equations, which are intended to work in tandem with the $V_{S30}$ scaling relations in the respective models. The resulting ground-motion hazards across the region result in minor (less than 10%) reductions at periods between 1 and 4 s and slightly higher increases (10%–25%) at 5–10 s periods compared to applying the NGA-West2 equations. We weight the new CyberShake-based amplification model as 0.25 because strong-motion data are abundant in southern California to constrain the GMMs, although it is recognized that the simulations reflect amplifications from predominantly large-magnitude earthquakes (refer to Table SA-7 of Electronic_Supplement_1.pdf for GMMs and weights in the Los Angeles basin region).

For the 2018 NSHMs, we applied Seattle amplifications based on $Z_{1.0}$ and $Z_{2.5}$ but we did not directly consider the M9 Project simulations (Frankel et al., 2018; Wirth et al., 2018b). Since the publication of the 2018 NSHM, end-users expressed concern that there are no data from interface earthquakes in Cascadia to inform the range of potential ground motions within the Seattle basin, and the engineering community recommended use of greater amplification within the Seattle basin based on the M9 Project results. These long periods could affect tall buildings (Chang et al., 2014; Wirth et al., 2018a). In this 2023 revision, we have applied additional period-dependent and $V_{S30}$-independent amplifications (up to a factor of 2) for long-period ground motions to account for the M9 simulations in the deep Seattle basin (Chang et al., 2014; $Z_{2.5} > 6$ km). At long periods, the new M9 ground-motion levels are similar to the AG20 empirical amplifications, which gives us confidence in the M9 results. However, the basin amplifications from the other NGA-Subduction GMMs for Cascadia (Kuehn et al., 2020; Parker et al., 2022) are lower than the AG20 and M9 amplifications, so we allow for alternative amplifications by setting a minimum for basin amplification in the deep parts of the Seattle basin for these two GMMs (Moschetti et al., 2023a). Consideration of these simulations along with the full suite of NGA-Subduction models provides a broad range of epistemic uncertainty. For the 2023 NSHM, we apply the new Seattle amplification model with 0.5 weight, with the other 0.5 weight given to the amplification models provided in the NGA-Subduction

GMMs for interface sources only. The M9 amplification factors are not used for intraslab sources. The simulations are important in this Pacific Northwest region where we lack empirical data for large subduction interface earthquakes and only have limited data for intraslab earthquakes. Therefore, we gave higher weight than usual for a branch of the logic tree that considers simulated data (refer to Tables SA-8 and SA-9 in Electronic_Supplement_1.pdf for GMMs and weights in the Seattle basin region).

### *Atlantic and Gulf Coastal Plain amplification models*

Several period-dependent amplification models were evaluated for amplifying ground motions on Gulf and Atlantic Coastal Plain sites that overlie deep wedges of sediments that continue offshore (Boyd et al., 2023 describe details of these models). We considered five amplification models for SAs based on sediment thickness and the distance traversed across the Gulf Coastal plain: Guo and Chapman (2019) and Chapman and Guo (2021, CG21), natural-site-period- and sediment-thickness-based models by Harmon et al. (2019), and the period-dependent and -independent NGA-East Gulf Coast adjustment factors that are path length dependent. Maps of coastal plain sediment thickness (generally Cretaceous and younger post-rift sediments) were compiled for this purpose (Boyd et al., 2023). In addition, ground-motion data from the CEUS for events $M > 3.5$ were also compiled and processed to develop a uniform database of earthquake records (Moschetti et al., 2023a). Boyd et al. (2023) used this database in addition to those prepared by CG21 and NGA-East (Goulet et al., 2021a, 2021b) to compare GMM predictions and found that the variance of total ground-motion residuals in the Coastal Plains could be reduced by about 20% using the CG21 amplification model. The other amplification models reduced residuals by about half as much. One complication with the CG21 model that was highlighted by the GMM review panel is that the amplification model is derived relative to reference stations outside of the Coastal Plain, shown in Figure 2, which do not have a $V_{S30}$ of 3000 m/s, the reference $V_{S30}$ assumed for the NGA-East GMMs. Boyd et al. (2023) sought to estimate the reference condition, finding a range of 1000–2000 m/s, indicating that the reference condition that would be best to use with CG21 is highly uncertain.

We apply a weight of 0.25 to the CG21 model to account for the amplification and deamplification effects of the Coastal Plains (refer to Table SA-5 of Electronic_Supplement_1.pdf for GMMs and weights in the CEUS coastal plain amplification region). The partial weight on the Coastal Plains amplification model was chosen because of the relative newness of the CG21 model and the uncertainty in the reference site condition. The new model has substantial impact on predicted ground motions (maximum reduction of ~80% at 0.03 s and maximum increase of ~100% at 2 s SA for 1 km of sediment), uncertainties about Coastal Plains' resonances and sediment velocity and thickness, and limited data from larger magnitude earthquakes and close-in stations. As future studies are expected to reduce the uncertainties and increase confidence in this modification, the weight on this branch of the logic tree can be expected to increase.

## CEUS-WUS attenuation boundary

Since the publication of the 1996 NSHM for CONUS (Frankel et al., 1996), the same eastern boundary of the Intermountain West region, separating active tectonic WUS crust from stable CEUS crust, has been used (Frankel et al., 1996, 2002; Petersen et al., 2008, 2014, 2020). This boundary is applied by separating earthquakes into CEUS and WUS regions. When calculating hazard at a site from a given fault or seismicity grid cell, the

GMMs appropriate for the source region (CEUS or WUS) are used (e.g. CEUS sources are always used with CEUS GMMs). For the 2018 NSHM, a transition zone between −115 and −100° west longitude (the overlap zone) was used to add rates of exceedances derived from CEUS and WUS GMMs together to compute total mean hazard. Recent studies of earthquakes in the overlap zone show that some of the areas classified as CEUS behave more like WUS GMMs (e.g. Darragh et al., 2019). Levandowski and McNamara (2022) performed surface wave crustal attenuation tomography and stress drop studies in the region that support these findings and have proposed a new boundary that slightly modifies the area around the Colorado Plateau and includes the central and northern portions of the Central and Southern Rocky Mountains in WUS instead of CEUS (Moschetti et al., 2023a; Figure 2 this article). A sensitivity analysis using the 2018 NSHM and transition zone methodology compared sites in the overlap zone using the old boundary and the new proposed boundary, resulting in small (<10% in most places for 2% exceedance in 50-year ground motions) changes in hazard (Moschetti et al., 2023a). We use 100% weight for this new model because it is an update of the older model that is based on additional tomography studies and stress drop analyses. The GMM review panel felt that this model was reasonable for use in the 2023 NSHMs. In the future, GMMs can be treated using alternative methods (e.g. dependence on the fraction of the paths in the CEUS and WUS).

## Hazard results and products

Seismic hazard calculations were performed using the probabilistic seismic hazard analysis computer code, *nshmp-haz* (Powers et al., 2022) and the following source models: 2023 CONUS NSHM (Powers and Altekruse, 2022a), 2023 Alaska NSHM (Powers and Altekruse, 2023), and 2021 Hawaii NSHM (Powers and Altekruse, 2022b).

### *Seismic hazard ground-motion maps and comparisons to older models*

The 2023 CONUS, 2023 Alaska, and 2021 Hawaii models apply the new ERF and GMMs with the proposed weights described above. Hazard results are generated for 2%, 5%, 10%, and other periods for PE in 50 years for SAs at 21 oscillator periods, 2 peak parameters (PGA, PGV), MMI, and 8 National Earthquake Hazards Reduction Program (NEHRP) site classes following past NSHMs (Shumway et al., 2021). These data sets can be found at the USGS ScienceBase Catalog (CONUS: Petersen et al., 2023, Alaska: Powers et al., 2023, Hawaii: Rukstales et al., 2021). A limited set of these results are presented here, along with comparisons to the past models.

The 2% PE in 50 years for 0.2 s SA at $V_{S30}$ of 760 m/s hazard maps for CONUS, Alaska, and Hawaii is shown in Figure 8. Seismic hazard is greater than 1 g along coastal California, Oregon, and Washington; across the eastern portion of California and western Nevada; along the Wasatch front in Utah and continuing north into the Yellowstone region of Wyoming, Montana, and Idaho; within the CEUS New Madrid region of Tennessee, Arkansas, Missouri, Illinois, and Kentucky, and eastern Tennessee, and the Charleston region of South Carolina; across the southern portions of Alaska; and within the Island of Hawai'i and Maui. The 2% PE in 50 years for 5 s SA at $V_{S30}$ of 260 m/s hazard maps for CONUS, Alaska, and Hawaii is shown in Figure 9. Seismic hazard that exceeds 0.1 g occurs in similar areas as those shown for the 1 g threshold at 0.2 s. The corresponding hazard maps for 10% in 50-year PE are shown in Figure SB-2 and SB-3 in Electronic_Supplement_1.pdf. Total mean hazard ground-motion maps (2% and 10% in 50-year PE, 0.2, 1.0, and 5.0 s SA, $V_{S30}$ of 760 m/s) for select regions (Puget Sound, San

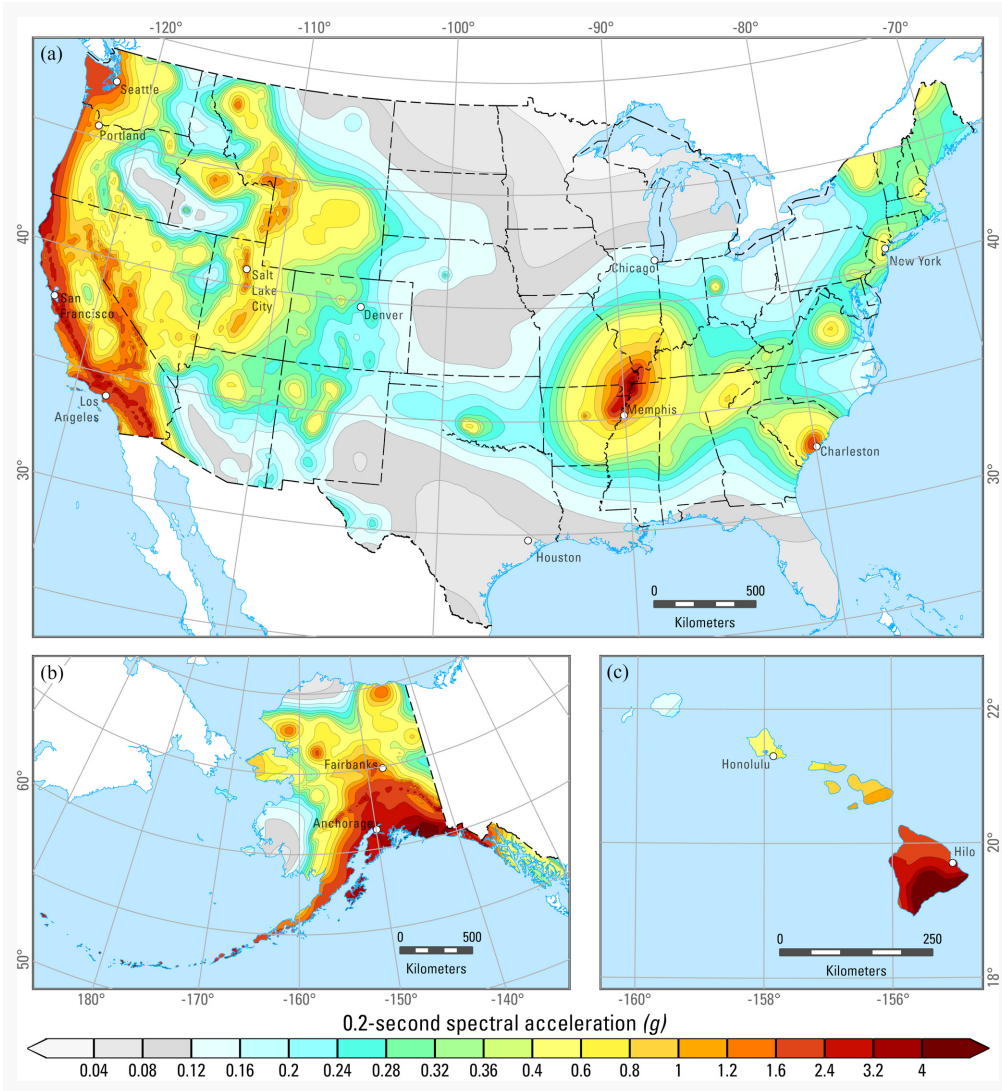


**Figure 8.** Maps of 0.2 s spectral acceleration total mean hazard for 2% probability of exceedance in 50 years, NEHRP site class boundary B/C ($V_{S30}$ = 760 m/s), calculated for the 2023 NSHM for (a) the conterminous United States, (b) Alaska, and (c) Hawaii.

Francisco Bay Area, Los Angeles Basin region, Wasatch Front region, NMSZ region, and the northern Eastern Seaboard) are shown in Electronic_Supplement_1.pdf (Figures SB-4 to SB-9, respectively).

The general map patterns of the 2023 NSHMs are very similar to previous NSHMs, but the details of ground-shaking differences (Figures 10 and 12) and ratios (Figures 11 and 13) can be substantial (these changes were reviewed by multiple panels, see Note 1). Comparisons of the 2018 NSHM and 2023 NSHM 0.2 and 1 s SA ground motions for 2% PE in 50 years on a uniform $V_{S30}$ = 760 m/s show that most sites are within about 50% of one another, but there also some that are higher or lower (refer to

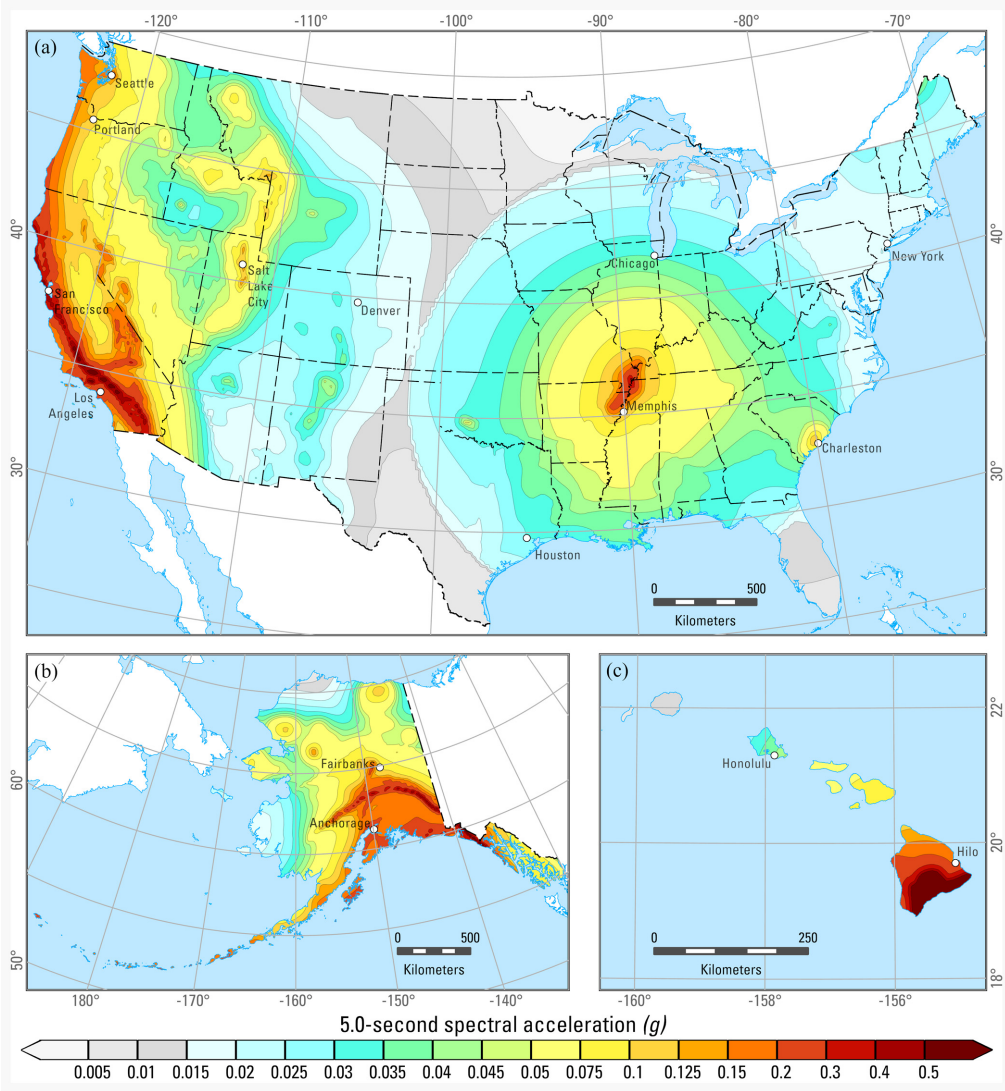


**Figure 9.** Maps of 5 s spectral acceleration total mean hazard for 2% probability of exceedance in 50 years, NEHRP site class D ($V_{S30}$ = 260 m/s), calculated for the 2023 NSHM for (a) the conterminous United States, (b) Alaska, and (c) Hawaii.

Electronic_Supplement_1.pdf, Appendix B, Figure SB-17). Many of the calculated changes in the model are caused by new fault and deformation models that have broad epistemic uncertainties and influence the immediate region surrounding the faults. Newly modeled faults across the region have increased the computed hazard, especially in low seismicity regions of the WUS. Within the CEUS, many of the broad changes in the model observed, especially in the ratio maps, are in low seismicity areas that are influenced by the gridded seismicity model or new newly applied fault zones. There are several reasons for the gridded seismicity changes: (1) catalog, (2) decluster models, (3) gridded seismicity models that consider full-catalog rates, (4) weighting of the fixed and adaptive smoothing models, (5) *b*-value changes, (6) application of the full versus declustered rates, and (7)

methodology changes caused by the catalog being cut-off at 104 degree longitude and a slightly altered CEUS-WUS attenuation/catalog boundary. In addition, there were several changes to the GMMs that result in changes in the 2023 NSHM. For example, we implemented new NGA-Subduction GMMs, which tend to lower the calculated ground motions beyond a few hundred kilometers of the coast in most places and for long-period GMMs (1 s). The computed ground motions are increased along a narrow strip of land located along coastal California, Oregon, and Washington for short periods (0.2 s) but decay with distance from the coast. The application of amplification models also makes significant long-period (1 s) changes to the maps. For example, adding Great Valley and Portland/Tualatin and updating the San Francisco Bay area and Los Angeles regions result in increased long-period hazard in the deepest portions of the sedimentary basins. Modifying the long-period ground motions with 3D simulations increases the computed hazard in Seattle and does not cause substantial changes in Los Angeles (Moschetti et al., 2023a). The application of the Coastal Plain amplification model causes changes in ground motions of about a factor of two, with decreases in computed hazard at short periods (0.2 s) and increases in hazard at long periods (>1 s). Alaska changes are also very substantial with changes along the Aleutian arc due to subduction zone rate model and GMM revisions. The Alaska review panel provided important information on the Alaska science that underlies these chanjes. We also convened the Tiger Team, which included NGA-Subduction modelers, to provide additional input and recommendations on the science behind these changes in Alaska hazard. Changes in interior Alaska are due to updates to gridded seismicity and crustal fault models. Hawaii changes are caused by the new fault-zone characterization, new time-dependent rate models, and new GMMs. For these return periods and short periods (0.2 s), the entire main island has ground motions that are higher than in the previous NSHM whereas the outer islands decrease due to these updates. For long periods (1 s), the changes are mixed with highs along the coasts and lows in a saddle across the middle of the Island of Hawai‘i and lower computed hazard again on the northern islands. These chanes were reviewed by the Hawaii review panel (Petersen et al., 2022).

Figures 10 to 13 are annotated to show where, why, and how the 2023 computed hazard changed compared to the past NSHMs. We published similar comparisons for the 2018 NSHM with the 2014 NSHM that show increases due to the GMMs in the CEUS and long-period amplifications due to sedimentary basin amplifications in the WUS (Petersen et al., 2021). Comparisons of the 2023 NSHM for CONUS with the 2018 NSHM for CONUS (Figures 10 to 13a to c and Table 1) indicate that ground motions decrease for short periods (0.2 s) near New Madrid and Charleston. The increase in hazard in areas in the CEUS, including along the mid and northern Atlantic seaboard, is attributed to changes in earthquake catalogs, *b*-values, declustering, and gridded seismicity parametric changes (refer to Electronic_Supplement_1.pdf, Appendix C, Figures SC-4 and SC-5). Increases can also be seen near the New Madrid, Saline River, and Central Virginia sources where fault zones were added or updated. The addition of the NGA-East amplification adjustment and Coastal Plain Amplification models bring down the hazard at short periods. Ground motions for longer periods (1 s SA) increased in regions of many CEUS regions due to coastal plain amplification modifications.

Within the WUS, the 2023 hazard varies with both substantial increases and decreases. Much of the California, Olympic Peninsula, and Rocky Mountain regions are elevated compared to the previous 2018 NSHM at 0.2 s SA 2% PE in 50 years. These increases are mostly due to changes in fault rates, earthquake catalogs, and for the Olympic Peninsula,

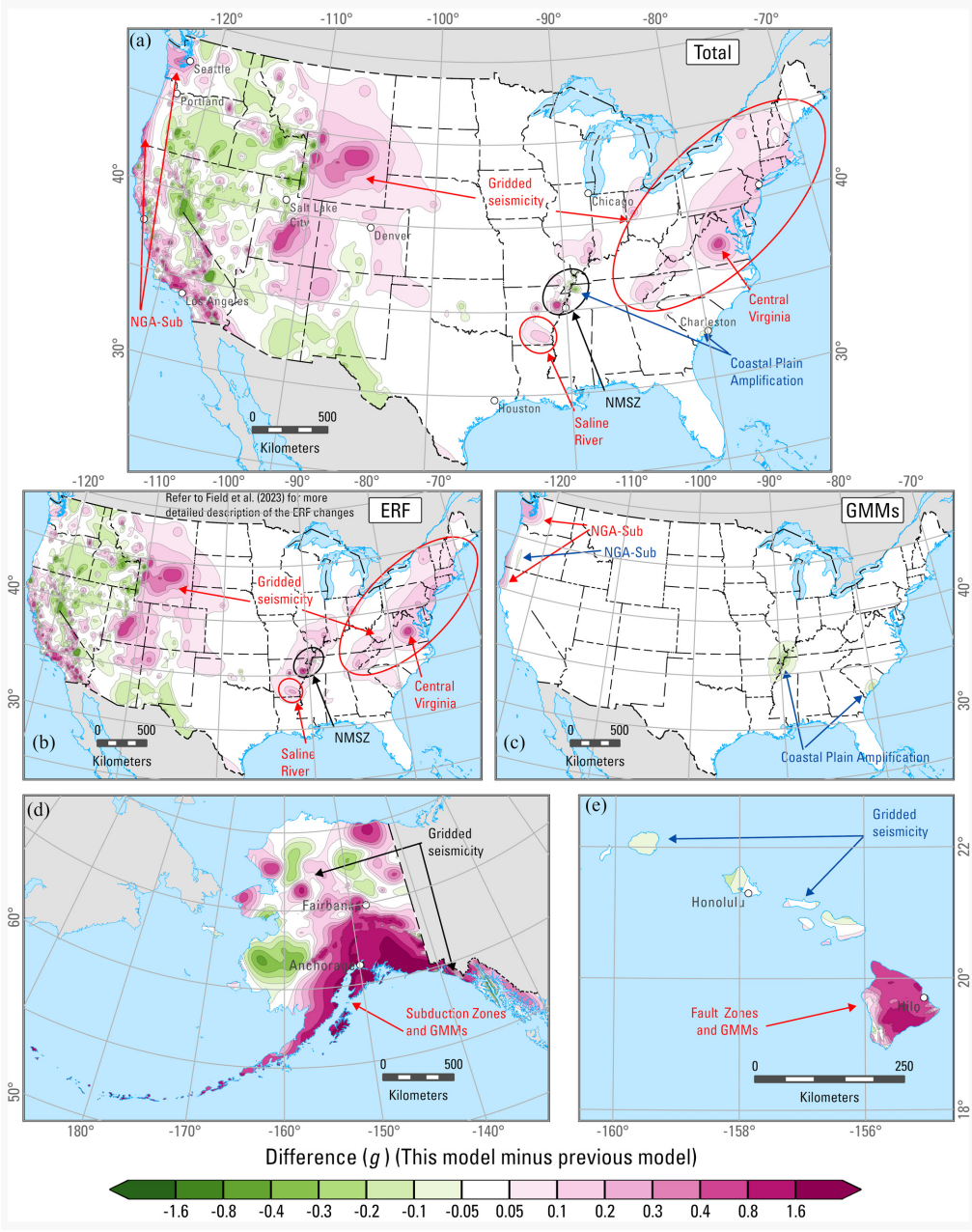


**Figure 10.** Difference maps for 0.2 s spectral acceleration showing comparisons between total mean hazard from (a, b, c) the 2023 CONUS NSHM and 2018 CONUS NSHM, (d) 2023 Alaska NSHM and 2007 Alaska NSHM, and (e) 2021 Hawaii NSHM and 2001 Hawaii NSHM for 2% probability of exceedance in 50 years, and NEHRP site class boundary B/C ($V_{S30}$ = 760 m/s). Red text and blue text represent areas where hazard went up or down, respectively, while black text indicates no change in hazard.

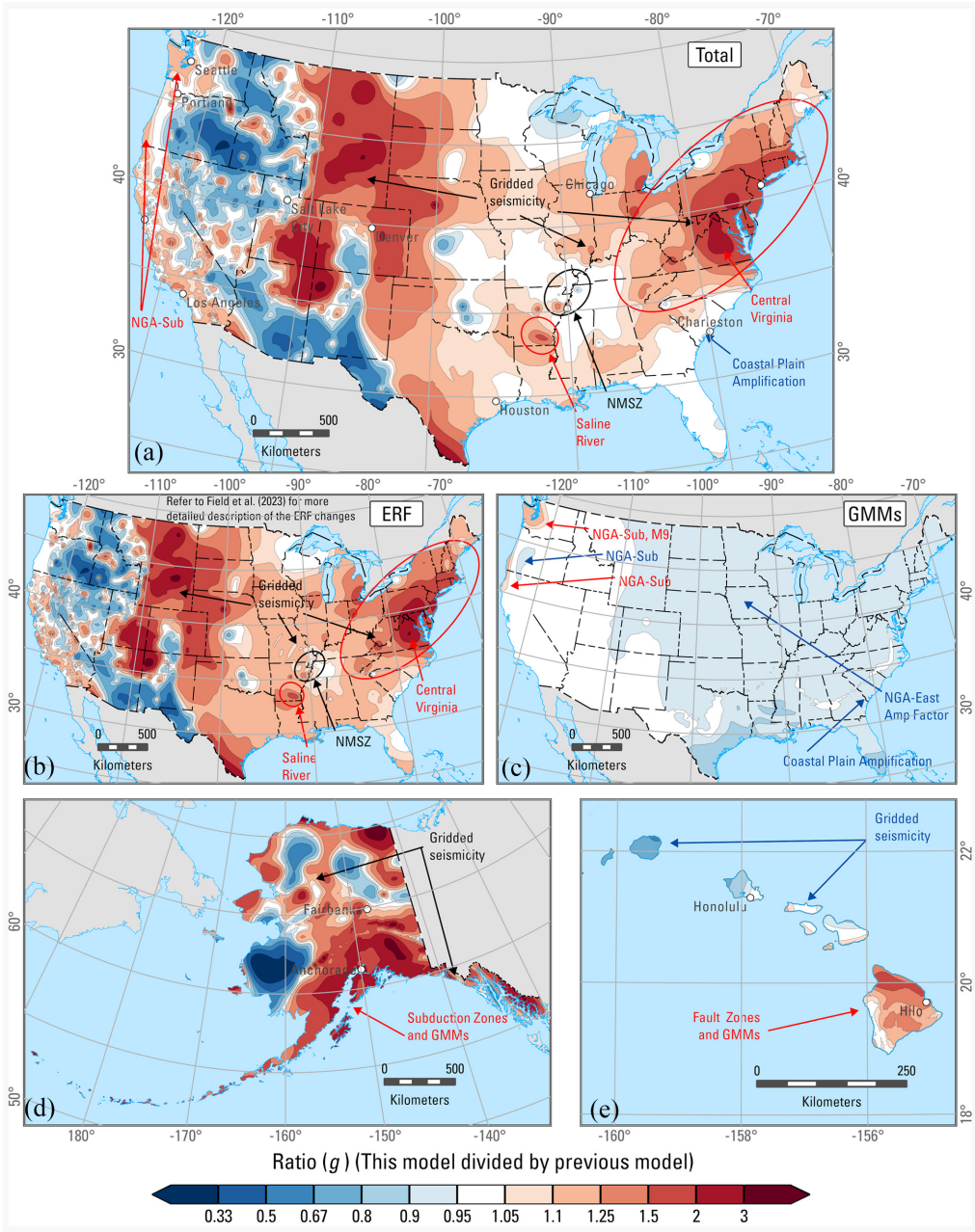


**Figure 11.** Ratio maps showing comparisons between total mean hazard for 0.2 s spectral acceleration from the (a, b, c) 2023 CONUS NSHM and 2018 CONUS NSHM, (d) 2023 Alaska NSHM and 2007 Alaska NSHM, and (e) 2021 Hawaii NSHM and 2001 Hawaii NSHM, 2% probability of exceedance in 50 years, and NEHRP site class boundary B/C ($V_{S30}$ = 760 m/s). Red text and blue text represent areas where hazard went up or down, respectively, while black text indicates no change in hazard.

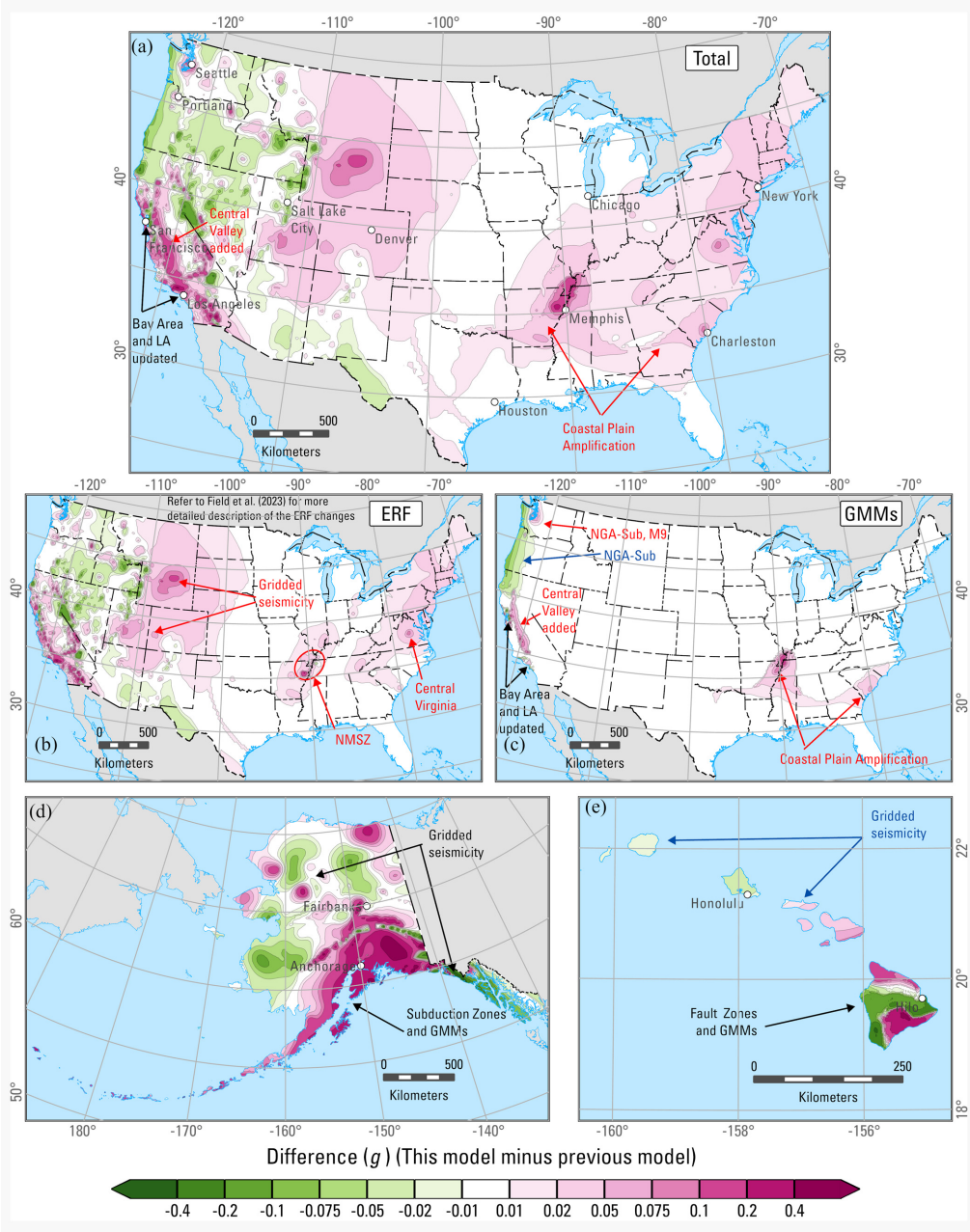


**Figure 12.** Difference maps showing comparisons between total mean hazard from the (a, b, c) 2023 CONUS NSHM and 2018 CONUS NSHM, (d) 2023 Alaska NSHM and 2007 Alaska NSHM, and (e) 2021 Hawaii NSHM and 2001 Hawaii NSHM for 1 s spectral acceleration, 2% probability of exceedance in 50 years, and NEHRP site class boundary B/C ($V_{S30}$ = 760 m/s). Red text and blue text represent areas where hazard went up or down, respectively, while black text indicates no change in hazard.

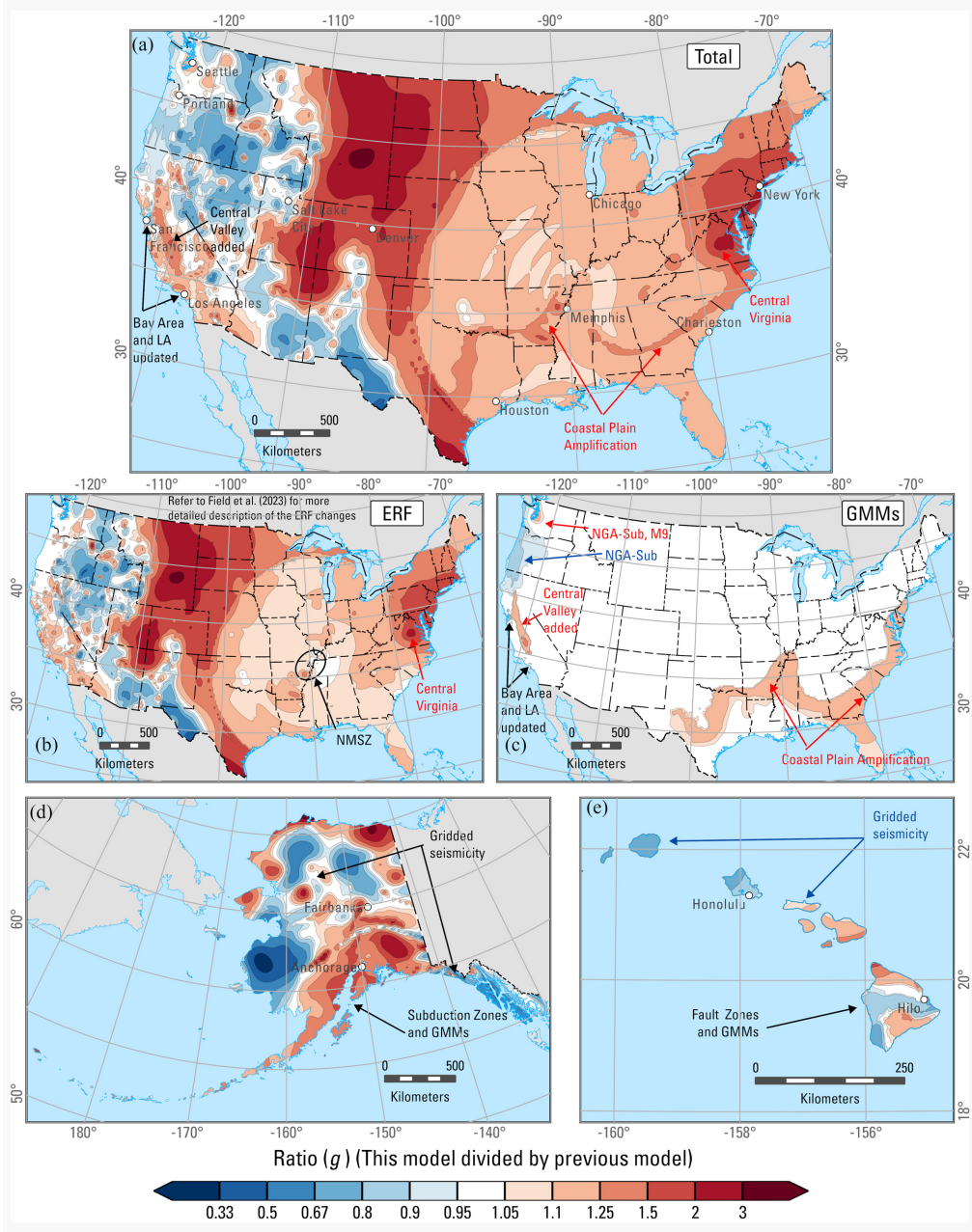


**Figure 13.** Ratio maps showing comparisons between total mean hazard for 1 s spectral acceleration from the (a, b, c) 2023 CONUS NSHM and 2018 CONUS NSHM, (d) 2023 Alaska NSHM and 2007 Alaska NSHM, and (e) 2021 Hawaii NSHM and 2001 Hawaii NSHM, 2% probability of exceedance in 50 years, and NEHRP site class boundary B/C ($V_{S30}$ = 760 m/s). Red text and blue text represent areas where hazard went up or down, respectively, while black text indicates no change in hazard.

**Table 1.** Comparison of total mean hazard for sites across the United States

| Site name | Latitude | Longitude | 2023 NSHM | 2021 NSHM | 2018 NSHM | 2007 NSHM | 2001 NSHM | Difference (g) | Ratio (%) |
|---|---|---|---|---|---|---|---|---|---|
| 0.2 s spectral acceleration | | | | | | | | | |
| Anchorage, Alaska | 61.20 | −149.90 | 3.36 | | | 1.55 | | 1.82 | 118 |
| Fairbanks, Alaska | 64.90 | −147.70 | 1.16 | | | 0.94 | | 0.22 | 24 |
| Los Angeles, California | 34.05 | −118.25 | 2.15 | | 2.07 | | | 0.08 | 4 |
| San Francisco, California | 37.75 | −122.40 | 1.95 | | 1.77 | | | 0.18 | 10 |
| Denver, Colorado | 39.75 | −105.00 | 0.25 | | 0.17 | | | 0.08 | 44 |
| Hilo, Hawaii | 19.70 | −155.06 | | 2.40 | | | 1.80 | 0.60 | 34 |
| Honolulu, Hawaii | 21.30 | −157.86 | | 0.60 | | | 0.61 | −0.02 | −3 |
| Chicago, Illinois | 41.85 | −87.65 | 0.16 | | 0.14 | | | 0.02 | 15 |
| New York, New York | 40.75 | −74.00 | 0.43 | | 0.25 | | | 0.19 | 77 |
| Portland, Oregon | 45.50 | −122.65 | 1.19 | | 0.68 | | | 0.52 | 76 |
| Charleston, South Carolina | 32.80 | −79.95 | 1.48 | | 1.57 | | | −0.09 | −6 |
| Memphis, Tennessee | 35.15 | −90.05 | 1.33 | | 1.26 | | | 0.07 | 5 |
| Houston, Texas | 29.75 | −95.35 | 0.08 | | 0.07 | | | 0.00 | 6 |
| Salt Lake City, Utah | 40.75 | −111.90 | 1.65 | | 1.71 | | | −0.06 | −3 |
| Seattle, Washington | 47.60 | −122.30 | 1.74 | | 1.44 | | | 0.30 | 21 |
| 1.0 s spectral acceleration | | | | | | | | | |
| Anchorage, Alaska | 61.20 | −149.90 | 0.96 | | | 0.61 | | 0.34 | 56 |
| Fairbanks, Alaska | 64.90 | −147.70 | 0.31 | | | 0.29 | | 0.02 | 7 |
| Los Angeles, California | 34.05 | −118.25 | 0.71 | | 0.64 | | | 0.07 | 12 |
| San Francisco, California | 37.75 | −122.40 | 0.65 | | 0.61 | | | 0.04 | 7 |
| Denver, Colorado | 39.75 | −105.00 | 0.07 | | 0.04 | | | 0.03 | 83 |
| Hilo, Hawaii | 19.70 | −155.06 | | 0.71 | | | 0.77 | −0.06 | −8 |
| Honolulu, Hawaii | 21.30 | −157.86 | | 0.16 | | | 0.18 | −0.02 | −12 |
| Chicago, Illinois | 41.85 | −87.65 | 0.07 | | 0.06 | | | 0.01 | 13 |
| New York, New York | 40.75 | −74.00 | 0.08 | | 0.04 | | | 0.04 | 86 |
| Portland, Oregon | 45.50 | −122.65 | 0.38 | | 0.33 | | | 0.05 | 17 |
| Charleston, South Carolina | 32.80 | −79.95 | 0.39 | | 0.34 | | | 0.05 | 15 |
| Memphis, Tennessee | 35.15 | −90.05 | 0.40 | | 0.33 | | | 0.08 | 24 |
| Houston, Texas | 29.75 | −95.35 | 0.04 | | 0.04 | | | 0.00 | 12 |
| Salt Lake City, Utah | 40.75 | −111.90 | 0.55 | | 0.57 | | | −0.02 | −4 |
| Seattle, Washington | 47.60 | −122.30 | 0.70 | | 0.59 | | | 0.12 | 20 |

*(continued)*

**Table 1.** (continued)

| Site name | Latitude | Longitude | 2023 NSHM | 2021 NSHM | 2018 NSHM | 2007 NSHM | 2001 NSHM | Difference (g) | Ratio (%) |
|---|---|---|---|---|---|---|---|---|---|
| 5.0 s spectral acceleration | | | | | | | | | |
| Anchorage, Alaska | 61.20 | −149.90 | 0.22 | | | | | | |
| Fairbanks, Alaska | 64.90 | −147.70 | 0.11 | | | | | | |
| Los Angeles, California | 34.05 | −118.25 | 0.23 | | 0.23 | | | −0.01 | −2 |
| San Francisco, California | 37.75 | −122.40 | 0.30 | | 0.34 | | | −0.04 | −12 |
| Denver, Colorado | 39.75 | −105.00 | 0.02 | | 0.01 | | | 0.01 | 136 |
| Hilo, Hawaii | 19.70 | −155.06 | | 0.21 | | | | | |
| Honolulu, Hawaii | 21.30 | −157.86 | | 0.04 | | | | | |
| Chicago, Illinois | 41.85 | −87.65 | 0.03 | | 0.03 | | | 0.01 | 36 |
| New York, New York | 40.75 | −74.00 | 0.02 | | 0.01 | | | 0.01 | 119 |
| Portland, Oregon | 45.50 | −122.65 | 0.13 | | 0.15 | | | −0.02 | −13 |
| Charleston, South Carolina | 32.80 | −79.95 | 0.09 | | 0.07 | | | 0.02 | 24 |
| Memphis, Tennessee | 35.15 | −90.05 | 0.13 | | 0.10 | | | 0.03 | 31 |
| Houston, Texas | 29.75 | −95.35 | 0.03 | | 0.02 | | | 0.01 | 66 |
| Salt Lake City, Utah | 40.75 | −111.90 | 0.15 | | 0.16 | | | 0.00 | −1 |
| Seattle, Washington | 47.60 | −122.30 | 0.23 | | 0.24 | | | −0.01 | −5 |

NSHM: National Seismic Hazard Model; NEHRP: National Earthquake Hazards Reduction Program.

The 2% probability of exceedance in 50 years for ground motions (g); NEHRP site class boundary B/C ($V_{S30}$ = 760 m/s) for 0.2 and 1 s spectral acceleration and NEHRP site class D ($V_{S30}$ = 260 m/s) for 5 s spectral acceleration. Red text and blue text represent areas where hazard went up or down, respectively, while black text indicates no change in hazard. Values have been rounded to two decimal places. Difference and ratio values were calculated prior to rounding.

the NGA-Subduction GMMs. Fault-based inversion models have lowered the hazard in parts of southern California and the intermountain west region (Field et al., 2023). Broad calculated decreases in ground-motion estimates for this region are caused by the ERF that links adjacent faults to make longer ruptures and, in the process, earthquakes use more moment per event—resulting in all multi-fault ruptures happening less frequently. Colorado, Wyoming, and Montana increased substantially due to changes in the methodology, which put earthquakes classified previously as CEUS into the WUS category for rates, allowing for a lower *b*-value, higher minimum magnitude threshold (which is the lower limit of hazard integrations), and other factors. The differences between the 2018 and 2023 NSHMs in the Rocky Mountain region are due to magnitude changes caused by the earthquake catalog prioritization, declustering, *b*-value changes from 1.0 to 0.94 in the CEUS and 0.82 to 0.81 in the WUS, and smoothing parameters. This is described in much more detail in Electronic_Supplement_1.pdf, Appendix C. Uniform floor zones were removed in areas of the Rocky Mountains, central California, Seattle, and Portland/Tualatin basins due to, respectively, addition of the new methodology for separating earthquake catalogs, Great Valley basins, NGA-Subduction and M9 3D simulations, and addition of basin-depth amplification models. Long-period ground motions decrease along the Pacific Northwest region at 1 s SA oscillator period due to addition of new GMMs (NGA-Subduction). For the Cascadia subduction zone region of the Pacific Northwest, our sensitivity studies holding either ERF or GMM models fixed to 2018 NSHM while varying the other parameters show that ground motions are slightly elevated near the coastline due to the addition of the NGA-Subduction models and slightly decreased inland due to the ERF model changes. Short-period ground motions are elevated in Seattle due to NGA-Subduction intraslab equations.

The 2023 NSHM for Alaska implies increases of greater than a factor of two of 2% in 50-year 0.2 s SA ground motions relative to the 2007 NSHM along the Aleutian arc and across south-central Alaska. For 1 s SA the increases are lower. These changes are due to subduction zone rate and GMM changes and updates to gridded seismicity and crustal fault models. In particular, the 3,440-km-long Aleutian megathrust subduction interface, which accommodates 60+ mm/yr of Pacific plate motion relative to stable North America, is characterized with a rupture rate model that is higher than in the 2007 NSHM. The geologic recurrence rates at the east end of the megathrust are marginally higher than in 2007. Paleoseismic and paleotsunami records only extended as far west as Kodiak Island and so geologic recurrence rates over the western Aleutians are based on a 200- to 210-year estimate of recurrence for the Fox Islands section. In the 2007 NSHM, rates in the western Aleutians were constrained with catalog seismicity rates that were somewhat lower. The geodetic recurrence rates over the length of the subduction zone are based on estimates of coupling and slip-deficit (Briggs et al., 2023) and are moment balanced against slip rate on the subduction zone. For those magnitude-area scaling relations that yield smaller rupture magnitudes, these ruptures consume less moment when moment-balancing and consequently have higher rates (several as short as a 50-yr return period) than their geologic counterparts, especially at the eastern end. The subduction interface GMMs and associated epistemic uncertainty branches yield slightly higher median ground motion at short periods. Substantially higher aleatory variability decreases the slope of the hazard curve and produces larger ground motions at 2% in 50-year return periods.

Changes to the distribution of intraslab seismicity (using Slab2 instead of uniform depth slices in the 2007 Alaska NSHM) also give rise to increases in hazard because intraslab point sources are somewhat closer to sites like Anchorage than they were in 2007.

Reductions in south central and southeast Alaska arise from fault-system modeling of the Queen Charlotte—Fairweather system that puts more moment into larger magnitude events and the removal of the Chatham Straight fault. Increases in this area are due to addition of numerous high slip rate strike-slip and reverse faults that accommodate the change from a transform plate boundary in southeast Alaska to compressive structures in the hanging wall of the subduction megathrust. Although the median subduction GMMs in the 2023 NSHM are generally lower than their 2007 counterparts, more so at long periods. At short distances, the medians are higher and thus further contribute to hazard increases close to and over the subduction interface. High sigmas in some of the GMMs also contribute to increases in hazard (Table SA-4 in Electronic_Supplement_1.pdf).

The Hawaii NSHM released in 2021 (Petersen et al., 2022) was based on declustered catalog rates which are about 10% lower than the full-catalog rates that are applied in CONUS and Alaska. Estimated hazard increased in portions of the Island of Hawai'i but decreased in areas to the north compared to the 2001 NSHM due to changes in the fault, gridded seismicity, and GMMs.

### *Mean hazard curves*

A comparison of total mean hazard curves for the 15 selected test sites are shown in Figure 14 for 0.2 and 1 s SA, $V_{S30}$ = 760 m/s. The 2023 hazard curves are shown with solid lines, and older model hazard curves are shown with dashed lines. For 0.2 and 1 s SA, at 2% PE in 50 years, Anchorage, Hilo, Los Angeles, San Francisco, Seattle, and Salt Lake City have the highest ground motions. CEUS hazard curves have different shapes than those in the WUS due to differences in WUS and CEUS GMMs, mostly due to crustal attenuation properties. Ground motions in the WUS decay faster with distance than those in the CEUS. Ground motions are substantially different at Denver, Chicago, New York, and Houston for both short and long periods compared to the previous NSHM. Hazard curves for sites in California are substantially higher than those in the CEUS.

## Uniform-hazard response spectra

Uniform-hazard response spectra (UHRS) were also generated for each of the 15 test sites for 2% PE in 50 years. UHRS for six of these sites are shown in Figure 15; ground motions for all six sites show similar response spectra shapes but differ for Anchorage where site conditions appear to be playing a significant role between 0.1 and 1 s SA, reaching >4 g at 0.3 s SA for NEHRP site class E ($V_{S30}$ = 150 m/s). Spectral ordinates at all these sites exceed 1 g acceleration for most site conditions and fall off for longer periods. CEUS sites have different UHRS characteristics than those in the WUS due to differences in WUS and CEUS GMMs and amplification models (i.e. the shape of the UHRS in Memphis differs from the others). Also, there is no discernible shift in PGA from rock to soft soil conditions due to differences between amplification models for NGA-East and for other regions.

### *Disaggregations*

For the 2023 NSHM, we examined disaggregations at several sites to determine the controlling features in the model. The NSHM webtool (www.earthquake.usgs.gov/nshmp/hazard/disagg) produces disaggregations for the 50-state 2023 model that can be generated

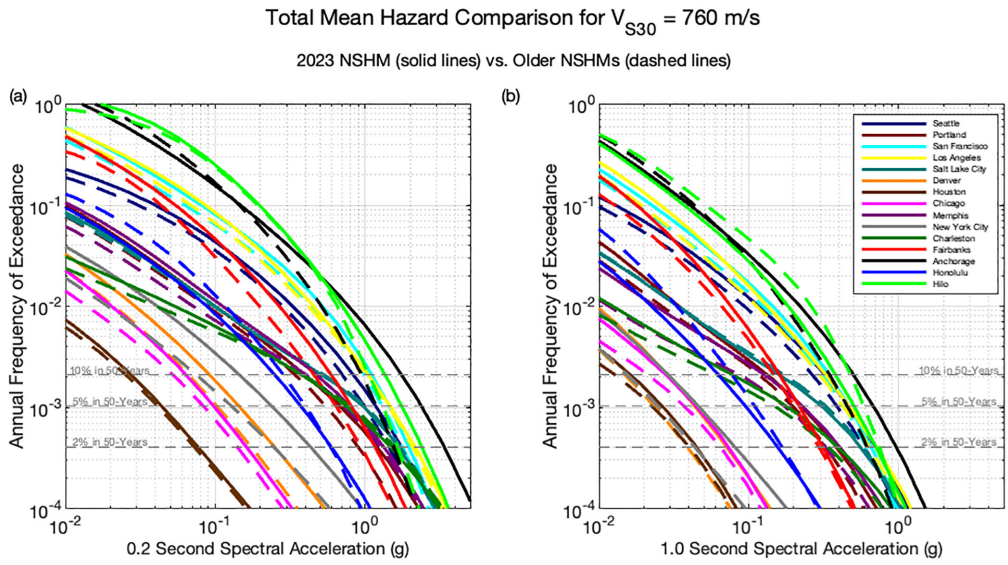


**Figure 14.** Comparison of total mean hazard curves for 15 sites across the United States is shown for the 2023 NSHM (CONUS and Alaska) and 2021 NSHM (Hawaii) (solid lines) versus the 2018 NSHM (CONUS, dashed lines), 2007 NSHM (Alaska, dashed lines), and 2001 NSHM (Hawaii, dashed lines). Hazard curves are plotted for (a) 0.2 s spectral acceleration and (b) 1 s spectral acceleration, NEHRP site class boundary B/C ($V_{S30}$ = 760 m/s).

for any site, location, period, or site class. For example, Figure 16 shows disaggregations for Los Angeles, California, 5 s SA at $V_{S30}$ = 329 m/s and 2% in 50-year PE. This site includes information from the new ERF, new basin-amplification model for CyberShake, and for NGA-West2. The controlling features are local faults (~98%) and grid sources (~2%). A list of all sources and their contributions to hazard (magnitude, distance, epsilon—difference in standard deviation units) are shown below the magnitude distance plots. A disaggregation for Seattle, Washington, is shown in Figure SB-10 in Electronic_Supplement_1.pfd, Appendix B.

## *Fractile hazard curves*

The mean hazard curves like those in Figure 14 consist of weighted averages across all the logic-tree branches of the ERF and GMMs summarized above. To quantify the epistemic uncertainty distribution corresponding to each mean hazard curve, it is common to also compute hazard curve fractiles (e.g. Figure 17). We calculate hazard fractiles at five sites - San Francisco, Salt Lake City, Honolulu, Los Angeles, and New York City - to show fractile differences in representative sites across Hawaii, WUS, and CEUS. An uncertainty analysis was also performed for Anchorage, but it was based on an earlier draft model. To avoid confusion, we have removed the Anchorage uncertainty results. The calculations differ in the level of completeness of the inputs because complete computation of fractile hazard curves is not yet available within the *nshmp-haz* and OpenSHA codes. At the Honolulu and New York sites, only the most important branches contributing at least 95%, in total, to the mean hazard are considered, based on disaggregation analysis. The New York site only accounts for the means of the four suites of GMMs; it does not fully

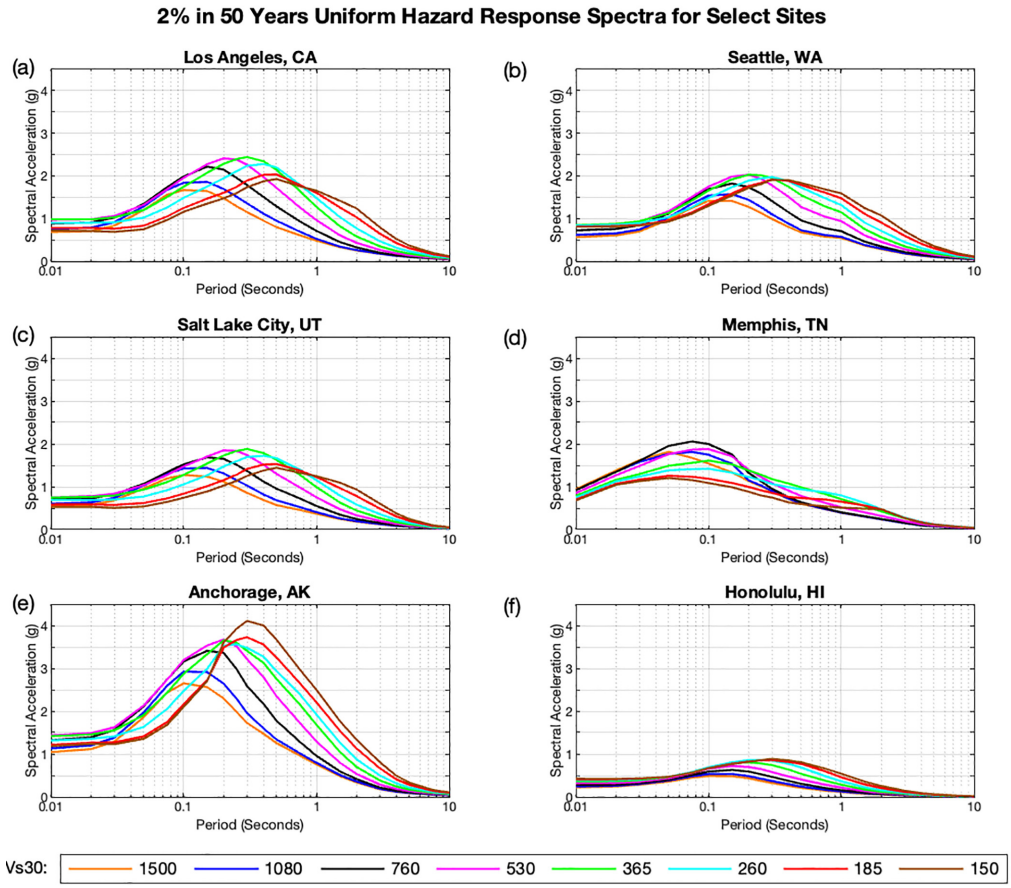


**Figure 15.** Uniform-hazard response spectra are plotted for six sites in the United States for a 2% probability of exceedance in 50 years. Values are calculated for NEHRP site classes B ($V_{S30}$ = 1080 m/s), C ($V_{S30}$ = 530 m/s), D ($V_{S30}$ = 260 m/s), and E ($V_{S30}$ = 150 m/s) and site class boundaries AB ($V_{S30}$ = 1500 m/s), BC ($V_{S30}$ = 760 m/s), CD ($V_{S30}$ = 365 m/s), and D/E ($V_{S30}$ = 185 m/s).

account for the spread in GMMs, as we averaged over the 17 NGA-East, 14 updated seed models, and the two adjusted NGA-East and seed models (described in section "GMM"). The sites in San Francisco, Los Angeles, and Salt Lake City are based on a more thorough uncertainty analysis of the logic tree but do not consider the basin-amplification models, which would add to the total uncertainty. Otherwise, the resulting fractile hazard curves represent distributions of hazard curves derived from traversing potential paths of the logic tree (ERF and GMM branches), with correlation assumptions mentioned below. This analysis is done to provide a first approximation of the overall hazard uncertainty, but future analyses could consider the other factors that may result in changes in the uncertainty assessment (e.g. basin-response, basin-edge uncertainties). The logic-tree uncertainty analysis here provides a general assessment of the range in ground motions or exceedances from the various fractiles, but more work would be needed to refine these estimates. In addition to more *nshmp-haz* development, further research requirements needed to improve the assessments are described in section "Discussion" and "Conclusion."

(a)

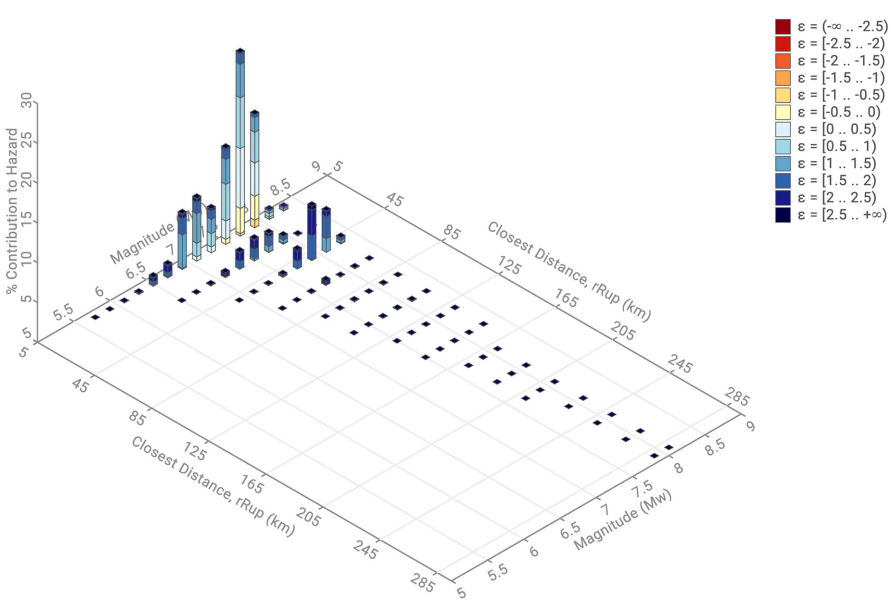


(b)

| Source Set ↳ Source | Type | r | m | $\varepsilon_0$ | lon | lat | az | % |
|---|---|---|---|---|---|---|---|---|
| WUS Branch Average | FaultSystem | | | | | | | 98.23 |
| Puente Hills (Los Angeles) (1) | | 4.67 | 7.52 | 0.53 | 118.272°W | 34.024°N | 214.81 | 18.96 |
| San Andreas (Mojave, south) (8) | | 55.55 | 7.96 | 1.91 | 117.983°W | 34.498°N | 26.13 | 14.68 |
| Compton (2) | | 14.48 | 7.66 | 0.64 | 118.354°W | 33.844°N | 202.79 | 13.97 |
| Elysian Park (upper) (1) | | 5.40 | 7.21 | 1.00 | 118.231°W | 34.076°N | 30.79 | 8.27 |
| Raymond (2) | | 8.76 | 7.44 | 0.99 | 118.224°W | 34.124°N | 16.33 | 5.91 |
| Sierra Madre (5) | | 19.91 | 7.87 | 1.15 | 118.179°W | 34.219°N | 19.24 | 4.89 |
| Newport - Inglewood (8) | | 11.70 | 7.66 | 0.75 | 118.361°W | 34.000°N | 241.55 | 4.12 |
| Hollywood (0) | | 8.34 | 7.50 | 0.88 | 118.264°W | 34.123°N | 351.13 | 3.89 |
| Puente Hills (Santa Fe Springs) (1) | | 12.82 | 7.55 | 0.84 | 118.144°W | 33.926°N | 144.47 | 2.34 |
| Whittier (7) | | 19.68 | 7.57 | 1.46 | 118.046°W | 33.999°N | 106.82 | 2 |
| Raymond (1) | | 12.80 | 7.48 | 1.26 | 118.142°W | 34.121°N | 51.27 | 1.94 |
| Palos Verdes (13) | | 27.12 | 7.36 | 2.03 | 118.439°W | 33.863°N | 220.02 | 1.73 |
| Compton (3) | | 14.62 | 7.22 | 1.20 | 118.414°W | 33.865°N | 216.36 | 1.68 |
| Santa Susana (0) | | 31.75 | 7.65 | 1.92 | 118.344°W | 34.324°N | 344.15 | 1.27 |
| WUS Branch Average (opt) | Grid | | | | | | | 1.77 |

**Figure 16.** (a) Disaggregation for a site in Los Angeles, California (34.05, −118.25). Results for 2% in 50-year probability of exceedance, 5 s SA, $V_{S30}$ = 329 m/s. (b) Example table showing percent contribution of sources which is available on the NSHMP website tools; for details of faults see references herein. r = distance, m = magnitude, $\varepsilon_0$ = epsilon, lon = longitude, lat = latitude, az = azimuth, % = percent contribution. For a map showing the site and contributing seismic sources, use webtool: USGS Earthquake Hazard Toolbox—https://earthquake.usgs.gov/nshmp/hazard/disagg.

For most of the sites in Figure 17, the separation between mean and median (50th fractiles) hazard curves is not very large, which could indicate a symmetric distribution of epistemic uncertainty. The 5th and 95th fractiles in Figure 17 show ground-motion uncertainties at 2% PE in 50 years that span about a factor of two or three. These uncertainties are from correlated propagation of GMM and ERF uncertainties, which increases their span compared to application of uncorrelated or partially correlated calculations at each site. On the contrary, the epistemic uncertainty represented is not necessarily complete, as disclaimed above, and future work that considers a more complete logic tree may

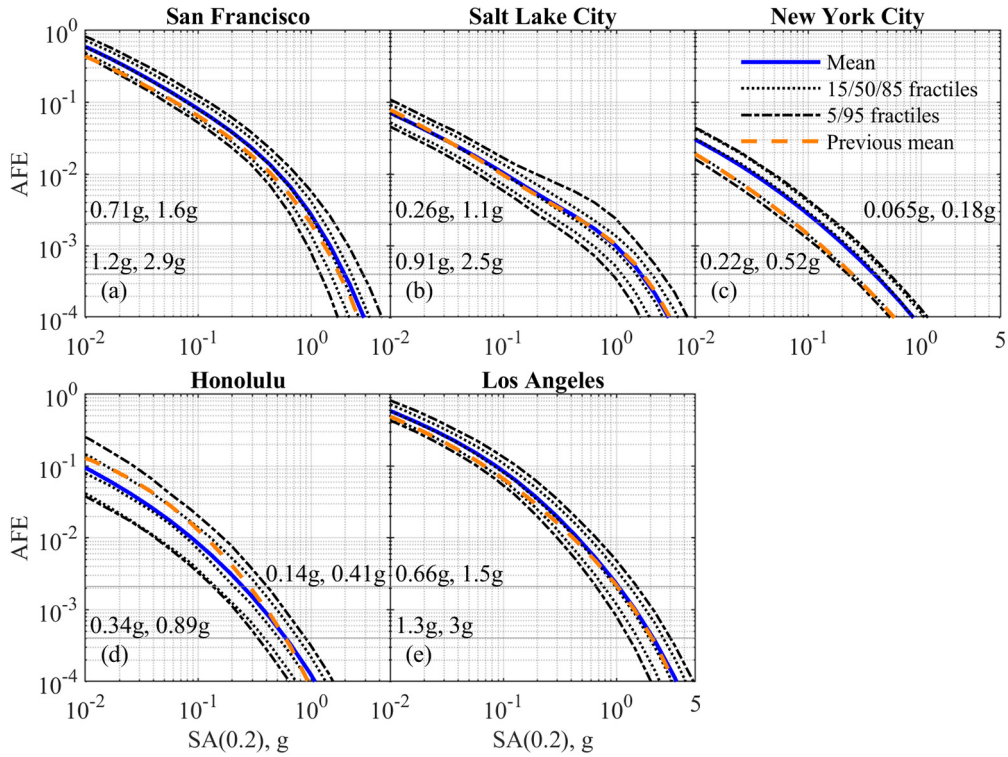


**Figure 17.** Example of uncertainty hazard curve fractiles (5th, 15th, 50th, 85th, and 95th) for sites across the United States and for 0.2 s pseudo-spectral acceleration with $V_{S30}$ = 760 m/s. The numbers labeled on the plot correspond to the 5th and 95th fractile ground motions with a 2% and 10% in 50-year probability of exceedance. The mean (2023 NSHM for CONUS and 2021 NSHM for Hawaii) and previous mean (2018 NSHM for CONUS and 2001 NSHM for Hawaii) are also shown.
AFE: annual frequency of exceedance.

lead to greater epistemic uncertainties than those depicted in this analysis. For most of the sites, the previous mean hazard curve (2018 NSHM for CONUS sites and 2001 NSHM for Honolulu) is within the 5th and 95th percentiles, although the New York City site shows previous mean curves that are close to the 5th percentiles and indicate more compact fractiles than the other sites. This compact nature of the uncertainty distribution is related to some trimming of logic trees and simplifications that were made to reduce the number of calculations. Figure SB-11 in Electronic_Supplement_1.pdf, Appendix B, shows the same results as Figure 17 but for 1.0 s SA.

We also explored the relative contribution of the ERF and GMM uncertainties for the sites in California, via the plots in Electronic_Supplement_1.pdf (Figures SB-12 to SB-15). We find that the two uncertainty components are often comparable in overall contribution to the total uncertainty, although the contributions can vary with location, annual frequency of exceedance (AFE), spectral period, and presumably (not yet explored) $V_{S30}$. Of note, the additional epistemic uncertainty applied to the NGA-West2 GMMs adds to the otherwise compact uncertainties observed in San Francisco and Los Angeles and indicates the importance of including this additional factor. However, this additional uncertainty

has been propagated in a fully correlated manner, which could overestimate its contribution. As we revise the additional uncertainty in future models, it is important to remember that this addition, and how it is propagated, may be an important factor that results in a more complete level of uncertainty.

### *Population exposure estimates*

We make use of the mean PGA hazard curve derived from the 2023 NSHM and previous (e.g. 2018 NSHMs for CONUS) at each mapped location assuming a reference rock site condition ($V_{S30}$ = 760 m/s) for performing shaking intensity-exposure analyses, analogous to our previous work (Figure 18, Jaiswal et al., 2015). The use of MMI as a shaking intensity measure type in portraying probabilistic seismic hazard offers several advantages over more traditional ground-motion intensity measures like PGA, PGV, or spectral accelerations at various periods/frequencies. The Worden et al. (2012) study provides regression relationships for converting PGA into a numeric value of MMI, which were rounded to integer values for further analyses. Gallahue and Abrahamson (2023) provide some important comparisons of the conversion equation impacts that can be addressed in future versions.

The exposure analysis relies on the latest 2022 global LandScan population database (Dobson et al., 2000; ~30 arc second resolution layer, roughly 1 km × 1 km grid) from the Oak Ridge National Laboratory as a baseline for deriving total population counts at each MMI bin. The probabilistic estimate of exceedance of intensities associated with various predefined recurrence thresholds (shown in Table 2) were used to sum and then tabulate the total population count at each intensity bin. This allows us to document changes in shaking estimates between successive map versions relying on same baseline population layer representing the current built environment. Clearly, the increase in population counts as shown in Table 2 at all shaking intensities and recurrence intervals highlight that the new mean hazard estimates have increased over previous map versions. The new hazard assessment identifies that nearly 49 million (an increase by 3% from our previous iteration of hazard), 188 million (an increase by 66%), and 290 million (an increase by 4%) are at risk of experiencing damaging shaking (MMI V or greater) with 50% (somewhat likely), 10% (uncommon), and 2% (rare) PE in the next 50 years (Figure 18 and Table 2). Table 2 shows a significant increase in population exposure (by ~75 million) at MMI V and above for 10 in 50 ground motions. Approximately 51 million of those people are located in Northeastern US covering parts of New York, New Jersey, Pennsylvania, Virginia, Maryland, Massachusetts, and Connecticut (Figure 10a) that have at least one intensity level increases in 10 in 50 hazard values. For Richmond, VA, the increase is even higher where the 10 in 50 hazard has increased by two levels (i.e. from MMI IV to VI) when compared with the 2018 model. Similarly, the hazard has also increased for the eastern front of the Rockies up from MMI IV to MMI V level where most of Colorado's population is located (Figure 10b).

### *Testing (CONUS only)*

Our NSHM-SC recommended that the NSHMs undergo testing, which is an important concept in developing science concepts and conclusions (Marzocchi and Jordan, 2018). GMM testing for the NSHMs is difficult because of the broad regional scope that spans many tectonic regimes, inherent complexity in natural earthquake systems, and the wide intra- and inter-event variability in the ground motions. For the first time, we evaluate the

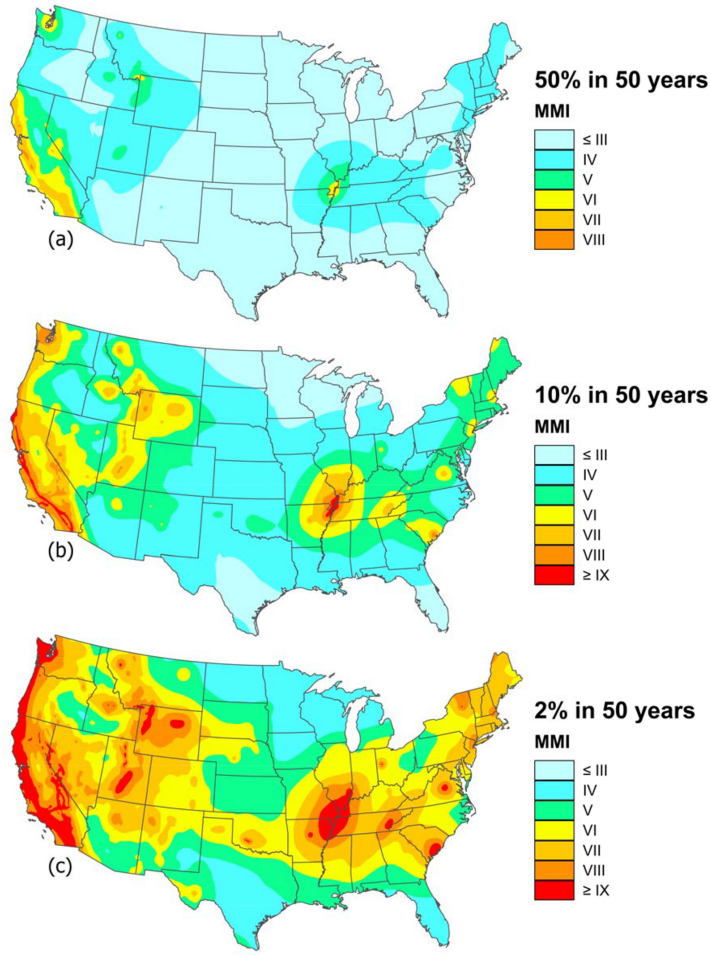


**Figure 18.** The 2023 Modified Mercalli Intensity (MMI) hazard maps of the conterminous United States showing estimates of earthquake shaking in terms of (1) 50% probability of exceedance (PE) in 50 years (somewhat likely), (b) 10% PE in 50 years (uncommon), and (c) 2% PE in 50 years (rare).

**Table 2.** Estimated counts of population (rounded up in 1000 s) in 50 US states using 2022 LandScan at various MMI shaking thresholds

| Map year | Total population estimates at MMI | | | | |
|---|---|---|---|---|---|
| | ⩾V | ⩾VI | ⩾VII | ⩾VIII | ⩾IX |
| 50% PE in 50 years (~72 years recurrence interval) | | | | | |
| Previous[a] | 47,343,000 | 35,349,000 | 12,625,000 | 229,000 | 6,000 |
| 2023 | 48,917,000 | 39,922,000 | 20,068,000 | 240,000 | 5,000 |
| 10% PE in 50 years (~475 years recurrence interval) | | | | | |
| Previous[a] | 113,112,000 | 68,770,000 | 49,956,000 | 32,019,000 | 3,963,000 |
| 2023 | 187,804,000 | 97,264,000 | 55,076,000 | 34,664,000 | 7,128,000 |
| 2% PE in 50 years (~2475 years recurrence interval) | | | | | |
| Previous[a] | 277,939,000 | 191,161,000 | 111,068,000 | 59,455,000 | 39,408,000 |
| 2023 | 290,126,000 | 233,434,000 | 158,607,000 | 82,743,000 | 40,606,000 |

MMI: Modified Mercalli Intensity; PE: probability of exceedance.
[a]CONUS 2018, AK 2007, and HI 2001.

performance of the 2023 NSHM (beta version) over much of the CONUS region simultaneously using estimates of past ground-shaking measurements that are independent of the GMM development. Input data sets and models are constantly being improved and incorporated, and these changes influence the final hazard estimate. Ideally, forecasts would be evaluated with data that were collected after the model was created. However, due to the nature of earthquakes and the infrequent occurrence of large magnitudes and strong ground motions, it is more advantageous to compare models with prior data that were not used in the NSHM. This data set provides a longer history of shaking.

Observed seismic intensity is a good source for assessing long-shaking histories and has the benefit of not being directly included in the hazard calculations, so these data provide an independent source for evaluation. Historical seismic intensities are derived from first-hand accounts of shaking by eyewitnesses, typically using a questionnaire, and are assigned a value by an expert or team or experts (Byerly and Dyk, 1936). Modern seismic intensities like the USGS Did You Feel It? (DYFI) product are collected via the Internet through multiple-choice questionnaires, then spatially aggregated and assigned an intensity by an algorithm (Wald et al., 1999). These two types of intensity data products have fundamental differences, although they are often combined to make longer histories. For example, the USGS ShakeMap product combines historical intensities, modern intensities, instrumental data, and earthquake source information with GMMs to achieve a more complete record of ground shaking (Marano et al., 2023). The Composite ShakeMap Atlas, which stacks ShakeMaps to reveal the history of shaking at a point and the maximum shaking over time, is particularly useful for the hazard model-evaluation exercise because it provides a comprehensive and spatially complete depiction of shaking for CONUS (Figure 19).

There are two ways to portray hazard spatially: point-based methods, as the hazard over different return periods (inverse of the frequency/PE) at a single location or area-based methods, as the hazard over an area at a single return period. Point-based evaluation methods have been applied in the past to the NSHM using historical intensities, with varied results: the hazard model was found to slightly exceed historical observations in the westernmost United States, while in the CEUS and the southern California subregion, the hazard tended to be lower than historical observations (Stirling and Petersen, 2006). In Oklahoma/Kansas, point-based results showed good agreement with modern DYFI intensities when applied to the short-term forecasts for natural and induced seismicity (White et al., 2018). Recent area-based evaluations of the NSHM have been applied to US subregions with similarly varied results (Ward, 1995). In California, area-based results showed the hazard model substantially exceeding historical intensities (Salditch et al., 2020). However, area-based results showed good agreement with modern intensities when applied to the short-term forecasts in Oklahoma/Kansas, similar to the point-based assessments in that region (Brooks et al., 2018, 2019). Area-based methods applied to the 2023 NSHM (beta version which is very similar to the final model) using modern intensity products show overall satisfactory agreement, indicating good performance of the model (Figure 19). This is illustrated in Figure 19 using established performance metrics: the M0 metric (difference between the observed and predicted fractional exceedance) is very close to the ideal value of zero, M1 (the sum of the squared difference at each point) is near the ideal value of zero, and the f/p metric (ratio of observed and predicted fractional exceedance) is near the ideal value of 1. The 2023 NSHM performs well against the independent set of observations using multiple metrics.

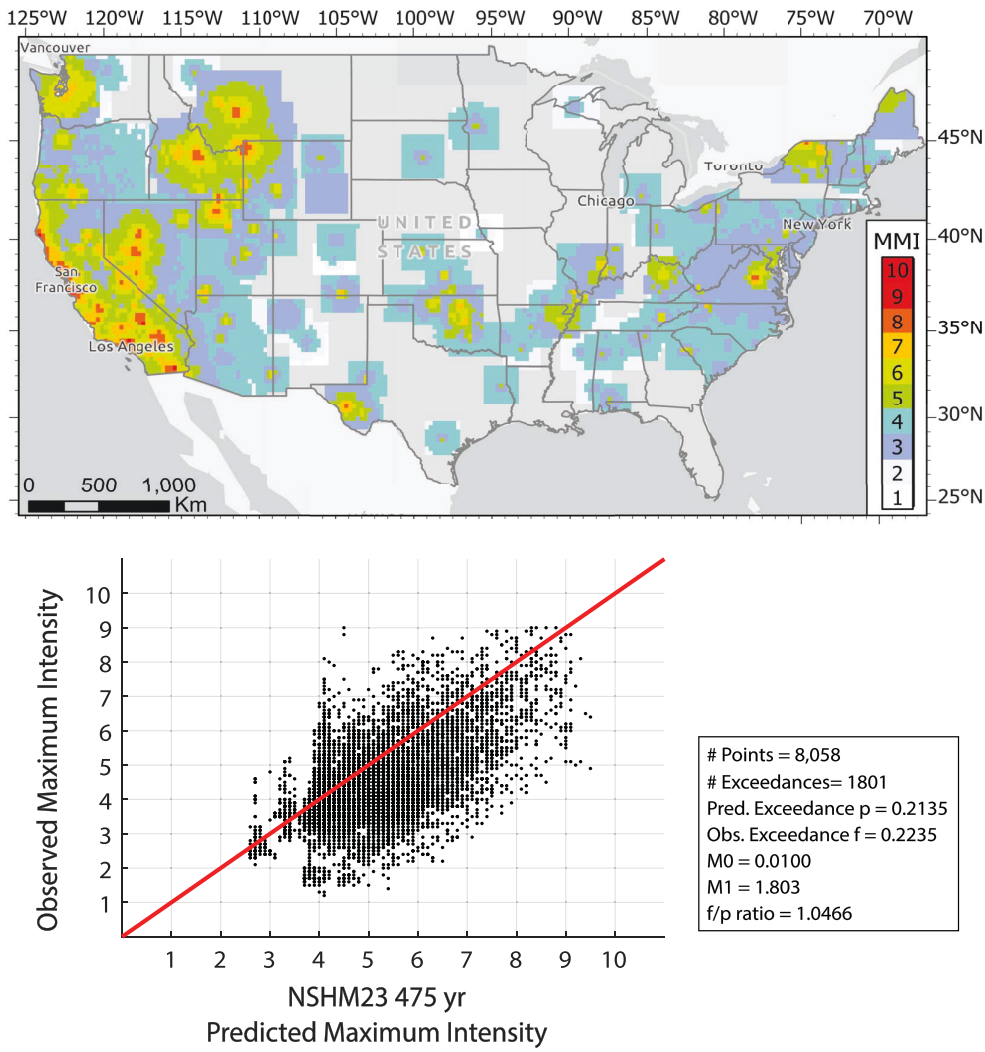


**Figure 19.** Top: maximum intensities from ShakeMap Composite Atlas 1906–2020. These augmented observations are used to compare against the predicted shaking from the 2023 NSHM. Intensity unit is Modified Mercalli Intensity (MMI). Bottom: performance metrics from comparison of NSHM23 10% in 50-year map, indicating good performance (M0 metric (difference between the observed and predicted fractional exceedance) is near the ideal value of zero, f/p metric (ratio of observed and predicted fractional exceedance) is near the ideal value of 1).

## Engineering and risk

### *Seismic scenarios in Hawaii and Salt Lake City that highlight newly mapped hazards*

Seismic scenarios serve a variety of different purposes and are traditionally developed to evaluate the seismic preparedness efforts in a given study region and most importantly to raise awareness about the underlying seismic risk. The USGS NSHM products (e.g. 2% in 50-year map) provide a probabilistic forecast of strong ground motions expected to occur within an observation window. Such products are largely targeted to be used within the

building code applications. As a part of NSHM 2023 effort, we also developed a set of new earthquake scenarios to highlight the underlying hazard and associated risk that the community faces, and where possible, incorporate new changes associated with the new model (e.g. new GMMs, source characteristics).

Accordingly, scenarios were developed for Hawaii (eight new scenarios), Utah (nine new scenarios), Alaska (10 new scenarios), and Virginia (one new scenario) to highlight the updates to the hazard characterization in these regions. Chase et al. (2022) have provided the rationale behind the need for the scenario development in the context of the new NSHM and discussed some of these scenarios in the context of community engagement. One scenario in the new Hawaii suite includes an M8.0 scenario on southern flank of the Island of Hawai'i near Hilo, consistent with the rupture of a décollement. Ground-shaking intensities are estimated to be an MMI of VII in Hilo with the potential for losses to exceed $1 billion and a few fatalities. In addition, the USGS Ground Failure earthquake product was used to find that there was a high probability of both liquefaction and landslides across the Island of Hawai'i.

### *Use of NSHM in US seismic provisions*

As with previous NSHM editions, the 2023 update will be proposed to serve as the basis for provisions in US seismic codes for buildings, bridges, railways, and defense facilities, among other types of infrastructure. The hazard curves at the 21 pseudo-spectral response periods, peak ground acceleration, peak velocity, and eight site classes produced by the NSHM are used as the primary inputs in the development of earthquake design load parameters for structural and geotechnical design and analysis. For seismic design guidelines that specify a uniform-hazard design basis (i.e. performance objectives that are conditional on a particular hazard level of ground shaking), design ground-motion parameters are interpolated from the NSHM-based hazard curves (Figure 14) at target annualized exceedance frequencies as specified by a particular design code. For example, the *American Society of Civil Engineers Seismic Evaluation and Retrofit of Existing Buildings* (ASCE 41 (ASCE, 2021)) design document specifies a range of design criteria that require design ground motions to be developed for return periods of 225 years (20% PE in 50 years), 975 years (5% PE in 50 years), and the 2475-year Maximum Considered Earthquake (MCE, 2% PE in 50 years). Similarly, the American Railway Engineering and Maintenance-of-Way Association (AREMA, 2019) design provisions require design ground motions for return periods ranging from 100 years (39% PE in 50 years) to the MCE. Within the context of seismic codes, ground-motion values extracted from the NSHM-based hazard curves are generally referred to as *probabilistic ground motions*.

Depending on the design code, probabilistic ground motions extracted from NSHM hazard curves are modified prior to their use as design values. In the case of guidelines that use uniform-risk performance criteria, rather than the uniform-hazard criteria described above, design motions are developed by integrating the full hazard curves with probabilistic representations of system fragility (e.g. Luco et al., 2007). The foregoing computations yield design parameters that produce uniform levels of system performance, such as a targeted annualized probability of structural collapse. For *National Earthquake Hazards Reduction Program (NEHRP) Recommended Seismic Provisions for New Buildings and Other* Structures (e.g. Building Seismic Safety Council (BSSC), 2020), (subsequently adopted in the ASCE 7 Minimum Design Loads for Buildings and Other Structures, e.g. ASCE, 2021), this risk target corresponds to a 1% in 50-year collapse probability, while

the forthcoming update to the American *Association of State Highway and Transportation Officials* (AASHTO, 2017) *Guide Specifications for LRFD Seismic Bridge Design* will use 1.5% in 75-year collapse risk target. The 2023 NSHM can also be used to compute deterministic ground-motion parameters, which often govern the seismic design in certain parts of the United States where they exceed probabilistic motions. As required by the 2020 NEHRP provisions, deterministic ground motions are calculated as the maximum 84th percentile SA computed from "scenario earthquakes on all known faults within the region," with the candidate scenario earthquakes determined from hazard disaggregation (Figure 16). Once adopted, design ground-motion parameters for a variety of code documents are computed and made freely available to users by the USGS through various means, such as web services (e.g. USGS, 2020) and online databases (e.g. Luco et al., 2021).

The 2023 NSHM update will be considered by the BSSC Provisions Update Committee (PUC) to serve as the basis for the 2026 update of the NEHRP provisions, with partial funding from FEMA. The NEHRP provisions update process began in 2022, involving hundreds of earthquake engineering experts from academia, industry, and public agencies—this includes USGS personnel, who serve as federal agency liaisons to the update committee. Many of those involved in the NEHRP provisions update also participate in NSHM workshops, such as user-needs workshops, throughout the model development process. More broadly, building code development occurs in parallel with NSHM updates, as the needs of users across different sectors can influence how NSHM data are made available and presented to the public.

### *Impact of epistemic uncertainties on seismic risk*

Several studies in the literature have highlighted the need to report epistemic uncertainties in the hazard (e.g. Bradley, 2009; Kennedy et al., 1980; Kulkarni et al., 1984; National Academies of Sciences, Engineering, and Medicine, 2019). From an engineering and risk perspective, incorporating the epistemic uncertainties in hazard enables estimates that are scientifically credible and defensible (e.g. risk-targeted ground motions, average annual loss). However, reporting estimates of epistemic uncertainties in the hazard involves various challenges (e.g. refer to fractile-based curves for six sites across the United States in Figure 17 and refer to further research described in section "Discussion" and "Conclusion").

Reporting epistemic uncertainties in hazard is important for understanding both hazard and risk. For example, the Kwong and Jaiswal (2023a, 2023b) studies provides specific example uses of fractile hazard curves, including visualization of epistemic uncertainties in maps of uniform-hazard ground motions (UHGMs), comparison of UHGMs over time, and an open-source Jupyter notebook (Kwong and Jaiswal, 2023a) for end-users of NSHM to interactively explore impacts of epistemic uncertainties in hazard in seismic risk assessments.

## Discussion

Our hazard assessment considers the best available science on earthquakes and related ground shaking available in the published literature as evaluated by the NSHM project members, review panels, and our NSHM-SC. This 2023 NSHM represents a major multi-year effort to improve the basis of the seismic hazard assessment across all 50 states with

many new ERF (Field et al., 2023) and GMM components (Moschetti et al., 2023a; Rezaeian et al., 2023). Dozens of researchers inside and outside of the USGS provided input data, methods, and models for this update. More than a hundred reviewers, scientists, and end-users provided important guidance, participated in workshops, and submitted public review comments in person and in written form. Although we were not able to accept all the technical requests recommended by our reviewers and other scientists, this 2023 hazard model builds on past NSHMs and uses many more data, input models, and methods than were available in developing the previous NSHMs. Our review panels generally felt that this new model represents a substantial improvement compared to past models.

For this update, we provide several types of outputs including (1) hazard curves for 21 spectral periods, PGV, PGA, MMI, and eight site conditions agreed upon with building code users, (2) ground-motion maps for these outputs as well as for MMI with topographic based amplification factors, and (3) deterministic-based earthquake rupture scenarios that could be useful for other end-users. One challege with the new Alaska models concerns the high calculated ground motions and how these could be truncated for various end-user applications. The NSHMs are considered for use by many end-users who each have different requirements for their respective use cases. Therefore, a variety of products would be beneficial to satisfy the needs of these alternative users, as debated in our user-needs workshop. The NSHM attempts to provide the models in the most efficient way to end-users and assist them in developing the products that they require for specific use cases. However, more could be done in this regard. Below, we examine several challenges in developing the NSHM.

### *Challenges in assessing epistemic uncertainties of input models*

Earthquakes are challenging to forecast, and it is important to keep in mind that epistemic uncertainties in the NSHMs are high and typically span factors of more than 2 in ground motion and factors of up to 10 in frequency of exceedance (e.g. Figure 17). Hazard uncertainties are high because there are gaps in our empirical database and knowledge regarding the possible faulting styles, rupture characteristics, coupling parameters, locations of future earthquakes, and ground-motion levels for alternative source properties, wave propagation characteristics, and site effects. To better assess epistemic uncertainty, the collection of new earthquake data would be beneficial for characterizing the full range of potential earthquake ruptures and developing alternative technically defensible interpretations. However, there are often many obstacles to collecting and analyzing the data needed to reduce these uncertainties. Seismicity, fault, and ground-motion data are difficult to collect and analyze and this requires a concerted and sustained effort by many trained scientists. For example, to better understand spatial and temporal variability of earthquake rupture properties requires extensive geologic and geophysical measurements and a unified effort with a quick response time following an earthquake to begin studies before the data perishes. Non-ergodic GMMs demand active and passive ground-motion collections and extensive subsurface modeling near a site of interest. Such studies can reduce epistemic uncertainty and possibly shift some portions of aleatory to epistemic through focused studies. This may result in better earthquake ground-motion forecasts. Other possible avenues for improvement include taking advantage of better science and computing capabilities by extrapolating data using physics-based principles into regions with fewer data, considering validated computer simulations to enhance the database of ground shaking, and developing global analogs to increase reliability.

*ERF.* Epistemic uncertainties are particularly high in places where data are sparse. For example, seismicity-based input component models have especially high uncertainties in regions with low seismic activity and especially those areas well away from known faults (e.g. parts of CEUS). To assess future earthquake rates in these areas, we use an earthquake catalog with uniform magnitudes, spatial smoothing kernels that account for how earthquakes are spatially distributed near past earthquakes, and MFDs based on statistical properties of seismicity. These data sets are used in constructing a smoothed seismicity–based MFD over a grid of sites that provides probabilistic estimates of future earthquake rates. The MFD uncertainties can, however, be quite high, especially in these lower seismic regions. For example, the seismicity-based models incorporate a grid of earthquake rates above some minimum magnitude-cutoff (typically M2.7 in CEUS or M4 in other regions). This rate is sensitive to slight changes in earthquake magnitudes compiled in seismicity catalogs. Earthquake magnitudes can change due to new analyses and data assessments. Earthquake catalog modifications may result in eliminating earthquakes or adding earthquakes to the NSHM earthquake catalog that fall above or below the minimum magnitude threshold. This can substantially change the rate of earthquakes in the model, especially in low seismicity areas. For example, our forensic analysis comparing the current and previous NSHMs shows substantial (~60%) increases in hazard ratios in lower seismic areas such as New York City due to treatment in prioritizing the input earthquake catalogs (resulting in magnitude adjustments) and MFD Gutenberg-Richter *b*-values. Calculated ground-motion differences are not as great at this site because the sparse seismicity in the area results in lower ground motions. Therefore, this hazard change may or may not be important to end-users. We can also observe similar sensitivities caused by methodology changes for assessing low seismicity areas near the boundary defined for the CEUS and WUS (104 degree longitude).

Another example of how data limitations affect hazard uncertainties can be observed in implementation of the deformation models. The five geologic and geologic–geodetic inversion models show very large between-model epistemic uncertainty caused by lack of knowledge of fault geometries, connections, and average slip rates (these differences often span factors between 2 and 10 or more). Our current fault model includes about 1000 faults, which represents a great achievement by the geologic community. Nevertheless, this number is only about half of the known fault sources mapped across the United States, with additional faults yet to be identified. For many of the major faults included in the assessment, the fault slip rates are derived from multiple detailed fault trenching and mapping studies by many investigators. This is important because these faults contribute most to hazard. For many of the other known faults, however, slip rates are typically sampled at only one or a few sites along the fault trace that are located either randomly or possibly at sites with unrepresentative faulting characteristics where surface effects (e.g. fault scarps) are more pronounced. This leads to considerable epistemic uncertainty for these less studied faults. Some faults in the model are not constrained by trenching data, resulting in the highest uncertainties. For example, most of the newly included 350 faults rely on geomorphologic characterizations gleaned from the Quaternary fault and fold database categories (Hatem et al., 2022a, 2022b). These new earthquake sources are thought to represent short faults (less than 20 km) with long recurrences (more than 5000 years). However, it is still important to study these faults to determine whether they are associated with other known or unknown rupture sources and to better quantify the prehistoric earthquake histories.

Slip rates are now modeled using both geology and GPS measurements, which increases our confidence in the deformation models and allow for a broader range of epistemic

uncertainty. These models are often limited by data availability. For example, many areas of the WUS, especially in the Intermountain West region, faults are modeled based on limited geologic studies as well as with widely spaced GPS recording sites that often span multiple faults. In addition, the deformation models are generated with alternative inputs and analytical methods that vary substantially between models—this is an important advantage in modeling the full range of science-based alternatives available on this topic. The deformation models would benefit from further validation studies and comparisons of alternative methods and data sets. It would be beneficial to know how to better rule out models that do not perform adequately and give more weight to those that are able to predict reasonable ranges of slip rates as discerned by empirical observations and physics-based constraints. However, we also do not want to limit models that are consistent with empirical data and simulations and that allow alternatives that are consistent with science and data. In addition, we currently allow for complex ruptures of known and inferred faults, but it would be helpful to extend the methodology to account for ruptures off the known faults using slip-rate information based on geology and geodesy studies. Inclusion of a wide but realistic range of input component models can further enhance the epistemic uncertainty estimation process and allow future reductions in the uncertainties through research and validation exercises.

Earthquake rate models also have large uncertainties that consider a broad range of earthquake ruptures that are derived from the widely varying deformation models to the varying earthquake rate models. There have been many debates about how we can best model future ruptures. Several recent large global earthquakes have occurred as the result of complex ruptures including both mapped and previously unmapped fault sections. This observation led to the development of the fault-system solution methodologies that form an innovative way to connect fault segments into complex but feasible rupture sources. However, we often lack information on fault parameters needed for making important modeling decisions (fault coupling properties, fault geometry, dynamic rupture fault connections, earthquake rates). For example, uncertainties associated with subsurface geometry of the Wasatch fault makes it difficult to assess the rupture sizes and connections with other faults. For example, the recent 2022 Magna, Utah, earthquake has ambiguous fault connections, and this rupture could be associated with a splay or antithetic fault or could be linked directly or indirectly with the Wasatch fault (Kleber et al., 2021). Even though the Wasatch fault is one of the most studied faults in the United States, improving our understanding of fault rupture properties (especially for the longest ruptures) and past rupture histories of neighboring faults may improve estimation of potential rupture lengths that drive hazard models in the Salt Lake City urban region.

We have implemented various models ranging from the classic to the fault-system solution inversion models to assess the rate of earthquakes considered in the ERF. The classic model is one end member that limits the number and sizes of earthquakes to be consistent with the past geologic record of inferred rupture sizes, prescribed MFDs, and moment rate calculations. However, this model results in a total MFD that has a bulge near M6.5 to M7.0 that led to the questioning of its viability by some in the science community, including several of the ERF review panel members (Jordan et al., 2023). The alternative fault-system solution inversion models allow for increasing numbers of additional ruptures by connecting adjacent ruptures based on connectivity constraints (fault rupture jump distances). These models result in a set of extended length ruptures that are consistent with earthquake statistics and physics-based simulations. However, most of the longest ruptures have not been recognized during the past 10,000-year record of paleoseismic studies and

the longest multi-fault ruptures are somewhat speculative but represent plausible rupture scenarios. This broad suite of models is thought to represent the current best available science range of potential sources along the Wasatch fault based on feedback from our ERF review panel. The differences between ground-motion hazard for the alternative ERF models (e.g. classic and the other inversion-based models and alternative deformation models) are large, and these models comprise some of the largest contributors to hazard uncertainties at urban sites (Electronic_Supplement_1.pdf, Figures SB-14 and SB-15). For example, Figures SB-14 and SB-15 show epistemic uncertainty in individual and combined ground motions that can span up to a factor of 10 between the various types of ERFs that consider alternative segmentation and deformation models. Therefore, additional global studies and physics-based simulations of multi-fault ruptures with strike-slip, normal, reverse, and subduction mechanisms can help improve future ERF models and help us better define the potential range of rupture sources.

Despite improvements, the new model is a limited representation of the system in terms of embodying assumptions, approximations, and data uncertainties. For example, we continue to differentiate between "on-fault" and "off-fault" ruptures, whereas nature will surely violate this model distinction. We also acknowledge that our fault model is a simplification of reality, and that future large ruptures will not exactly match it.

While we believe the logic-tree branch weights are a reasonable representation of current expert judgments, adjustments may be warranted in certain situations. For example, a 10% weight on the Classic and no-segmentation branches seems rational for site-specific hazard (because the actual connectivity of nearby faults may be more or less than implied by the fault model), but the likelihood that either of these branches applies to all faults in a region is more doubtful, so weight adjustments might be appropriate, especially for spatially distributed hazard and risk metrics (e.g. state-wide portfolio losses).

Another presently unresolved issue is the best way to combine sources that have completely different logic-tree branches. For example, if Cascadia has $X$ branches, do we combine these with all $N$ WUS branches, yielding $N^X$ branches? Alternatively, should we keep them separate and combine the consequent hazard PDFs, or resort to Monte Carlo sampling, both of which might complicate quantifying the influence of different branches? Or do we construct philosophically similar sets of branches for each source and assume perfect correlation? Until we address these questions, full consideration of all epistemic uncertainties will remain a challenge in hazard and risk analyses.

Future efforts are planned to focus on adding time-dependent components to the NSHM (e.g. elastic rebound, spatiotemporal clustering, induced seismicity, and swarms). For example, the 2023 NSHM may not characterize seismicity rates appropriately for return periods much less than about 475 years (Jordan et al., 2023). To improve the shorter-term forecasts, time-dependent seismicity rate calculations and other adjustments would be critical for use cases such as risk analysis and functional recovery building design applications. But in terms of improving the time-independent model presented here, effort is clearly warranted with respect to improving the deformation models, as fault slip rates continue to be one of the most influential factors on seismic hazard. Given that the five deformation models applied here differ substantially from one another, attention could be given to not only the viability of different modeling approaches, but also consideration to how each model maps out any solution range of different models that fit the data equally well (null space). In fact, it would be ideal if each approach provided a suite of viable models that represents both a systematic traversal of different models that fit the data equally

well and a basis for determining slip-rate covariance. We also want to improve the reliability of the off-fault deformation estimates from these models, both in terms of total moment rate and the spatial distribution of off-fault earthquakes (on which we have made no progress since UCERF3 (Field et al., 2014)).

It may also be beneficial to explore applicability of fault-system solutions in other areas (New Madrid and Alaska faults, and the Cascadia and the Aleutian subduction zones), in part to enable computing implied attributes, such as subduction slip rates, and for adding time dependencies. Another high priority is better quantification of epistemic uncertainties associated with the gridded seismicity model, especially given the limited sample of instrumental and historical earthquakes; better procedures are needed for quantifying the implications of this sampling error.

*GMM.* The current ergodic GMMs applied in the NSHMs and the related amplification models also show substantial between-model aleatory variability and epistemic uncertainties. Further work would be useful to separate the quantities and refine these models. We received suggestions from our reviewers that we should separate the mean/median and aleatory variability in future NSHM logic trees to account for variable knowledge of these two possibly independent quantities. Over the years, we have also received comments on the need for the NSHMs to better account for additional epistemic uncertainty, which account for unknown unknowns in the models. Several reviewers of the current model felt that this should be a primary focus of future updates because epistemic uncertainties influence differences in risk models. There are several reasons why we think that the NGA-West-2 GMMs as a group may not represent a wide enough epistemic uncertainty and why we have applied additional epistemic uncertainties to these models. For example, some of the GMMs were developed in collaborative projects where modelers formed general agreements on inputs, best practices, and data processing techniques. Differences between models arose mostly from modeling preferences and data selection criteria. This collaboration is very valuable in ensuring data quality and reasonable methodologies; however, it could also result in limiting the epistemic uncertainties when applying the potentially correlated models. This limited epistemic uncertainty represented by the different GMMs alone can be observed in the San Francisco and Los Angeles plots, which show very low epistemic uncertainties obtained from runs without additional epistemic uncertainty (Electronic_Supplement_1.pdf, Figures SB-12 to SB-14). Comparison of these plots with and without additional epistemic uncertainty indicates that the NSHMs should continue to apply some form of additional epistemic uncertainty to broaden the epistemic uncertainty to a more reasonable range. There are several examples of how modelers can better account for a reasonable range of uncertainties. The CEUS GMMs account for a very broad range of epistemic uncertainty resulting from the Sammons methods used for NGA-East (Goulet et al., 2021a, 2021b). New subduction zone GMMs from NGA-Subduction provide estimates of epistemic uncertainty for each model (Bozorgnia et al., 2022). These are both reasonable methods that allow modelers to account for epistemic uncertainty based on the available modeled data sets.

The GMMs are mostly built on smaller- to moderate-sized earthquakes or global (ergodic) observations of large earthquakes because large local earthquake strong-motion observations are not readily available for densely sampled sites distributed across urban regions. Therefore, it is difficult to assess a reasonable range of epistemic uncertainty for these urban regions. Despite relatively high modern seismicity rates in California, the largest historical events, such as the M7.9 1857 Fort Tejon and M7.8 1906 San Francisco San

Andreas Fault earthquakes, predated the advent of modern strong-motion instrumentation. Many other faults in California, the Cascadia subduction zone, and the Wasatch fault have not ruptured in several hundreds or thousands of years; therefore, few large earthquake recordings are available for estimating ground motions for these large earthquake ruptures. We have access to some earthquake strong-motion records from earthquakes with magnitude less than 7 (e.g. 1989 M6.9 Loma Prieta and 1994 M6.7 Northridge earthquakes) in urban areas, which can be helpful in improving our understanding of potential but unmeasured shaking levels caused by large earthquakes. We also have new international data from sequences such as the M7.8 2023 Turkiye earthquake that can add data to future GMMs, and ground-motion modelers can rely on these global analogs or simulations for assessing these large earthquake ground motions. To account for this lack of data, we apply equal weight to the NGA-West2 basin depth–based amplification models and to the average NGA-West2 models for sites across the San Francisco Bay area and Los Angeles regions. This contrasts with the 2018 NSHM that did not allow for the NGA-West2 basin deamplifications for shallow soil sites and only applied the average models. New models are being implemented as we gain confidence in the outputs, understand implications, and assess the uncertainties and variabilities. The new NGA-West models with basin considerations require detailed basin-depth and shape characterizations that amplify or deamplify ground motions based on multiple reflections and refractions off layers of the complex basin lithology and structure. The average GMMs that do not consider basin depths may account for additional epistemic uncertainties related to a relative lack of large earthquake strong-motion records and for unaccounted contributions from directivity or other unmodeled factors that influence the shaking. Epistemic and aleatory variability warrant consideration based on new parametric inputs in these GMMs. We have included both models in assessing urban ground shaking until more data are collected that rules out or lends support to these or other alternatives. Continued research would be helpful in establishing a more reasonable weighting.

Large epistemic uncertainties are also related to the rock/soil deamplification/amplifications. Amplification models for various soil types currently use broad proxies such as $V_{S30}$ or depth to shear-wave velocity horizons ($Z_{1.0}$ or $Z_{2.5}$) to estimate shaking levels. These models are insightful but uncertain site- and basin-response estimation vehicles. The response of shallow basins—such as those near Salt Lake City, Reno, and Portland—remains poorly understood, and amplification models may need to be modified for these basins, which have different $V_S$ gradients compared to the deeper basins in the WUS, such as the Los Angeles basin from which much of the NGA-West2 database is derived. There is only a weak correlation between CEUS and Hawaii soil amplifications and $V_{S30}$. Much of the northeastern CEUS is characterized by a soil layer over a harder rock, which results in a sharp impedance contrast that is not tied to $V_{S30}$ but to the depth of the soil layer. Modifications may also be needed for amplification factors that incorporate a proxy of the depth of sediments to model amplification in the deeper sediments associated with the Atlantic and Gulf Coastal plains and deamplification of shallow soils outside of basins (with respect to the centered equations of NGA-West2 as a function of $V_{S30}$) in urban areas. Models do not explicitly incorporate known ground-shaking effects (e.g. directivity or topographic amplification). New models could be developed that apply alternative input parameters, but this would take time and research. As for the GMM model components, new earthquakes will be informative, and additional dense networks of strong-motion instruments would be useful to record the shaking and improve these forecasts of the ground motions.

### Challenges in assigning logic-tree branch weights

A very important element of the hazard assessment is the assignment of branch weights. This assessment represents our perception of the best available science and knowledge of which of the models in the logic tree is most optimal at forecasting earthquake sources and ground motions. These weight analyses are based on the following: comparisons with empirical data, comparisons with physical principles, comparisons with other models and their ability to reduce residuals with observations, and expert judgments. This weighting depends on considerations of whether a new model is mature and vetted enough to justify a large weight, whether an older model still has merit and should continue to be considered in the analysis, whether it is time to retire an older model that does not perform as well, whether to consider an older model with lower weight to better capture the appropriate range of epistemic uncertainty, whether to allow for viable alternatives to better represent the epistemic uncertainty, and how to produce more scientifically defensible results for end-users. The inclusion of an input model ideally is based on a robust assessment of the available science data and expert judgments and ideally is not biased by either a desire to maintain the status quo or to quickly adopt new methods that lack proper testing and validation. There is a delicate balance between applying new models that are perhaps not as mature and accepted in the science community or including older models that have considered many of the same data but were evaluated in a different way using alternative and perhaps simpler techniques. The challenge is to constrain or limit these uncertainties using physics, geology, and observations and to ruptures that are well defined and supported by observations or theoretical-based consensus of opinion. Our project members, NSHM-SC, and review panels evaluate whether a new model is better at modeling sources or predicting ground motions than previous models, how to construct and constrain the full epistemic uncertainty and whether new or old models better define this range, and evaluate whether the model is sufficiently mature to include in the policy application or if we should opt to include it in the research and development model for further testing and scrutiny. We have tried to follow the internal USGS weighting assessments as well as consensus-based input from the scientific community and review panels in assigning weights to these models. It is important that outside hazard analysts assess the weights in the NSHMs instead of individual modeling teams providing weights for their own models that can easily result in potential biases.

### Challenges in presenting uncertainity in the models

As introduced above, computing hazard curve fractiles remains future work that entails both additional development of *nshmp-haz* and OpenSHA to implement Monte Carlo simulations of epistemic uncertainties and further research. Mean hazard curves like those computed in prior NSHM updates are not affected by the partitioning of epistemic versus aleatory uncertainties (of the ERF and GMM), but hazard curve fractiles are, so this partitioning for the NSHM is one research need. Another is research and deliberate decisions on the extent to which the various epistemic uncertainties (logic-tree branches on, for example, segmentation, *b*-value, or fault dip) are correlated across the earthquake sources. For example, the epistemic uncertainty in forecasted seismicity rate can be propagated as either fully (and positively) correlated or uncorrelated across the earthquake sources, or perhaps more realistically but difficultly, partially correlated. The same can be said of the logic-tree branches of GMMs and the other epistemic uncertainties. The decisions on the appropriate amount of correlation can be resolved based on how each epistemic uncertainty was developed and the characteristics of the earthquake sources to which the

uncertainty is applied. Relative to partial (and positive) correlation, assuming full correlation will increase the spread of the fractiles (i.e. the standard deviation), and assuming no correlation will decrease it. Thus, best estimates of the correlations of the various epistemic uncertainties are needed to avoid knowingly biasing the quantification of hazard curve fractiles. Unbiased estimation of the spread of the fractiles is important because they can be used to ascertain whether changes in the mean hazard are statistically significant. Overestimation of the spread would downplay the significance of mean hazard changes, which could lead some users to ignore the updated NSHM. Of course, underestimation of the spread of the fractiles would make the changes in mean hazard appear more significant than they are, which is also undesirable. Thus, extensive review of the hazard curve fractiles is needed to check whether their spread aligns with expectations across different geographic regions (e.g. WUS vs CEUS), return periods and spectral periods (short vs long), and site classes (firm vs soft). Review may identify sources of epistemic uncertainty that require further research for more rigorous quantification. Finally, to optimize the usefulness of the modeled uncertainties, further research on the "use cases" (end-user applications) would be beneficial.

### *Policy and research and development models*

The 2023 NSHM represents a policy model, which we interpret to mean that it is thoroughly reviewed and suitable for use by entities outside the USGS to set policy for building codes, risk mitigation, seismic safety, and other applications. The USGS does not prescribe policy on the use of the hazard model by those outside entities. The policy model is a single hazard model that is primarily made for a specific range of applications that are based on well-accepted data, models, and methods, and that have been adequately tested and vetted with published and peer-reviewed papers documenting the advantages and limitations of each input component model. These models only apply input components that are deemed by the scientific and user communities to represent best available science.

During development of the policy model, the USGS often considers model components that are ultimately deemed too immature for inclusion. In addition, we consider input components that would provide guidance for some end-users but may be incompatible for other applications. For example, in this update, we considered directivity in ground-motion modeling, but there are multiple published directivity models with widely varying parameterizations (Withers et al., 2023). We also considered time-dependence in this update but ultimately left it out of the policy model because it would disrupt established practices of the building code community. Nevertheless, time-dependence is a core requirement of the risk and insurance industries, and we plan to provide those users access to a USGS-endorsed version of the NSHM that includes time-dependence. We aim to provide end-users access to what has been developed thus far and future additions and modifications. Within the National Seismic Hazard Model Project (NSHMP), there is work underway to develop additional intensity measures, such as arias intensity and cumulative average velocity. Adding support for these in the hazard codes does not affect the policy model outputs but will ultimately broaden the NSHM user base. Engineers have also expressed interest in the USGS providing ground motions for damping scaling factors other than 5%. Another element of the research model in the near term could be inclusion of non-ergodic GMMs.

Following release of the 2023 update of the NSHM, the USGS will continue to support collection of new data and the development of improved methods and component models.

Our goal is that new data, methods, or component models are continuously being developed, implemented, evaluated, and tested within a dedicated research and development environment. The aggregate set of input component models and resulting hazard calculations are made available by the USGS to end-users for exploring effects of the new models on a particular site, portfolio or inventory. Some of new model components (e.g. alternative intensity measures and damping scaling factors) may make their way into the core USGS hazard codes and online web services and applications; others (e.g. directivity effects) may be made available only to users who run the hazard codes directly. Maintenance of the research and development environment will include the use of strict version control of USGS hazard codes and input files.

Ideally, all new models/data/research should be implemented first in the research model for testing and review, before they are considered for implementation in future updates of the policy model. How and when newly developed model components are deployed will depend largely on how they are implemented and their impacts on end-user models. Ultimately, this approach to research and development serves two purposes: First, it allows the USGS to provide end-user access to experimental features and components. Second, it supports progress toward future policy model updates while engaging with end-users throughout the update process.

## Conclusion

The US NSHM was updated in 2023 for all 50 states using the best available science related to earthquake seismicity, fault rupture characterization, ground-motion distribution, and hazard estimation techniques to produce a standard of practice for public policy applications (Field et al., 2023-CONUS ERF; Moschetti et al., 2023a-GMM; Rezaeian et al., 2023-NGA-Sub; Appendix D of Electronic_Supplement_1.pdf-Alaska; Petersen et al., 2022-Hawaii). This probabilistic seismic hazard model provides important new data, models, and methods that improve the hazard characterization and usefulness of the new model. Changes across the country are generally larger than in previous model updates because the 2023 NSHM applies so many new data, methods, and models for both ERF and GMM inputs. In improving the input component models, it is essential that we ensure that the new modeling changes are consistent with the best available science; that input component models are defensible; and results are robust, tested as well as possible, and reproducible. Our review panels provided a consensus (but not always unanimous) affirmation that these new models represent an improvement in forecasting earthquake sources and ground motions. The testing of the intensity outputs indicate that this model is consistent with the ShakeMap database, which lends confidence in the outputs of the model. Nevertheless, additional testing of these models is needed to ensure that the NSHM and its input components are consistent with all the data.

In this hazard assessment, we attempted to better categorize aleatory variability and epistemic uncertainty and analyzed the uncertainty at several sites spread across the country to identify relative model contributions and sensitivities. We have appreciated the extensive hazard community support in producing this complex model. External scientists provided new input models, feedback at dozens of public workshops, extensive recommendations from multiple review committees, and public comments on inputs and user-based outputs (Appendix E in Electronic_Supplement_1.pdf). This NSHM represents a high level of consensus within the science community. Nevertheless, it is not easy to capture a reasonable center, body, and scientifically based range of epistemic uncertainty and to use

these to estimate hazard uncertainty. Uncertainty assessments differ considerably at various sites and are dependent on the correlations in the models and details on how they are applied in the analysis. We have included many available proponent input models in this update but this may not always be sufficient to capture a broad enough epistemic uncertainty range. Sometimes this uncertainty assessment requires, arguably, adding additional input models or additional epistemic uncertainty when the available models do not span a broad enough range that is consistent with our knowledge of uncertainties. There are several ways we can improve the assessment of epistemic uncertainty including continuing to develop more robust backbone uncertainty approaches, encouraging modeler defined epistemic uncertainties, and involving the science community more fully in assessing regionalized epistemic uncertainty (Atkinson et al., 2014). The fully correlated uncertainty bounds we calculated for the 2023 NSHM span a factor of two or three at the 5% and 95% confidence levels. These distributions are mostly consistent with the 2018 NSHMs, with some exceptions. Uncertainty assessments performed in this analysis have provided important insights into the model inputs and outputs, and these analyses ideally would be expanded in future applications to include all NSHM sites.

Some of the challenges in developing and applying the 2023 NSHM are related to the following input component models:

1. We accounted for a new earthquake catalog, declustering methods, and spatial smoothing methods to produce a new seismicity model that is quite sensitive to modeling choices such as M thresholds and *b*-values. For this new model, we considered full-catalog rates rather than declustered earthquake rates applied previously in NSHMs. These changes result in increases in hazard >10% and may be significant to some users. Additional time-dependent studies and consideration of spatial and temporal clustering for earthquakes with very short recurrences (less than about 475 years) would be beneficial. This improvement would influence risk/insurance rate models, which are dependent on shorter recurrence earthquakes (less than 500-year recurrence) but are not well defined in the hazard models presented here (Field et al., 2023).
2. We included a suite of deformation models that included two additional and vastly different geodetic deformation models (i.e. expanded from three previous models up to five current models) that are all somewhat consistent with the available data and weighted in the 2023 ERF. The epistemic uncertainty between these geodetic-based models is quite wide with some models differing by factors of more than 2–10 compared to the geologic and geodetic-based models that were the basis of past NSHMs. Additional comparisons and revisions of inputs and constraints (e.g. modeling techniques, new data, global and regional plate rate constraints, and other geologic-based constraints) can improve the viability of these deformation models.
3. We applied new earthquake rupture rate models including new broad inversion-based fault-system solutions of ERF for the entire WUS (rather than just California in the previous models) as well as a classic prescriptive earthquake rate modeling treatment for CEUS, Alaska, and Hawaii. In future versions, we plan to apply more uniform methods, more uniformly processed and analyzed data sets, and more stable results. However, we continue to recognize that there are fundamental differences between various regions of the 50 states and allow for the best techniques to be applied regionally, including non-ergodic considerations.

Earthquake ruptures have large uncertainties as fault data and recurrence information are often obscured, which limits slip-rate and recurrence assessments. Fault ruptures with recurrences beyond 10,000-year recurrences are not well constrained and require additional attention.

4. We applied several new GMMs in the 2023 NSHM. The new NGA-Subduction GMMs are supplemented with older equations, which increase epistemic uncertainty, especially for long-period ground motions. We modified GMMs in CEUS to reduce data residuals and better account for non-linearity and a bias recognized in some GMMs. Additional epistemic uncertainty was added to active crustal GMMs, but new and better constrained methods of accounting for this uncertainty component would be helpful. CEUS and WUS spectra and site amplification factors differ considerably, and these need to be better understood and explained. Along with the CEUS and subduction GMMs, we applied new GMMs for Alaska and Hawaii. New bias adjusted GMMs are based on region specific Alaska subduction interface and CEUS strong motion data. Hawaii GMMs were selected based on comparisons with Hawaii volcanic generated earthquakes. Improvements in the median and standard deviations could allow for better seismic hazard and uncertainty assessments.
5. We accounted for new sedimentary basin-depth models in San Francisco, Los Angeles, and Seattle and for Coastal Plain amplification models that increase long-period ground motions and reduce short-period motions. A better understanding of the reference site condition for Atlantic and Gulf Coastal Plain amplification model is needed as well as a methodology to improve the implementation of these sediment effects with the current CEUS GMMs. We applied or modified GMMs using 3D ground-motion simulations to improve the basin-amplification models in places where data are scarce. Better understanding of the appropriate adjustment factors for the CEUS and WUS basin models can improve confidence in these models and result in increased weight assignments. Increased information on site specific soil and rock conditions and alternative proxies for assessing site amplification may also improve these models.
6. We developed several new components of hazard models that could be considered in future research and development models including a new directivity model for active faults in California, which is not implemented in the policy model, and a new time-dependent model for Cascadia. Other new models may better account for non-ergodic GMMs and improved site response proxies. Further assessments of the directivity for strike-slip, reverse, and normal faults and associated epistemic uncertainty and aleatory variability may improve models and make them more useful in future policy-based models. New time-dependent hazard models may improve the short return periods of seismicity models and the long return periods of fault models.
7. We have held more than 25 workshops with end-users of the NSHMs to enhance the consensus basis of the 2023 NSHMs. These models also benefited from extensive review by external panels that provided important advice and support in producing broad consensus-based hazard models. Continued work with the informed community will help in assessing how we can best fulfill the needs of each of the end-users of these products.

We plan to continue to update these models as new technology, science-based studies, and techniques allow us to better define the hazard and uncertainties across the United

States. We welcome any comments, suggestions, research, and inputs that can help us improve models in the future.

## Acknowledgments

The authors acknowledge the NSHM Steering Committee, the Deformation, ERF, and GMM Review Panels for CONUS, the Alaska Review Panel, and the Hawaii Earthquake and Tsunami Advisory Committee, who acted as the Hawaii Review Panel, and the Tiger Team. We want to especially thank the panel members and chairs of these panels including: Norm Abrahamson, John Anderson, Rhett Butler, Kaj Johnson, Tom Jordan, Jon Stewart, and Mike west for all their hard work and contributions. We thank the experts who provided additional advice on the Alaska geodetic-based subduction interface earthquake rate model: Rob Wesson and Jeff Freymueller. The authors also thank the state geological surveys who provided insights into the quality and usefulness of these models. The authors also thank participants in the workshops and public review for their insights and assistance in defining the best available science. The authors thank reviewers and editors of Earthquake Spectra and USGS reviewers. Also, the authors acknowledge Julian Bommer, Nilesh Shome, an anonymous reviewer from Earthquake Spectra, John Anderson, David Wald, and Ryan Gold for helpful feedback on the model and inputs. Any use of trade, firm, or product names is for descriptive purposes only and does not imply endorsement by the US Government.

## Declaration of conflicting interests

The author(s) declared no potential conflicts of interest with respect to the research, authorship, and/or publication of this article.

## Funding

The author(s) disclosed receipt of the following financial support for the research, authorship, and/or publication of this article: The authors wish to thank the USGS Earthquake Hazards Program for funding the development of the 2023 50-State NSHM.

## ORCID iDs

Mark D Petersen https://orcid.org/0000-0001-8542-3990
Allison M Shumway https://orcid.org/0000-0003-1142-7141
Peter M Powers https://orcid.org/0000-0003-2124-6184
Morgan P Moschetti https://orcid.org/0000-0001-7261-0295
Kishor S Jaiswal https://orcid.org/0000-0002-5803-8007
Sanaz Rezaeian https://orcid.org/0000-0001-7589-7893
Andrea L Llenos https://orcid.org/0000-0002-4088-6737
Andrew J Michael https://orcid.org/0000-0002-2403-5019
Jason M Altekruse https://orcid.org/0000-0002-8798-9514
Sean K Ahdi https://orcid.org/0000-0003-0274-5180
Kyle B Withers https://orcid.org/0000-0001-7863-3930
Robert E Chase https://orcid.org/0000-0002-8155-6830
Nicolas Luco https://orcid.org/0000-0002-5763-9847
Julie A Herrick https://orcid.org/0000-0003-0682-760X
Oliver S Boyd https://orcid.org/0000-0001-9457-0407
Eileen L Evans https://orcid.org/0000-0002-7290-5269
Andrew J Makdisi https://orcid.org/0000-0002-8239-0692
Brian R Shiro https://orcid.org/0000-0001-8756-288X
James A Smith https://orcid.org/0000-0002-5565-9254
Eric M Thompson https://orcid.org/0000-0002-6943-4806

## Supplemental material

Supplemental material for this article is available online.

## Note

1. NSHM Steering Committee: John Anderson (Chair), Gail Atkinson, Jack Baker, Ken Campbell, Heather DeShon, Tom Jordan, Keith Kelson, Nilesh Shome, and Jon Stewart; CONUS Deformation Review Panel: Kaj Johnson (Chair), Bill Hammond, and Ray Weldon; CONUS ERF Review Panel: Tom Jordan (Chair), Norm Abrahamson, John Anderson, Glenn Biasi, Kenneth Campbell, Timothy Dawson, Heather DeShon, Matt Gerstenberger, Nick Gregor, Keith Kelson, Yajie Lee, Nicolas Luco, Warner Marzocchi, Badie Rowshandel, David Schwartz, Nilesh Shome, Seth Stein, Gabriel Toro, Ray Weldon, and Ivan Wong; CONUS GMM Review Panel: Jon Stewart (Chair), Norm Abrahamson, John Anderson, Gail Atkinson, Ken Campbell, Chris Cramer, Michal Kolaj, and Grace Parker; Alaska Review Panel: Mike West (Chair), Norm Abrahamson, John Adams, John Thorley, Rob Wesson, and Ivan Wong; Tiger Team: Norm Abrahamson (Chair), Yousef Bozorgnia, Ken Campbell, Christine Goulet, Nick Gregor, Nico Kuehn, Jon Stewart, Grace Parker, Shahram Pezeshk, Mike West, and Ivan Wong; Hawaii Review Panel: Members of the Hawaii Earthquake and Tsunami Advisory Committee (HETAC); Publication Reviewers: Julian Bommer, Nilesh Shome, and an anonymous reviewer for Earthquake Spectra, John Anderson, David Wald, and Ryan Gold for the USGS, and several members of the NSHM Steering Committee.

## References

Aagaard BT (2023a) *Ground-Motion Records and Basin Depth Models for Portland, Oregon, 2005–2022* (US Geological Survey data release). DOI: 10.5066/P990DSA7.

Aagaard BT (2023b) *Ground-Motion Records and Basin Depth Models for Reno, Nevada, 2008–2022* (US Geological Survey data release). DOI: 10.5066/P93I5PU4.

Aagaard BT (2023c) *Ground-Motion Records and Basin Depth Models for the Great Valley, California, 2000–2022* (US Geological Survey data release). DOI: 10.5066/P9YKF031.

Aagaard BT and Hirakawa ET (2021) *San Francisco Bay Region 3D Seismic Velocity Model V21.1* (US Geological Survey data release). DOI: 10.5066/P9TRDCHE.

Abrahamson NA and Gülerce Z (2022) Summary of the Abrahamson and Gülerce NGA-SUB ground-motion model for subduction earthquakes. *Earthquake Spectra* 38(4): 2638–2681.

Abrahamson NA, Gregor N and Addo K (2016) BC Hydro ground motion prediction equations for subduction earthquakes. *Earthquake Spectra* 32(1): 23–44.

Abrahamson NA, Silva WJ and Kamai R (2014) Summary of the ASK14 ground motion relation for active crustal regions. *Earthquake Spectra* 30(3): 1025–1055.

Ahdi SK, Aagaard BT, Moschetti MP, Parker GA, Boyd OS and Stephenson WJ (2023) Empirical response of select basins in the western United States. *Earthquake Spectra* 40(1): 5–88.

Algermissen ST and Perkins DM (1976) *A probabilistic estimate of the maximum acceleration in rock in the contiguous United States*. Open-file report no. 76-416. Reston, VA: US Geological Survey. DOI: 10.3133/ofr76416.

American Association of State Highway and Transportation Officials (AASHTO) (2017) *AASHTO LRFD Bridge Design Specifications, Customary U.S. Units*. Washington, DC: American Association of State Highway and Transportation Officials.

American Railway Engineering and Maintenance-of-Way Association (AREMA) (2019) *Manual for Railway Engineering*. https://www.arema.org/files/pubs/mre/2019/AREMA_MRE_Chapter_9_2019.pdf

American Society of Civil Engineers (ASCE) (2021) *Minimum design loads and associated criteria for buildings and other structures* (ASCE/SEI 7-22). Reston, VA: ASCE.

Ancheta TD, Darragh RB, Stewart JP, Seyhan E, Silva WJ, Chiou BSJ, Wooddell KE, Graves RW, Kottke AR, Boore DM, Kishida T and Donahue JL (2014) NGA-West2 database. *Earthquake Spectra* 30(3): 989–1005.

Atkinson GM (2010) Ground-motion prediction equations for Hawaii from a referenced empirical approach. *Bulletin of the Seismological Society of America* 100(2): 751–761.

Atkinson GM and Macias M (2009) Predicted ground motions for great interface earthquakes in the Cascadia subduction zone. *Bulletin of the Seismological Society of America* 99(3): 1552–1578.

Atkinson GM, Bommer JJ and Abrahamson NA (2014) Alternative approaches to modeling epistemic uncertainty in ground motions in probabilistic seismic-hazard analysis. *Seismological Research Letters* 85(6): 1141–1144.

Baker JW, Bradley BA and Stafford PJ (2021) *Seismic Hazard and Risk Analysis*. Cambridge University Press. Available at: https://www.cambridge.org/core/books/seismic-hazard-and-risk-analysis/177B4BA01FC2600AA53A22B27598A06C (accessed 22 November 2023).

Bender AM, Haeussler PJ and Powers PM (2021) *Geologic Inputs for the 2023 Alaska Update to the U.S. National Seismic Hazard Model (NSHM)* (US Geological Survey data release). DOI: 10.5066/P97NRR0F.

Boore DM, Stewart JP, Seyhan E and Atkinson GM (2014) NGA-West2 equations for predicting PGA, PGV, and 5% damped PSA for shallow crustal earthquakes. *Earthquake Spectra* 30(3): 1057–1085.

Boyd OS, Churchwell D, Moschetti MP, Thompson EM, Chapman MC, Ilhan O, Pratt TL, Ahdi SK and Rezaeian S (2023) Sediment thickness and ground motion amplification along the United States Atlantic and Gulf Coastal Plains Sediment thickness map of Atlantic and Gulf Coastal Plain strata, central and eastern U.S., and their influence on earthquake ground motions. *Earthquake Spectra*.

Bozorgnia Y, Abrahamson NA, Ahdi SK, Ancheta TD, Al Atik L, Archuleta RJ, Atkinson GM, Boore DM, Campbell KW, Chiou BS-J, Contreras V, Darragh RB, Derakhshan S, Donahue JL, Gregor N, Gulerce Z, Idriss IM, Ji C, Kishida T, Kottke AR, Kuehn N, Kwak DY, Kwok AOL, Lin P, Mazzoni S, Midorikawa S, Muin S, Parker GA, Rezaeian S, Si H, Silva WJ, Stewart JP, Walling M, Wooddell K and Youngs RR (2022) NGA-Subduction research program. *Earthquake Spectra* 38(2): 783–798.

Bozorgnia Y, Abrahamson NA, Al Atik L, Ancheta TD, Atkinson GM, Baker JW, Baltay A, Boore DM, Campbell KW, Chiou BS-J, Darragh RB, Day S, Donahue J, Graves RW, Gregor N, Hanks T, Idriss IM, Kamai R, Kishida T, Kottke AR, Mahin SA, Rezaeian S, Rowshandel B, Seyhan E, Shahi S, Shantz T, Silva WJ, Spudich P, Stewart JP, Watson-Lamprey JA, Wooddell KE and Youngs RR (2014) NGA-West2 research project. *Earthquake Spectra* 30(3): 973–987.

Bradley BA (2009) Seismic hazard epistemic uncertainty in the San Francisco Bay Area and its role in performance-based assessment. *Earthquake Spectra* 25(4): 733–753.

Briggs RW, Witter RC, Freymueller JT, Powers PM, Haeussler PJ, Ross SL, Dura T, Engelhart SE, Koehler RD and Thio H-K (2023) An Alaska-Aleutian subduction zone interface earthquake recurrence model from geology and geodesy. In: Ruppert N, Jadamec M and Freymueller J (eds) *Tectonics and Seismicity of Alaska and WESTERN CANADA: Earthscope and Beyond*. Washington, DC: American Geophysical Union. https://essopenarchive.org/users/699055/articles/686652-an-alaska-aleutian-subduction-zone-interface-earthquake-recurrence-model-from-geology-and-geodesy

Brooks EM, Neely J, Stein S, Spencer BD and Salditch L (2019) Assessments of the performance of the 2017 one-year seismic hazard forecast for the Central and Eastern United States via simulated earthquake shaking data. *Seismological Research Letters* 90(3): 1155–1167.

Brooks EM, Stein S, Spencer BD, Salditch L, Petersen MD and McNamara DE (2018) Assessing earthquake hazard map performance for natural and induced seismicity in the central and eastern United States. *Seismological Research Letters* 89(1): 118–126.

Building Seismic Safety Council (BSSC) (2020) *NEHRP recommended seismic provisions for new buildings and other structures*. Federal Emergency Management Agency (FEMA) report no. P-2082-1, 2020 edition. Available at: https://www.fema.gov/sites/default/files/2020-10/fema_2020-nehrp-provisions_part-1-and-part-2.pdf (accessed 22 November 2023).

Butler R (2020) The 1871 Lānaʻi earthquake in the Hawaiian Islands. *Seismological Research Letters* 91(6): 3612–3621.

Byerly P and Dyk H (1936) The questionnaire program for collecting earthquake data. In: Heck NH (ed.) *Earthquake Investigations in California, 1934–1935* (Special Publication No. 201). Washington, DC: US Department of Commerce Coast and Geodetic Survey, pp. 43–48.

Campbell KW (2020) Proposed methodology for estimating the magnitude at which subduction megathrust ground motions and source dimensions exhibit a break in magnitude scaling: Example for 79 global subduction zones. *Earthquake Spectra* 36(3): 1271–1297.

Campbell KW and Bozorgnia Y (2014) NGA-West2 ground motion model for the average horizontal components of PGA, PGV, and 5% damped linear acceleration response spectra. *Earthquake Spectra* 30(3): 1087–1115.

Campbell KW and Gupta N (2018) Modeling diffuse seismicity in probabilistic seismic hazard analysis: Treatment of virtual faults. *Earthquake Spectra* 34(3): 1135–1154.

Chang SW, Frankel AD and Weaver CS (2014) *Report on workshop to incorporate basin response in the design of tall buildings in the Puget Sound region, Washington*. Open-file report no. 2014-1196. Reston, VA: US Geological Survey. DOI: 10.3133/ofr20141196.

Chapman MC and Guo Z (2021) A response spectral ratio model to account for amplification and attenuation effects in the Atlantic and Gulf Coastal Plain. *Bulletin of the Seismological Society of America* 111(4): 1849–1867.

Chase RE, Jaiswal KS and Petersen MD (2022) Earthquake scenario development in the 2023 USGS National Seismic Hazard Model Update. Seismological Society of America Annual Meeting April 19–23, 2022 Bellevue, Washington, the Seismological Society of America.

Chiou BS-J and Youngs RR (2014) Update of the Chiou and Youngs NGA model for the average horizontal component of peak ground motion and response spectra. *Earthquake Spectra* 30(3): 1117–1153.

Cornell CA (1968) Engineering seismic risk analysis. *Bulletin of the Seismological Society of America* 58(5): 1583–1606.

Darragh R, Wong I and Silva W (2019) Evaluating kappa, Q(f), and stress parameter in the southern Rocky Mountains of central Colorado. *Bulletin of the Seismological Society of America* 109(2): 586–599.

Dobson JE, Bright EA, Coleman PR, Durfee RC and Worley BA (2000) LandScan: A global population database for estimating populations at risk. *Photogrammetric Engineering and Remote Sensing* 66(7): 849–857.

Elliott J and Freymueller JT (2020) A block model of present-day kinematics of Alaska and western Canada. *Journal of Geophysical Research: Solid Earth* 125: e2019JB018378.

Evans EL (2022) A dense block model representing western continental United States deformation for the 2023 update to the National Seismic Hazard Model. *Seismological Research Letters* 93(6): 3024–3036.

Field EH, Arrowsmith RJ, Biasi GP, Bird P, Dawson TE, Felzer KR, Jackson DD, Johnson KM, Jordan TH, Madden C, Michael AJ, Milner KR, Page MT, Parsons T, Powers PM, Shaw BE, Thatcher WR, Weldon RJ and Zeng Y (2014) Uniform California earthquake rupture forecast, version 3 (UCERF3)—The time-independent model. *Bulletin of the Seismological Society of America* 104(3): 1122–1180.

Field EH, Biasi GP, Bird P, Dawson TE, Felzer KR, Jackson DD, Johnson KM, Jordan TH, Madden C, Michael AJ, Milner KR, Page MT, Parsons T, Powers PM, Shaw BE, Thatcher WR, Weldon RJ and Zeng Y (2013) *Uniform California earthquake rupture forecast (ver. 3) (UCERF3)—The time-independent model*. Open-file report no. 2013-1165. Reston, VA: US Geological Survey. Available at: https://pubs.usgs.gov/of/2013/1165/ (accessed 22 November 2023).

Field EH, Dawson TE, Felzer KR, Frankel AD, Gupta V, Jordan TH, Parsons T, Petersen MD, Stein RS, Weldon RJ and Wills CJ (2009) Uniform California earthquake rupture forecast (ver. 2) (UCERF 2). *Bulletin of the Seismological Society of America* 99(4): 2053–2107.

Field EH, Jordan TH and Cornell CA (2003) OpenSHA: A developing community-modeling environment for seismic hazard analysis. *Seismological Research Letters* 74(4): 406–419.

Field EH, Milner KR and Page MT (2021) Generalizing the inversion-based PSHA source model for an interconnected fault system. *Bulletin of the Seismological Society of America* 111(1): 371–390.

Field EH, Milner KR, Hatem AE, Powers PM, Pollitz FF, Llenos AL, Zeng Y, Johnson KM, Shaw BE, McPhillips DF, Thompson Jobe JA, Michael AJ, Shen Z-K, Evans EL, Hearn EH, Shumway AM, Mueller CS, Frankel AD, Petersen MD, DuRoss CB, Briggs RW, Page MT, Rubinstein JL and Herrick JA (2023) The USGS 2023 conterminous U.S. Time-independent earthquake rupture forecast. *Bulletin of the Seismological Society of America*.

Frankel AD (1995) Mapping seismic hazard in the central and eastern United States. *Seismological Research Letters* 66(4): 8–21.

Frankel AD, Mueller CS, Barnhard TP, Perkins DM, Leyendecker EV, Dickman N, Hanson SL and Hopper MG (1996) *National seismic-hazard maps: Documentation June 1996*. Open-file report no. 96-532. Reston, VA: US Geological Survey. Available at: https://pubs.usgs.gov/of/1996/532/ (accessed 22 November 2023).

Frankel AD, Petersen MD, Mueller CS, Haller KM, Wheeler RL, Leyendecker EV, Wesson RL, Harmsen SC, Cramer CH, Perkins DM and Rukstales KS (2002) *Documentation for the 2002 update of the national seismic hazard maps*. Open-file report no. 02-420. Reston, VA: US Geological Survey. Available at: https://pubs.usgs.gov/of/1996/532/ (accessed 22 November 2023).

Frankel AD, Stephenson W and Carver D (2009) Sedimentary basin effects in Seattle, Washington: Ground-motion observations and 3D simulations. *Bulletin of the Seismological Society of America* 99: 1579–1611.

Frankel AD, Wirth E, Marafi N, Vidale J and Stephenson W (2018) Broadband synthetic seismograms for magnitude 9 earthquakes on the Cascadia megathrust based on 3D simulations and stochastic synthetics, Part 1: Methodology and overall results. *Bulletin of the Seismological Society of America* 108(5A): 2347–2369.

Gallahue M and Abrahamson N (2023) New methodology for unbiased ground-motion intensity conversion equations. *Bulletin of the Seismological Society of America* 113(3): 1133–1151.

Gardner JK and Knopoff L (1974) Is the sequence of earthquakes in southern California, with aftershocks removed, Poissonian? *Bulletin of the Seismological Society of America* 64(5): 1363–1367.

Gerstenberger MC, Bora S, Bradley B, DiCaprio C, Kaiser Manea E, Nicol A, Rollins C, Stirling M, Thingbaijam K, Van Dissen R, Atkinson G, Chamberlain C, Christophersen K, Clark K, Coffey G, de la Torre CA, Ellis S, Fraser J, Graham K, Griffin J, Hamling I, Hill M, Hulsey A, Hutchinson J, Iturrieta P, Johnson K, Jurgens V, Kirkman R, Langridge R, Lee R, Litchfield N, Maurer J, Milner K, Rastin S, Rattenbury M, Rhoades D, Ristau J, Seebeck H, Shaw S, Townend J, Schorlemmer D, Stafford PJ, Villamor P, Wallace L, Weatherill G, Williams C and Wotherspoon L (2023) The 2022 New Zealand National Seismic Hazard Model: Process, overview and results. *Bulletin of the Seismological Society of America*.

Goldfinger C, Galer S, Beeson J, Hamilton T, Black B, Romsos C, Patton J, Nelson CH, Hausmann R and Morey A (2017) The importance of site selection, sediment supply, and hydrodynamics: A case study of submarine paleoseismology on the northern Cascadia margin, Washington USA. *Marine Geology* 384: 4–46.

Goulet CA, Bozorgnia Y, Kuehn N, Al Atik L, Youngs RR, Graves RW and Atkinson GM (2021a) NGA-east ground-motion characterization model part 1: Summary of products and model development. *Earthquake Spectra* 37(1): 1231–1282.

Goulet CA, Kishida T, Ancheta TD, Cramer CH, Darragh RB, Silva WJ, Hashash YMA, Harmon J, Parker GA, Stewart JP and Youngs RR (2021b) PEER NGA-east database. *Earthquake Spectra* 37: 1331–1353.

Graizer V (2018) GK17 ground-motion prediction equation for horizontal PGA and 5% damped PSA from shallow crustal continental earthquakes. *Bulletin of the Seismological Society of America* 108(1): 380–398.

Graves R, Jordan TH, Callaghan S, Deelman E, Field EH, Juve G, Kesselman C, Maechling P, Mehta G, Milner K, Okaya D, Small P and Vahi K (2011) CyberShake: A physics-based seismic hazard model for southern California. *Pure and Applied Geophysics* 168(3–4): 367–381.

Guo Z and Chapman MC (2019) An examination of amplification and attenuation effects in the Atlantic and Gulf Coastal Plain using spectral ratios. *Bulletin of the Seismological Society of America* 109(5): 1855–1877.

Gutenberg B and Richter CF (1944) Frequency of earthquakes in California. *Bulletin of the Seismological Society of America* 34(4): 185–188.

Haeussler PJ, Bender AM, Powers PM, Koehler RD and Brothers DS (2023) Updating the crustal seismic sources for the 2023 National Seismic Hazard Model for Alaska. In: Ruppert NA, Jadamec M and Freymueller JT (eds) *Tectonics and Seismicity of Alaska and Western Canada: Earthscope and Beyond* (American Geophysical Union Geophysical Monograph Series). Washington, DC: American Geophysical Union.

Harmon J, Hashash YMA, Stewart JP, Rathje EM, Campbell KW, Silva MJ, Xu B, Musgrove M and Ilhan O (2019) Site amplification functions for central and eastern North America–Part 1: Simulation data set development. *Earthquake Spectra* 35(2): 787–814.

Hashash YMA, Ilhan O, Harmon JA, Parker GA, Stewart JP, Rathje EM, Campbell KW and Silva WJ (2020) Nonlinear site amplification model for ergodic seismic hazard analysis in central and eastern North America. *Earthquake Spectra* 36(1): 69–86.

Hatem AE, Collett CM, Briggs RW, Gold RD, Angster SJ, Powers PM, Field EH, Anderson M, Ben-Horin JY, Dawson T, DeLong S, DuRoss C, Thompson Jobe JA, Kleber E, Knudsen KL, Koehler R, Koning D, Lifton Z, Madin I, Mauch J, Morgan M, Pearthree P, Pollitz FF, Scharer K, Sherrod B, Stickney M, Wittke S and Zachariasen J (2022a) *Earthquake Geology Inputs for the U.S. National Seismic Hazard Model (NSHM) 2023 (Western US)* (Ver. 2.0, US Geological Survey data release). DOI: 10.5066/P9AU713N.

Hatem AE, Reitman NG, Briggs RW, Gold RD, Thompson Jobe JA and Burgette RJ (2022b) Western U.S. geologic deformation model for use in the U.S. National Seismic Hazard Model 2023. *Seismological Research Letters* 93(6): 3053–3067.

Hayes GP, Moore GL, Portner DE, Hearne M, Flamme H, Furtney M and Smoczyk GM (2018) Slab2, a comprehensive subduction zone geometry model. *Science* 362: 58–61.

Hearn E (2022) "Ghost transient" correction to the southern California GPS velocity field from San Andreas fault seismic cycle model. *Seismological Research Letters* 96(6): 2973–2989.

Heath DC, Wald DJ, Worden CB, Thompson EM and Smoczyk GM (2020) A global hybrid VS30 map with a topographic slope–based default and regional map insets. *Earthquake Spectra* 36(3): 1570–1584.

Jaiswal KS, Petersen MD, Rukstales KS and Leith WS (2015) Earthquake shaking hazard estimates and exposure changes in the conterminous United States. *Earthquake Spectra* 31(S1): S201–S220.

Jaiswal KS, Rozelle J, Tong M, Sheehan A, McNabb S, Kelly M, Zuzak C, Bausch D and Simms J (2023) *Hazus estimated annualized earthquake losses for the United States*. Report no. P-366. Washington, DC: Federal Emergency Management Agency. Available at: https://www.fema.gov/sites/default/files/documents/fema_p-366-hazus-estimated-annualized-earthquake-losses-united-states.pdf (accessed 22 November 2023).

Johnson KM, Murray JR and Wespestad CE (2022) Creep rate models for the 2023 US National Seismic Hazard Model: Physically constrained inversions for the distribution of creep on California faults. *Seismological Research Letters* 93(6): 3151–3169.

Jordan TH, Abrahamson N, Anderson JG, Biasi G, Campbell K, Dawson T, DeShon H, Gerstenberger M, Gregor N, Kelson K, Lee Y, Luco N, Marzocchi W, Rowshandel B, Schwartz D, Shome N, Toro G, Weldon R and Wong I (2023) Panel review of the USGS 2023 conterminous U.S. Time-independent earthquake rupture forecast. *Bulletin of the Seismological Society of America*.

Keefer DL and Bodily SE (1983) Three-point approximations for continuous random variables. *Management Science* 29(5): 595–609.

Kennedy RP, Cornell CA, Campbell RD, Kaplan S and Perla HF (1980) Probabilistic seismic safety study of an existing nuclear power plant. *Nuclear Engineering and Design* 59(2): 315–338.

Kleber EJ, McKean AP, Hiscock AI, Hylland MD, Hardwick CL, McDonald GN, Anderson ZW, Bowman SD, Willis GC and Erickson BA (2021) Geologic setting, ground effects, and proposed

structural model for the 18 March 2020 Mw 5.7 Magna, Utah, earthquake. *Seismological Research Letters* 92(2A): 710–724.

Klein FW, Frankel AD, Mueller CS, Wesson RL and Okubo PG (2001) Seismic hazard in Hawaii: High rate of large earthquakes and probabilistic ground-motion maps. *Bulletin of the Seismological Society of America* 91(3): 479–498.

Kuehn N, Bozorgnia Y, Campbell K and Gregor N (2020) Partially non-ergodic ground-motion model for subduction regions using the NGA subduction database. *PEER reports, Pacific Earthquake Engineering Research Center, University of California, Berkeley, CA*, 1 September.

Kulkarni RB, Youngs RR and Coppersmith KJ (1984) Assessment of confidence intervals for results of seismic hazard analysis. In: *Proceedings of the eighth world conference on earthquake engineering*, San Francisco, CA, 21–28 July pp. 263–270. Earthquake Engineering Research Institute.

Kwong NS and Jaiswal KS (2023a) *brit: Bridge Risk Interactive Tool for Exploring Impacts From Epistemic Uncertainties in USGS NSHMs*. USGS Software Release. DOI: 10.5066/P9N5QTIN.

Kwong NS and Jaiswal KS (2023b) Uses of epistemic uncertainties in the USGS National Seismic Hazard Models. *Earthquake Spectra* 39(2): 1058–1087.

Lee E-J, Chen P, Jordan TH, Maechling PB, Denolle MAM and Beroza GC (2014) Full-3-D tomography for crustal structure in southern California based on the scattering-integral and the adjoint-wavefield methods. *Journal of Geophysical Research* 119(8): 6421–6451.

Levandowski W and McNamara DE (2022) Delineating the crustal seismic attenuation boundary between the central/eastern and western United States. *Seismological Research Letters* 93(2B): 1353.

Luco N, Ellingwood BR, Hamburger RO, Hooper JD, Kimball JK and Kircher CA (2007) Risk-targeted versus current seismic design maps for the conterminous United States. In: *Proceedings, structural engineer association of California 2007 convention*, Squaw Creek, CA, 26–29 September pp. 13. Structural Engineers Association of California.

Luco N, Rezaeian S, Rukstales KS, Powers PM, Shumway AM, Martinez EM and Smoczyk GM (2021) *Gridded earthquake ground motions for the 2020 NEHRP recommended seismic provisions and 2022 ASCE/SEI 7 standard* (US Geological Survey data release). DOI: 10.5066/P9I0R4O6.

McNamara DE, Wolin E, Powers PM, Shumway AM, Moschetti MP, Rekoske J, Thompson EM, Mueller CS and Petersen MD (2020) Evaluation of ground-motion models for US Geological Survey seismic hazard forecasts: Hawaii tectonic earthquakes and volcanic eruptions. *Bulletin of the Seismological Society of America* 110(2): 666–688.

McPhillips D (2022) Revised earthquake recurrence intervals in California, U.S.A.: New paleoseismic sites and application of event likelihoods. *Seismological Research Letters* 93(6): 3009–3023.

Magistrale H, Olsen KB and Pechmann JC (2008) *Construction and verification of a Wasatch Front community velocity model*. USGS Technical report no. HQGR.060012. Reston, VA: US Geological Survey. Available at: https://earthquake.usgs.gov/cfusion/external_grants/reports/06HQGR0009.pdf (accessed 22 November 2023).

Marano KD, Hearne M, Jaiswal KS, Thompson EM, Worden CB and Wald DJ (2023) ShakeMap Atlas 4.0 and AtlasCat: An archive of recent and historical earthquake ShakeMaps and impacts for global hazard analyses and loss model calibration. *Seismological Research Letters*. DOI: 10.1785/0220220324

Marzocchi W and Jordan TH (2018) Experimental concepts for testing probabilistic earthquake forecasting and seismic hazard models. *Geophysical Journal International* 215(2): 780–798.

Marzocchi W and Taroni M (2014) Some thoughts on declustering in probabilistic seismic-hazard analysis. *Bulletin of the Seismological Society of America* 104(4): 1838–1845.

Mazzoni S, Tadahiro K, Ahdi SK, Ancheta TD, Contreras V, Darragh RB, Kuehn NM, Kwak D, Kwok AO, Chiou BS-J, Silva WJ, Bozorgnia Y and Stewart JP (2021) *NGA-Sub Flatfile* (R211022). DOI: 10.34948/N3Z59T.

Michael AJ and Llenos AL (2022) An efficient, analytic solution using order statistics for probabilistic seismic-hazard assessment without the Poisson assumption. *Bulletin of the Seismological Society of America* 112(3): 1678–1693.

Milner KR and Field EH (2023) A comprehensive fault system inversion approach: Methods and application to NSHM23. *Bulletin of the Seismological Society of America*.

Milner KR, Shaw BE and Field EH (2022) Enumerating plausible multifault ruptures in complex fault systems with physical constraints. *Bulletin of the Seismological Society of America* 112(4): 1806–1824.

Moschetti MP (2015) A long-term earthquake rate model for the central and eastern United States from smoothed seismicity. *Bulletin of the Seismological Society of America* 105(6): 2928–2941.

Moschetti MP, Aagaard BT, Ahdi SK, Altekruse JA, Boyd OS, Frankel AD, Herrick JA, Petersen MD, Powers PM, Rezaeian S, Shumway AM, Smith JA, Stephenson WJ, Thompson EM and Withers KB (2023a) The 2023 U.S. National Seismic Hazard Model: Ground-motion characterization for conterminous U.S. *Earthquake Spectra*.

Moschetti MP, Withers K and Thompson EM (2023b) Basin effects from 3D simulated ground motions in the Greater Los Angeles region for use in seismic-hazard analyses. *Earthquake Spectra*.

Mueller CS (2019) Earthquake catalogs for the USGS national seismic hazard maps. *Seismological Research Letters* 90(1): 251–261.

Mueller CS, Frankel A, Petersen MD and Leyendecker E (2010) New seismic hazard maps for Puerto Rico and the U.S. Virgin Islands. *Earthquake Spectra* 26(1): 169–185.

Mueller CS, Haller KM, Luco N, Petersen MD and Frankel AD (2012) *Seismic hazard assessment for Guam and the Northern Mariana Islands*. Open-file report no. 2012-1015. Reston, VA: US Geological Survey. Available at: https://pubs.usgs.gov/of/2012/1015/ (accessed 22 November 2023).

National Academies of Sciences, Engineering, and Medicine (NASEM) (2019) *Reproducibility and Replicability in Science*. Washington, DC: The National Academies Press.

Nelson AR, DuRoss CB, Witter RC, Kelsy HM, Engelhart SE, Mahan SA, Gray HJ, Hawkes AD, Horton BP and Padgett JS (2021) A maximum rupture model for the central and southern Cascadia subduction zone—Reassessing ages for coastal evidence of megathrust earthquakes and tsunamis. *Quaternary Science Reviews* 261: 106922.

Nweke CC, Stewart JP and Brandenberg SJ (2020) *Site response of southern California sedimentary basins and other geomorphic provinces*. Report GIRS-2020-12. Los Angeles, CA: B. John Garrick Risk Institute, Natural Hazards Risk and Resiliency Research Center, UCLA. Available at: https://doi.org/10.34948/N3159F (accessed March 2022).

Nweke CC, Stewart JP, Graves RW, Goulet CA and Brandenberg SJ (2022a) Validating predicted site response in sedimentary basins from 3D ground motion simulations. *Earthquake Spectra* 38(3): 2135–2161.

Nweke CC, Stewart JP, Wang P and Brandenberg SJ (2022b) Site response of sedimentary basins and other geomorphic provinces in southern California. *Earthquake Spectra* 38(4): 2341–2370.

Ogata Y (1988) Statistical models for earthquake occurrences and residual analysis for point processes. *Journal of the American Statistical Association* 83(401): 9–27.

Ogata Y (1998) Space-time point-process models for earthquake occurrences. *Annals of the Institute of Statistical Mathematics* 50(2): 379–402.

Page MT, Field EH, Milner KR and Powers PM (2014) The UCERF3 grand inversion: Solving for the long-term rate of ruptures in a fault system. *Bulletin of the Seismological Society of America* 104(3): 1181–1204.

Parker GA, Stewart JP, Boore DM, Atkinson GM and Hassani B (2022) NGA-Subduction global ground motion models with regional adjustment factors. *Earthquake Spectra* 38(1): 456–493.

Petersen MD, Bryant WA, Cramer CH, Cao T, Reichle MS, Frankel AD, Lienkaemper JJ, McCrory PA and Schwartz D (1996) *Probabilistic seismic hazard assessment for the State of California*. US Geological Survey Open-file report no. 96-706. Reston, VA: US Geological Survey. DOI: 10.3133/ofr96706.

Petersen MD, Cao T, Campbell KW and Frankel AD (2007) Time-independent and time-dependent seismic hazard assessment for the state of California: Uniform California earthquake rupture forecast model 1.0. *Seismological Research Letters* 78(1): 99–109.

Petersen MD, Cramer CH and Frankel AD (2002) Simulations of seismic hazard for the Pacific Northwest of the United States from earthquakes associated with the Cascadia subduction zone. *Pure and Applied Geophysics* 159(9): 2147–2168.

Petersen MD, Frankel AD, Harmsen SC, Mueller CS, Haller KM, Wheeler RL, Wesson RL, Zeng Y, Boyd OS, Perkins DM, Luco N, Field EH, Wills CJ and Rukstales KS (2008) *Documentation for the 2008 update of the United States National Seismic Hazard Maps* (Version 1.1). Open-file report no. 2008-1128. Reston, VA: US Geological Survey. DOI: 10.3133/ofr20081128.

Petersen MD, Harmsen SC, Rukstales KS, Mueller CS, McNamara DE, Luco N and Walling M (2012) *Seismic hazard of American Samoa and neighboring South Pacific Islands—Methods, data, parameters, and results*. Open-file report no. 2012-1087. Reston, VA: US Geological Survey. Available at: https://pubs.usgs.gov/of/2012/1087/ (accessed 22 November 2023).

Petersen MD, Moschetti MP, Powers PM, Mueller CS, Haller KM, Frankel AD, Zeng Y, Rezaeian S, Harmsen SC, Boyd OS, Field EH, Chen R, Rukstales KS, Luco N, Wheeler RL, Williams RA and Olsen AH (2014) *Documentation for the 2014 update of the United States national seismic hazard maps*. Open-file report no. 2014-1091. Reston, VA: US Geological Survey. DOI: 10.3133/ofr20081128.

Petersen MD, Moschetti MP, Powers PM, Mueller CS, Haller KM, Frankel AD, Zeng Y, Rezaeian S, Harmsen SC, Boyd OS, Field EH, Chen R, Rukstales KS, Luco N, Wheeler RL, Williams RA and Olsen AH (2015a) The 2014 United States National Seismic Hazard Model. *Earthquake Spectra* 31(S1): S1–S30.

Petersen MD, Mueller CS, Moschetti MP, Hoover SM, Llenos AL, Ellsworth WL, Michael AJ, Rubinstein JL, McGarr AF and Rukstales KS (2016a) *2016 one-year seismic hazard forecast for the Central and Eastern United States from induced and natural earthquakes*. Open-file report no. 2016-1035. Reston, VA: US Geological Survey. DOI: 10.3133/ofr20161035.

Petersen MD, Mueller CS, Moschetti MP, Hoover SM, Llenos AL, Ellsworth WL, Michael AJ, Rubinstein JL, McGarr AF and Rukstales KS (2016b) Seismic hazard forecast for 2016 including induced and natural earthquakes in the central and eastern United States. *Seismological Research Letters* 87(6): 1327–1341.

Petersen MD, Mueller CS, Moschetti MP, Hoover SM, Rubinstein J, Llenos AL, Ellsworth W and Holland AA (2015b) *Incorporating induced seismicity in the 2014 United States National Seismic Hazard Models: Workshop and sensitivity studies*. Open-file report no. 2015-1-70. Reston, VA: US Geological Survey. DOI: 10.3133/ofr20151070.

Petersen MD, Mueller CS, Moschetti MP, Hoover SM, Rukstales KS, McNamara DM, Williams RA, Shumway AM, Powers PM, Earle PS, Llenos AL, Michael AJ, Rubinstein JL, Norbeck J and Cochran ES (2018) 2018 one-year seismic hazard forecast for the central and eastern United States from induced and natural earthquakes. *Seismological Research Letters* 89(3): 1049–1061.

Petersen MD, Mueller CS, Moschetti MP, Hoover SM, Shumway AM, McNamara DE, Williams RA, Llenos AL, Ellsworth WL, Michael AJ, Rubinstein JL, McGarr AF and Rukstales KS (2017) 2017 one-year seismic hazard forecast for the central and eastern United States from induced and natural earthquakes. *Seismological Research Letters* 88(3): 772–783.

Petersen MD, Shumway AM, Powers PM, Field EH, Moschetti MP, Jaiswal KS, Milner KR, Rezaeian S, Frankel AD, Llenos AL, Michael AJ, Altekruse JM, Ahdi SK, Withers KB, Mueller CS, Zeng Y, Chase RE, Salditch LM, Luco N, Rukstales KS, Herrick JA, Girot DL, Aagaard BT, Bender AM, Blanpied ML, Briggs RW, Boyd OS, Clayton BS, DuRoss CB, Evans EL, Haeussler PJ, Hatem AE, Haynie KL, Hearn EH, Johnson KM, Kortum ZA, Kwong NS, Makdisi AJ, Mason HB, McNamara DE, McPhillips DF, Okubo PG, Page MT, Pollitz FF, Rubinstein JL, Shaw BE, Shen Z-K, Shiro BR, Smith JA, Stephenson WJ, Thompson EM, Thompson Jobe JA, Wirth EA and Witter RC (2023) *Data Release for the 2023 U.S. 50-State National Seismic Hazard Model: Overview and Implications* (US Geological Survey data release). DOI: 10.5066/P9GNPCOD.

Petersen MD, Shumway AM, Powers PM, Moschetti MP, Llenos AL, Michael AJ, Mueller CS, Frankel AD, Rezaeian S, Rukstales KS, McNamara DE, Okubo PG, Zeng Y, Jaiswal KS, Ahdi SK, Altekruse JM and Shiro BR (2022) 2021 US National Seismic Hazard Model for the state of Hawaii. *Earthquake Spectra* 38(2): 856–916.

Petersen MD, Shumway AM, Powers PM, Mueller CS, Moschetti MP, Frankel AD, Rezaeian S, McNamara DE, Luco N, Boyd OS, Rukstales KS, Jaiswal KS, Thompson EM, Hoover SM, Clayton BS, Field EH and Zeng Y (2020) The 2018 update of the US National Seismic Hazard Model: Overview of model and implications. *Earthquake Spectra* 36(1): 5–41.

Petersen MD, Shumway AM, Powers PM, Mueller CS, Moschetti MP, Frankel AD, Rezaeian S, McNamara DE, Luco N, Boyd OS, Rukstales KS, Jaiswal KS, Thompson EM, Hoover SM, Clayton BS, Field EH and Zeng Y (2021) The 2018 update of the US National Seismic Hazard Model: Where, why, and how much probabilistic ground motion maps changed. *Earthquake Spectra* 37(2): 959–987.

Petersen MD, Zeng Y, Haller KM, McCaffrey R, Hammond WC, Bird P, Moschetti MP and Thatcher WR (2013) *Geodesy- and geology-based slip-rate models for the Western United States (excluding California) national seismic hazard maps*. Open-file report no. 2014-1091. Reston, VA: US Geological Survey. Available at: https://pubs.usgs.gov/of/2014/1091/ (accessed 22 November 2023).

Pollitz FF (2022) Viscoelastic fault-based model of crustal deformation for the 2023 update to the US National Seismic Hazard Model. *Seismological Research Letters* 93(6): 3087–3099.

Pollitz FF, Evans EL, Field EH, Hatem AE, Hearn EH, Johnson K, Murray JR, Powers PM, Shen Z-K, Wespestad CE and Zeng Y (2022) Western U.S. deformation models for the 2023 update to the U.S. National Seismic Hazard Model. *Seismological Research Letters* 93(6): 3068–3086.

Powers PM, Altekruse JM, Llenos AL, Michael AJ, Haynie KL, Haeussler PJ, Bender AM, Rezaeian S, Moschetti MP, Smith JA, Briggs RW, Witter RC, Mueller CS, Zeng Y, Girot DL, Herrick JA, Shumway AM and Petersen MD (2023) *Data Release for the 2023 Alaska National Seismic Hazard Model* (US Geological Survey data release). DOI: 10.5066/P9EVWWFZ.

Powers PM and Altekruse JM (2022a) *National Seismic Hazard Model for the conterminous U.S. (NSHM-CONUS)* (US Geological Survey software release). DOI: 10.5066/P9J1OVR6.

Powers PM and Altekruse JM (2023) *National Seismic Hazard Model for the state of Alaska (NSHM-AKALASKA)* (US Geological Survey software release). Available at: https://code.usgs.gov/ghsc/nshmp/nshms/nshm-alaska/ (accessed 22 November 2023). doi:10.5066/P961IMZX

Powers PM and Altekruse JM (2022b) *National Seismic Hazard Model for the state of Hawaii (NSHM-Hawaii)* (US Geological Survey software release). DOI: 10.5066/P97SQ3AQ.

Powers PM, Clayton BS and Altekruse JM (2022) *National Seismic Hazard Model project hazard applications and web services (NSHMP-haz)* (US Geological Survey software release). DOI: 10.5066/P9STF5GK.

Ramos-Sepúlveda M, Stewart J, Parker G, Moschetti M, Thompson E, Brandenberg S, Hashash YMA and Rathje EM (2023) Bias of NGA-East Ground Motion and Site Amplification Models Relative to Central and Eastern North America Ground Motion Database. *Earthquake Spectra*.

Reasenberg PA (1985) Second-order moment of central California seismicity, 1969–1982. *Journal of Geophysical Research: Solid Earth* 90(B7): 5479–5495.

Rezaeian S, Petersen MD and Moschetti MP (2015) Ground motion models used in the 2014 U.S. National Seismic Hazard Maps. *Earthquake Spectra* 31(1_suppl): S59–S84.

Rezaeian S, Powers PM, Altekruse JA, Ahdi SK, Petersen MD, Shumway AM, Frankel AD, Wirth EA, Smith JA, Moschetti MP and Withers KB (2023) The 2023 U.S. National Seismic Hazard Model: Subduction ground motion models. *Earthquake Spectra*.

Rezaeian S, Powers PM, Shumway AM, Petersen MD, Luco N, Frankel AD, Moschetti MP, Thompson EM and McNamara DE (2021) The 2018 update of the US National Seismic Hazard Model: Ground motion models in the central and eastern U.S. *Earthquake Spectra* 37(Suppl. 1): 1354–1390.

Rukstales KS, Shumway AM and Petersen MD (2021) *Data Release for the 2021 Update of the U.S. National Seismic Hazard Model for Hawaii* (U.S. Geological Survey data release). DOI: 10.5066/P91V4SDT.

Salditch LM, Gallahue MM, Lucas MC, Neely JS, Hough SE and Stein S (2020) California Historical Intensity Mapping Project (CHIMP): A consistently reinterpreted dataset of seismic

intensities for the past 162 yr and implications for seismic hazard maps. *Seismological Research Letters* 91(5): 2631–2650.

Shah AK and Boyd OS (2018) *Depth to basement and thickness of unconsolidated sediments for the western United States—Initial estimates for layers of the U.S. Geological Survey National Crustal Model*. Open-file report no. 2018-1115. Reston, VA: US Geological Survey. DOI: 10.3133/ofr20181115.

Shaw BE (2023) Magnitude and slip scaling relations for fault-based seismic hazard. *Bulletin of the Seismological Society of America* 113(3): 924–947.

Shen Z-K and Bird P (2022) NeoKinema deformation model for the 2023 update to the US National Seismic Hazard Model. *Seismological Research Letters* 93(6): 3037–3052.

Shumway AM, Petersen MD, Powers PM, Rezaeian S, Rukstales KS and Clayton BS (2021) The 2018 update of the US National Seismic Hazard Model: Additional period and site class data. *Earthquake Spectra* 37(2): 1145–1161.

Shumway AM, Petersen MD, Toro G, Powers PM, Altekruse JM, Thompson Jobe JA, Hatem AE, Herrick JA and Girot DL (2023) Earthquake rupture forecast model construction for the 2023 50-state National Seismic Hazard Model update: Central and eastern U.S. fault and area source models. *Seismological Research Letters*.

Simpson AR and Louie JN (2020) *Measurements and Predictions of VS30, Z1.0, and Z2.5 in Nevada*. Reno, NV: Nevada Seismological Laboratory, University of Nevada, Reno.

Stephenson WJ (2007) *Velocity and density models incorporating the Cascadia subduction zone for 3D earthquake ground motion simulations*. Open-file report no. 2007-1348. Reston, VA: US Geological Survey. DOI: 10.3133/OFR20071348.

Stephenson WJ, Reitman NG and Angster SJ (2017) *P- and S-wave velocity models incorporating the Cascadia subduction zone for 3D earthquake ground motion simulations*. Open-file report no. 2017-1152. Reston, VA: US Geological Survey. DOI: 10.3133/ofr20171152.

Stewart JP, Parker GA, Atkinson GM, Boore DM, Hashash YMA and Silva WJ (2020) Ergodic site amplification model for central and eastern North America. *Earthquake Spectra* 36(1): 42–68.

Stirling MW and Petersen MD (2006) Comparison of the historical record of earthquake hazard with seismic-hazard models for New Zealand and the continental United States. *Bulletin of the Seismological Society of America* 96(6): 1978–1994.

Thompson Jobe JA, Hatem AE, Gold RD, DuRoss CB, Reitman NG, Briggs RW and Collett CM (2022a) *Earthquake Geology Inputs for the National Seismic Hazard Model (NSHM) 2023 (Central and Eastern United States)* (Version 1.0) (US Geological Survey data release). DOI: 10.5066/P94HLE5G.

Thompson Jobe JA, Hatem AE, Gold RD, DuRoss CB, Reitman NG, Briggs RW and Collett CM (2022b) Revised earthquake geology inputs for the central and eastern United States and southeast Canada for the 2023 National Seismic Hazard Model. *Seismological Research Letters* 93(6): 3100–3120.

US Geological Survey (USGS) (2018) East vs west coast earthquakes. Available at: https://www.usgs.gov/news/featured-story/east-vs-west-coast-earthquakes (accessed 22 November 2023).

US Geological Survey (USGS) (2020) NEHRP-2020 web service documentation. Available at: https://earthquake.usgs.gov/ws/designmaps/nehrp-2020.html (accessed April 2022).

US Geological Survey, Earthquake Hazards Program (ComCat) (2022) *Advanced National Seismic System (ANSS) Comprehensive Catalog of Earthquake Events and Products*. DOI: 10.5066/F7MS3QZH.

US Nuclear Regulatory Commission (CEUS–SSCn) (2012) Central and Eastern United States seismic source characterization for nuclear facilities. *US Nuclear Regulatory Commission, Office of Nuclear Regulatory Research*. Available at: https://www.nrc.gov/docs/ML1204/ML12048A804.pdf (accessed 22 November 2023).

Valentini A, DuRoss CB, Field EH, Gold RD, Briggs RW, Visini F and Pace B (2020) Relaxing segmentation on the Wasatch Fault Zone: Impact on seismic hazard. *Bulletin of the Seismological Society of America* 110: 83–109.

Wald DJ and Allen TI (2007) Topographic slope as a proxy for seismic site conditions and amplification. *Bulletin of the Seismological Society of America* 97(5): 1379–1395.

Wald DJ, Quitoriano V, Dengler LA and Dewey JW (1999) Utilization of the internet for rapid community intensity maps. *Seismological Research Letters* 70(6): 680–692.

Wang S, Werner MJ and Yu R (2022) How well does Poissonian probabilistic seismic hazard assessment (PSHA) approximate the simulated hazard of epidemic-type earthquake sequences? *Bulletin of the Seismological Society of America* 112(1): 508–526.

Ward SN (1995) Area-based tests of long-term seismic hazard predictions. *Bulletin of the Seismological Society of America* 85(5): 1285–1298.

Watson-Lamprey JA (2018) *Capturing directivity effects in the mean and aleatory variability of the NGA-West2 ground-motion prediction equations*. PEER 2018-04, November. Berkeley, CA: Pacific Earthquake Engineering Research Center.

Wesson RL, Boyd OS, Mueller CS, Bufe CG, Frankel AD and Petersen MD (2007) *Revision of time-independent probabilistic seismic hazard maps for Alaska*. Open-file report no. 2007-1043. Reston, VA: US Geological Survey. Available at: https://pubs.usgs.gov/of/2007/1043/ (accessed 22 November 2023).

Wesson RL, Frankel AD, Mueller CS and Harmsen SC (1999) *Probabilistic seismic hazard maps of Alaska*. Open-file report 99-36. Reston, VA: US Geological Survey. DOI: 10.3133/ofr9936.

White IJO, Liu T, Luco N and Liel AB (2018) Considerations in comparing the U.S. Geological Survey one-year induced-seismicity hazard models with "Did You Feel It?" and instrumental data. *Seismological Research Letters* 89(1): 127–137.

Wirth EA, Chang SW and Frankel AD (2018a) *2018 report on incorporating sedimentary basin response into the design of tall buildings in Seattle, Washington*. Open-file report no. 2018-1149. Reston, VA: US Geological Survey. DOI: 10.3133/ofr20181149.

Wirth EA, Frankel AD, Marafi N, Vidale JE and Stephenson WJ (2018b) Broadband synthetic seismograms for magnitude 9 earthquakes on the Cascadia megathrust based on 3D simulations and stochastic synthetics, Part 2: Rupture parameters and variability. *Bulletin of the Seismological Society of America* 108(5A): 2370–2388.

Withers K, Moschetti M, Powers P, Petersen M, Graves R, Aagaard BT, Baltay A, Luco N, Wirth E, Rezaeian S and Thompson E (2023) Evaluation and integration of rupture directivity models for the USGS National Seismic Hazard Model. *Earthquake Spectra*.

Wong IG, Silva WJ, Darragh R, Gregor N and Dober M (2015) A ground motion prediction model for deep earthquakes beneath the Island of Hawaii. *Earthquake Spectra* 31(3): 1763–1788.

Worden CB, Gerstenberger MC, Rhoades DA and Wald DJ (2012) Probabilistic relationships between ground motion parameters and modified Mercalli intensity in California. *Bulletin of the Seismological Society of America* 102(1): 204–221.

Zaliapin I and Ben-Zion Y (2020) Earthquake declustering using the nearest-neighbor approach in space-time-magnitude domain. *Journal of Geophysical Research: Solid Earth* 125(4): e2018JB017120.

Zeng Y (2022a) A fault-based crustal deformation model with deep driven dislocation sources for the 2023 update to the US National Seismic Hazard Model. *Seismological Research Letters* 93(6): 3170–3185.

Zeng Y (2022b) GPS velocity field of the western United States for the 2023 National Seismic Hazard Model update. *Seismological Research Letters* 93(6): 3121–3134.

Zhao JX, Zhang J, Asano A, Ohno Y, Oouchi T, Takahashi T, Ogawa H, Irikura K, Thio HK, Somerville PG, Fukushima Y and Fukushima Y (2006) Attenuation relations of strong ground motion in Japan using site classification based on predominant period. *Bulletin of the Seismological Society of America* 96(3): 898–913.